ANKARA UNIVERSITY
GRADUATE SCHOOL OF NATURAL AND APPLIED SCIENCE

MASTER THESIS

3D BIOPRINTING OF OSTEOCHONDRAL GRAFTS USING INFRAPATELLAR FAT PAD DERIVED STEM CELLS

Ebru TALAK

DEPARTMENT OF BIOMEDICAL ENGINEERING

ANKARA
2022

All rights reserved

ABSTRACT

M.Sc. Thesis

3D BIOPRINTING OF OSTEOCHONDRAL GRAFTS USING INFRAPATELLAR FAT PAD DERIVED STEM CELLS

Ebru TALAK

Ankara University

Graduate School of Natural and Applied Sciences

Department of Biomedical Engineering

Supervisor: Prof. Dr. Pınar YILGÖR HURİ

The utilization of stem cells in tissue engineering is an important research and application area. The multipotent characteristics and proliferation capacities of mesenchymal stem cells are the main reasons for their use in this field. In recent years, studies with mesenchymal stem cells obtained from adipose tissue (AL-ASC) have gained importance in tissue engineering applications since it is easily available with liposuction method and abundant in the body. As an alternative to the abdominal lipoaspirate, ASC cells can be isolated from the infrapatellar fat pad in the knee (IPFP-ASCs). With its high osteogenic and chondrogenic differentiation capacity, IPFP-ASCs are a significant cell source, especially for bone and cartilage tissue engineering applications. They also become important for the treatment of the old age population because they do not lose their ability to proliferate and differentiate depending on age. With this thesis, it is aimed to analyze the use of IPFP-ASCs in the production of osteochondral grafts in comparison with AL-ASC cells with tissue engineering approach. For this, osteogenic and chondrogenic differentiation capacities of IPFP- and AL-ASCs isolated from two different patient populations, 25-40 and 50-65 years were evaluated. 3D bioprinting which has an ever-increasing role in tissue engineering was used to form osteochondral scaffold with hydrogel combination including alginate, gelatin, and carboxymethylcellulose. The inner pattern of the cartilage and bone part of the osteochondral scaffold was designed grid and snowflake, respectively. In order to induce the differentiation of the IPFP- and AL-ASCs on the scaffold, controlled release of the PCL capsules loaded with BMP-2 for osteogenic; PCL capsules loaded with TGF-β for chondrogenic were used.

January 2022, 110 Pages

Keywords: Osteochondral tissue engineering; 3D bioprinting; Infrapatellar fat pad derived adipose stem cells; Controlled release of growth factor

ÖZET

Yüksek Lisans Tezi

İNFRAPATELLAR YAĞ YASTIĞI KAYNAKLI KÖK HÜCRELERİN 3B BİYOBASKILAMAYLA OSTEOKONDRAL GREFT ÜRETİMİNDE KULLANIMI

Ebru TALAK

Ankara Üniversitesi

Fen Bilimleri Enstitüsü

Biyomedikal Mühendisliği Anabilim Dalı

Danışman: Prof. Dr. Pınar YILGÖR HURİ

Doku mühendisliğinde kök hücrelerin kullanımı önemli bir araştırma ve uygulama alanıdır. Sıklıkla tercih edilen mezenkimal kök hücrelerin multipotent karakteri ve çoğalma kapasiteleri bu alandaki kullanımlarının başlıca sebebidir. Son yıllarda liposuction yöntemiyle kolaylıkla elde edilebilir olması ve vücutta bol miktarda bulunması sebebiyle yağ dokusundan elde edilen mezenkimal kök hücrelerle (AL-ASC) yapılan çalışmalar gerek hücresel tedavilerde gerekse doku mühendisliği uygulamalarında hız kazanmıştır. Abdominal lipoaspirata alternatif olarak, diz içinde bulunan infrapatellar yağ yastığından da ASC hücreleri izole edilebilmektedir (IPFP-ASC). Yüksek osteojenik ve kondrojenik farklılaşma kapasitesi gibi özellikleriyle IPFP-ASC hücreleri özellikle kemik ve kıkırdak doku mühendisliği uygulamaları için umut verici bir hücre kaynağıdır. Yaşa bağlı olarak çoğalma ve farklılaşma yeteneklerini kaybetmemeleri nedeniyle ayrıca ileri yaş popülasyonun tedavisi için de önemli hale gelmektedir. Bu çalışmada IPFP-ASC hücrelerinin, AL-ASC hücreleriyle karşılaştırmalı şekilde, tek hücre kaynağı olarak osteokondral greft üretiminde kullanımının doku mühendisliği yaklaşımı ile incelenmesi amaçlanmaktadır. Bunun için 25-40 yaş ve 50-65 yaş olmak üzere iki farklı hasta popülasyonundan izole edilen IPFP- ve AL-ASC'lerin osteojenik ve kondrojenik farklılaşma kapasiteleri değerlendirildi. Aljinat, jelatin ve karboksimetilselüloz içeren hidrojel kombinasyonu ile osteokondral iskele oluşturmak için doku mühendisliğinde giderek artan bir role sahip olan 3D biyo-baskı kullanıldı. Osteokondral iskelenin kıkırdak ve kemik kısmının iç dizaynı sırasıyla kare ve kar deseni olarak tasarlandı. İskelede IPFP- ve AL-ASC'lerin farklılaşmasını indüklemek için, osteojenik için BMP-2 ile yüklenmiş PCL kapsüllerinin kontrollü salımı; kondrojenik için TGF-β ile yüklenmiş PCL kapsüller kullanıldı.

Ocak 2022, 110 Sayfa

Anahtar kelimeler: Osteokondral doku mühendisliği;3 boyutlu biyobaskılama;

Infrapatellar yağ yastığı kaynaklı kök hücreler; Kontrollü büyüme faktörü salımı

ACKNOWLEDGEMENTS

Ebru TALAK

Ankara, January 2022

CONTENTS

LIST OF FIGURES

LIST OF TABLES

ABBREVIATIONS

3D	Three-Dimensional
ACI	Autogenous Chondrocytes Implantation
ADA	Alginate Dialdehyde
AL-ASCs	Abdominal Lipoaspirate Derived Adipose Stem Cells
AlgMc	Alginate-Methylcellulose
AM	Additive Manufacturing
ASCs	Adipose-Derived Stem Cells
APG	Agarose-Polydopamine
APS	Ammonium Persulfate
BMP	Bone Morphogenetic Protein
BMSCs	Bone Marrow Mesenchymal Stem Cells
BSA	Bovine Serum Albumin
b-TCP	b-Tricalcium Phosphate
CAD	Computer-Aided Design
CMC	Carboxymethylcellulose
CPC	Calcium Phosphate Cement
CT	Computerized Tomography
C2C12	Mouse Myoblast Cell Line
DAPI	4′,6-Diamidino-2-Phenylindole
DCM	Dichloromethane
dECM	Decellularized Extracellular Matrix
DMEM	Dulbecco’s Modified Eagle Medium
DMSO	Dimethyl Sulfoxide

DPSC	Dental Pulp Stem Cells
ECM	Extracellular Matrix
ESCs	Embryonic Stem Cells
FBS	Fetal Bovine Serum
FDM	Fused Deposition Method
FGF	Fibroblast Growth Factor
GAG	Glycosaminoglycan
GELMA	Gelatin Methacrylate
HA	Hydroxyapatite
HaCaT	Human Immortalized Keratinocyte
HCEpC	Human Corneal Epithelial Cells
hCh	Human Chondrocytes
hESCs	Human Embryonic Stem Cells
HepG2	Human Liver Cancer Cells
IPFP-ASCs	Infrapatellar Fat Pad Derived Adipose Stem Cells
IPSCs	Induced Pluripotent Stem Cells
MBAAm	Methylene Bisacrylamide
MC3T3-E1	Mouse Calvaria Pre-Osteoblast
MRC-5	Human Fetal Lung Fibroblast
MSCs	Mesenchymal Stem Cells
MRI	Magnetic Resonance Imaging
NIH/3T3	Mouse Embryonic Fibroblasts
P/S	Penicillin/Streptomycin
pASCs	Porcine Adipose Derived Stem Cells
PBS	Phosphate Buffer Saline

PCL	Poly (ε-Caprolactone)
PFA	Paraformaldehyde
PGA	Poly (Glycolic) Acid
PLA	Polylactic Acid
PLGA	Polylactic-co-Glycolic Acid
PRP	Platelet-Rich Plasma
PU	Polyurethane
PTL-CS	N-Pentenyl Chitosan
PVA	Polyvinyl Alcohol
SEM	Scanning Electron Microscopy
SLA	Stereolithography
SLS	Selective Laser Sintering
TCP	Tricalcium Phosphate
TE	Tissue Engineering
TEA	Triethanolamine
Temed	Tetramethyl Ethylene Diamine
TGF-β	Transforming Growth Factor Beta
UCB-MSCs	Umbilical Cord Blood Mesenchymal Stem Cells
V-2-P	N-Vinyl-2-Prrolidinone

1. INTRODUCTION

Articular cartilage is often damaged by effects such as aging and trauma, especially, the knee joint is a fairly common problem. More than 2 million arthroscopic knee surgeries are performed worldwide annually and 60% of these surgeries are performed because of osteochondral tissue damage. The articular cartilage does not contain vascular and nerve structures and its potential to regenerate itself is very low, if it is damaged owing to the presence of a small number of chondrocytes (E. B. Hunziker, 1999; Temenoff & Mikos, 2000). Due to its nerve-free structure, the damage can progress and cause subchondral bone tissue damage in addition to cartilage tissue damage over time. Osteochondral tissue regeneration can only be provided by surgical operation because of the lack of effective drug treatment. Treatments such as microfracture method, autologous and allogeneic tissue transplantation are used to provide osteochondral regeneration in the clinic. However, instead of hyaline articular cartilage, fibrocartilage formation with different mechanical properties can occur and decrease the success of treatment (Bedi, Feeley, & Williams, 2010; Panseri et al., 2012). In addition, risks such as the limited amount of autologous tissue that can be transplanted and disease transmission in allogeneic transplants lead to the need for bioactive osteochondral grafts in treatment. In order to produce a solution to this need, studies on the production of osteochondral grafts have gained speed with a tissue engineering approach by using autologous cells, biomaterials, and bioactive molecules. Osteochondral graft prepared in a complex structure that can mimic cartilage and subchondral bone tissue and should be biocompatible and aimed to stimulate tissue regeneration. It is formed in accordance with the natural structures of the tissues by using various bioactive molecules and/or different biomaterials to create cartilage and bone tissues. To imitate this complex structure, scaffold design and production methods gain importance.

In this thesis, the osteochondral differentiation ability of the infrapatellar fat pad-derived adipose stem cells (IPFP-ASCs), which have an important potential to be an excellent cell source for cell therapy and tissue engineering applications due their age-independent proliferation and differentiation ability, were examined and compared with abdominal lipoaspirate derived stem cells (AL-ASCs). The osteogenic and chondrogenic

differentiation potential of IPFP-ASC and AL-ASC cells in osteochondral grafts, which were created by 3D bioprinting, were compared for the first time.

2. LITERATURE SURVEY

2.1 Osteochondral Tissue

The osteochondral unit consisting of articular cartilage, subchondral bone, and calcified cartilage layers enables the movement and stability of the skeleton. The articular cartilage layer located in the upper region of the osteochondral tissue covers the distal ends of bones and protects bone against friction and the damage it can cause. The extracellular matrix (ECM) of it mainly includes water, collagen Type-II, and proteoglycans, which protects bones. Articular cartilage is a type of tissue that contains small number of chondrocytes (1-2% of total cartilage volume) and has no nerve and blood supply (E. B. Hunziker, 1999; Ernst B. Hunziker, Lippuner, & Shintani, 2014; Temenoff & Mikos, 2000). All these reasons cause the tissue to have a low regeneration and repair mechanism. Aging, diseases, or traumatic events can cause cartilage damage and the minor damage leads to a huge amount of problems in joint until subchondral bone damage due to avascular and aneural nature of cartilage (CHANG, LIN, CHOU, LIN, & LIU, 2005; Correia et al., 2013). Subchondral bone part provides mechanical strength to the osteochondral unit. The extracellular matrix of the subchondral bone part includes proteins such as type I collagen, proteoglycans, glycosaminoglycans, and hydroxyapatite minerals that give the bone its hardness (Stewart & Kawcak, 2018; van der Harst et al., 2004). The majority of bone tissue extracellular matrix consists of hydroxyapatite mineral as the inorganic phase, type 1 collagen as the organic phase (X. Lin, Patil, Gao, & Qian, 2020). Unlike cartilage which only consists of chondrocytes, bone tissue contains various cell types like osteoblasts, osteoclasts, osteocytes, and mesenchymal stem cells (MSCs).

The calcified cartilage layer that is mainly composed of type-X collagen, is located between the articular cartilage and subchondral bone. The calcified cartilage interface is responsible for the arrangement of cartilage-to-bone transition and maintenance of structural integrity (Gadjanski & Vunjak-Novakovic, 2015).

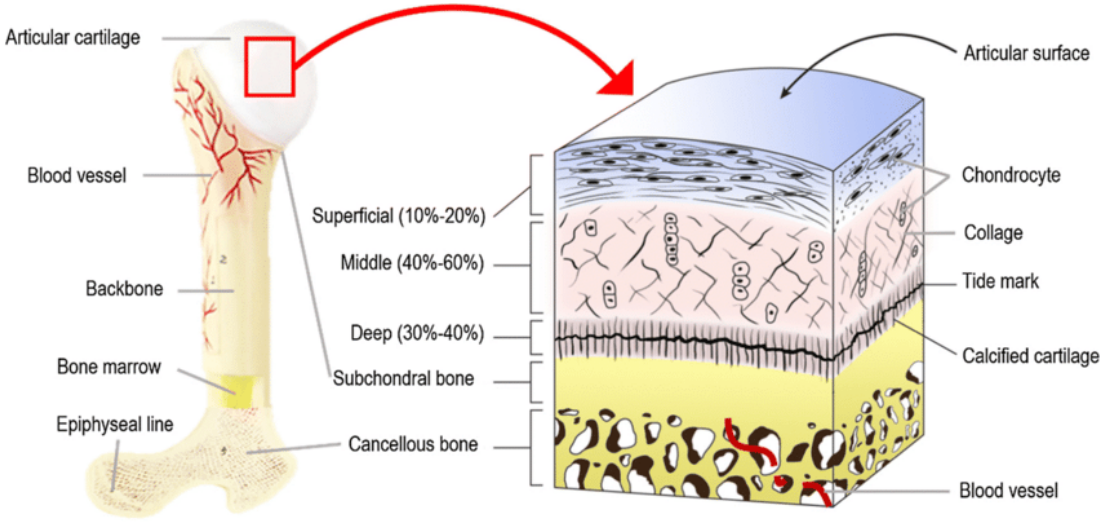

Figure 2. 1 Structure of the osteochondral tissue (Hu et al., 2020)

2.1.1 Cartilage tissue

Cartilage is a connective tissue found in the articular surfaces of the long bones, trachea, bronchi, ear, nose, and larynx (Sharma, Gautam, Dinda, & Mishra, 2011). Articular cartilage located in the knees carries all the weight of the body and, it prevents the bones from being damaged by rubbing against each other and ensures the transmission of force. Articular cartilage tissue has less cell density compared to other tissues and includes chondrocyte and precursor cells; chondroblasts. It is liable for the formation and healing of the ECM including proteins and glycosaminoglycans of the cartilage tissue. Articular cartilage contains the range of 65–85% water, 12–24% collagen, 3–6% glycosaminoglycan (GAG) (Hoemann, 2004). The extracellular matrix of cartilage mostly composed of collagen type II and GAGs bound to proteoglycans. Unlike bone, cartilage contains no blood vessels or nerves, so it does not supply the nutrient and oxygen supply. Diffusion provides the oxygen and nutrient needs of the cells. Because of the having the smaller number of chondrocytes, nerve-free and avascular nature, the regeneration ability of cartilage tissue is insufficient (E. B. Hunziker, 1999; Temenoff & Mikos, 2000). If any damage occurs in cartilage, with time it causes the progress of the damage.

There are three different cartilage tissues: hyaline cartilage, elastic cartilage, and fibrocartilage. All of them have distinct mechanical, chemical, and morphological properties. Hyaline cartilage is the most abundant type of cartilage and majorly type II

collagen found on its extracellular matrix. It can be a bluish white colour or a frosted glass appearance. It is very resistant to pressure. The entire skeleton in the embryo, nasal cartilage, trachea, cartilages found on bone surfaces in synovial joints, and cartilage in large bronchi are hyaline-type cartilage (Kheir & Shaw, 2009). Elastic cartilage is cartilage that is more transparent than hyaline cartilage and is yellowish and can bend. It is found in the outer ear, wall of auditory canals, Eustachian tube, small bronchioles, wings of the nose (Parsons, 1998). Fibrocartilage looks in grayish-white colour. It includes collagen type II and type I, and the high number of collagens fibers that give it to its stiffness. It is found in several specific areas, meniscus, symphysis pubis, at the connection areas of tendons to bones (Benjamin & Evans, 1990).

2.1.2 Bone tissue

Bone tissue is a connective tissue that has an important role in our skeleton, protecting organs, organizing movement with muscle, storing minerals, and production of blood cells. Mature bone tissue is divided into two according to their structure cortical (compact) bone and cancellous (trabecular) bone (Tzelepi, Tsamandas, Zolota, & Scopa, 2009). Cortical bones form the outer surface of the bones. It is a continuous bone tissue and contains vascular channels. It gives strength to the skeleton. The cortical bone structure consists of osteons that are interconnected by Haversian canals (Augat & Schorlemmer, 2006). The outer surfaces of all bones have a cortical bone structure. It is found especially in the diaphysis of long bones. Cancellous bone is located within the bone layers contains trabeculae that include bone marrow where blood cells are produced. In addition, cancellous bone increases mechanical strength by providing internal support to the bone. Cancellous bone is mainly present at the end of long bones, close parts of joints, and the inner parts of the flat bones (TOPALOĞLU, KETANİ, & SARUHAN, 2017). Based on the porosity, macrostructure, and mineral content, the mechanical properties of bones can be variable (Rho, Kuhn-Spearing, & Zioupos, 1998). Cortical bone has high compressive strength than cancellous bone due to such reasons (Cowin & Telega, 2003).

The part at the end of the bone covered with cartilage tissue in the joints is called the subchondral bone (G. Li et al., 2013). It has a responsibility to support the joint. Cartilage

tissue can be damaged because of aging, traumatic events, or disease conditions, and this damage can lead to the subchondral bone defect because of the low regeneration ability of cartilage (H. Madry, van Dijk, & Mueller-Gerbl, 2010). Treatment is needed because this defect causes a painful situation and affects the quality of life.

There are different cells for bone tissue; osteoblasts, osteoclasts, osteocytes, and mesenchymal stem cells (MSCs). Osteoblasts are specialized mesenchymal cells that play role in bone formation. Osteoclasts are multinucleated cells responsible for the breaks down bone tissue for the development and remodelling of bone. Osteocytes are bone cells derived from osteoblasts.

The extracellular matrix of the bone is mainly composed of the organic phase, and the rest is the mineral/inorganic phase. This phase includes type I collagen that is more than 90%, glycoproteins and proteoglycans (Gelse, Pöschl, & Aigner, 2003; Robey, 2002). The inorganic phase of ECM includes hydroxyapatite.

2.2 Osteochondral Defects

The osteochondral defect is combined damage caused by both cartilage and subchondral bone tissue injuries. Trauma, aging, tumour, disease such as osteoarthritis can cause damage to cartilage tissue. Osteoarthritis is a painful disease caused by genetic and biological factors that affect the quality of people life over the age of 60 (Woolf & Pfleger, 2003). Articular cartilage tissue has a very low self-renewal potential in case of damage due to its characteristic features, such as nerve-free network and avascular structure, and containing a small number of chondrocytes (E. B. Hunziker, 1999; Temenoff & Mikos, 2000). This situation causes damage to the subchondral bone tissue over time, causing osteochondral defects. Because of the low regeneration potential of the cartilage, damages are irreversible and can leads to osteochondral defect.

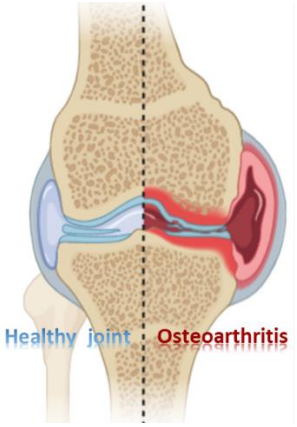

Figure 2. 2 Healthy and damaged osteochondral tissue

2.3 Clinical Treatments for Osteochondral Defects

There are some treatment options against to osteochondral injury such as mosaicplasty, autogenous chondrocytes implantation (ACI) or marrow stimulating techniques, such as multiple drilling or microfracture (Gillogly, Voight, & Blackburn, 1998). However, all techniques have some limitations to treat of cartilage injury. Marrow stimulating techniques result in the formation of fibrocartilage instead of hyaline cartilage (Mitchell & Shepard, 1976; Panseri et al., 2012). Fibrocartilage has different mechanic properties and limited repair capacity. Microfracture technique can be applied to young and middle-age patients, and the size of the defect should be less than 2 square centimeters. Small holes are formed on the subchondral bone part that triggers the stem cells gathering to defect area, then eventually form fibrocartilage tissue at that site. In mosaicplasty, the autologous transfer of the tissue leads to donor site morbidity and there is a limited amount of autogenous tissue (E. B. Hunziker, 2002). End-stage treatment of the osteochondral defect is joint replacement surgery. However, having the limited lifespan of the prosthesis and adverse side effects, such as inflammation decrease the success of the treatment.

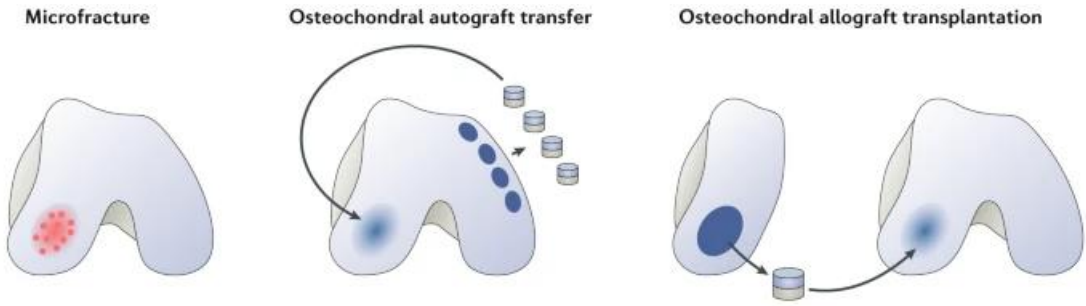

Figure 2. 3 Surgical treatment strategies for osteochondral defects (Kwon et al., 2019)

2.4 Tissue Engineering

Many people in the world experience organ/tissue loss for various reasons and their treatments are tried to provide as autogenic or allogenic tissue/organ transplantation. However, the number of patients awaiting organ/tissue transplantation is increasing day by day due to the limited amount of autologous tissue for transfer, and the limited number of volunteer donors, and the possibility of immune response in allogeneic transfer (Altinörs, 2020). At that point, tissue engineering has been working with increasing importance in recent years, aiming the treatment with an alternative approach for tissue/organ insufficiency.

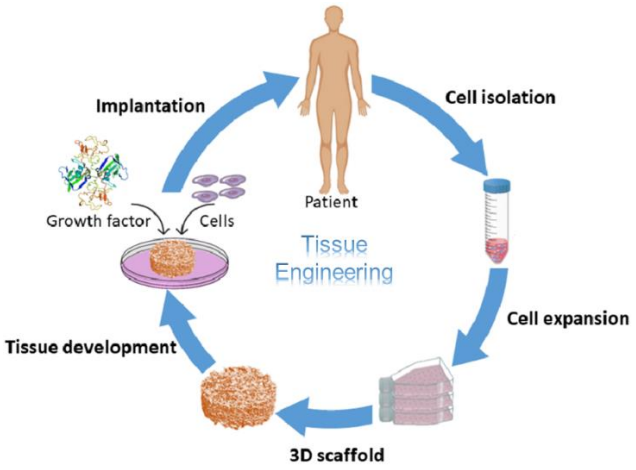

Figure 2. 4 Schematic representation of tissue engineering

Tissue engineering (TE) is the interdisciplinary research field that brings biology, chemistry, engineering, and health science together to generate functional tissues and organs. There are three key ingredients in tissue engineering: cell, biomaterial and

signalling molecule (growth factor). According to the desired tissue's mechanical, morphological, and chemical features, the biomaterial is selected. Again, based on intended tissue, cell source and growth factors, if necessary, are determined. The aim here is to regenerate and heal the tissue by providing an environment that can mimic the natural extracellular matrix of cells.

2.4.1 Osteochondral tissue engineering

Osteochondral tissue engineering includes both cartilage and bone tissue engineering (Martin, Miot, Barbero, Jakob, & Wendt, 2007). Because the natural osteochondral unit has cartilage and bone tissues, intended tissue becomes having specific properties of them (Nukavarapu & Dorcemus, 2013). Cartilage and bone have distinct mechanical, structural, and chemical features. To achieve success, a scaffold should be created, and cells should be selected, taking into account the properties of tissues. The scaffold is the biomaterial-based structure that imitates the native extracellular matrix of the tissues. In osteochondral tissue engineering, having two or more different phases of the scaffold is a factor that increases the success of forming osteochondral unit (Levingstone et al., 2016). The role of the multi-layered collagen-based scaffold in the treatment of in vivo rabbit osteochondral defect was investigated, and the damage has been observed to heal based on macroscopic, microscopic, and histological staining, obtained when compared with the control group (Levingstone et al., 2016). There are many sources in the literature regarding the use of biphasic or multiphasic scaffolds in osteochondral tissue engineering (Bernhardt, Paul, & Gelinsky, 2018; Seo, Mahapatra, Singh, Knowles, & Kim, 2014; Shimomura, Moriguchi, Murawski, Yoshikawa, & Nakamura, 2014; Singh, Moses, Bhunia, Nandi, & Mandal, 2018).

2.4.2 Cells in tissue engineering

Tissue-specific primary cells such as chondrocytes and osteoblasts can be used as the source of cells in cartilage and bone tissue engineering applications. However, stem cells are widely used as an alternative source due to the complexity in the isolation and culture of primary cells. Especially mesenchymal stem cells are frequently preferred, including clinical applications, due to their high proliferation and differentiation capacities.

2.4.2.1 Stem cells

Stem cells are unspecialized, undifferentiated cells having self-renewal and differentiation ability. Life begins with fertilized egg is the type of stem cells called totipotent stem cells. They have ability to form an organism means that totipotent stem cells can differentiate into whole kind of cells even extra embryonic cells. After 4-5 day of fertilization blastocyst occurs. Inner cell mass of blastocyst can be used to isolate another stem cell called pluripotent stem cells or embryonic stem cells (ESCs). They have capacity for differentiation of all kinds of cells inside the mature body. However, they cannot form organism normally, because of the lack of the formation ability of extra embryonic tissues. In order to isolate pluripotent stem cells, blastocyst should be disrupted to take cells from inner cell mass. If no intervention, the blastocyst will develop into the embryo, later, give rise to an organism. Because of that, isolation and use of pluripotent stem cells cause an ethical dilemma.

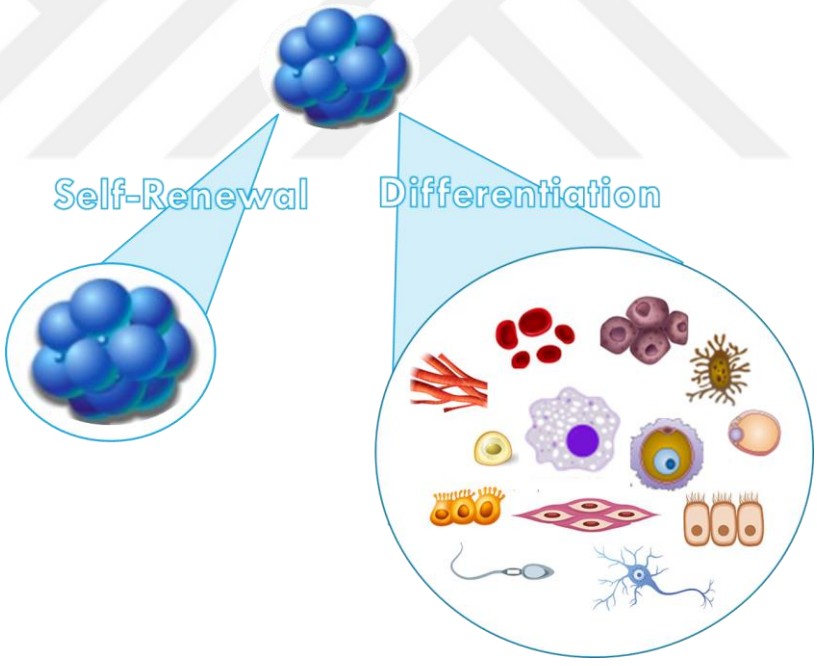

Figure 2. 5 Key features of the stem cells; self-renewal capacity and differentiation potential

An alternative cell source for pluripotent stem cells is induced pluripotent stem cells (IPSCs). John B. Gurdon and Shinya Yamanaka were awarded 2012 Nobel Prize with their discovery of “mature cells can be reprogrammed into pluripotent state”. Specific growth factors: Oct ¾, Klf4, c-Myc and Sox2 called Yamanaka factors introduced

fibroblast cells by viral vectors and changed the transcription profile of the cells then convert mature cells to pluripotent state (Takahashi & Yamanaka, 2006). Since IPSCs do not cause any ethical problems, it can be widely used in regenerative medicine research. However, use of the viral vector in the transfection procedure limits its clinical applicability. Scientists are trying to overcome this problem by working on transferring genes in a different way (Eggenschwiler & Cantz, 2009; C. H. Lee et al., 2011; Okita, Nakagawa, Hyenjong, Ichisaka, & Yamanaka, 2008; H. Y. Park et al., 2012).

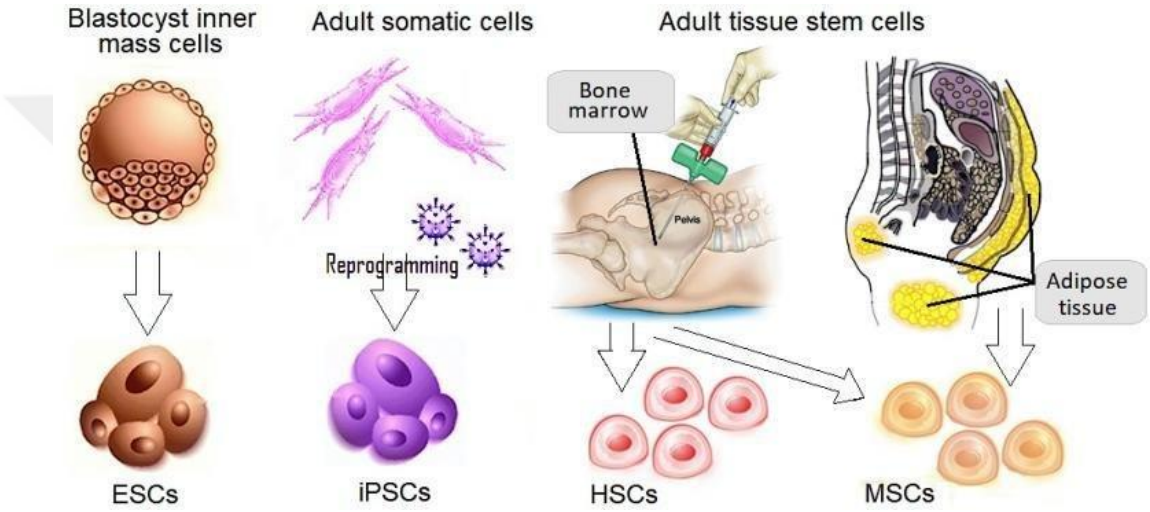

Figure 2. 6 Schematic illustration of stem cells and their sources (Baranova, 2018)

2.4.2.1.1 Adipose-derived stem cells (ASCs)

The isolation of the multipotent adipose-derived stem cells (ASCs) is carried out easily and is obtained a high number of cells due to the abundance of the fat tissue. It has been shown in several studies that these cells are very efficient in terms of proliferation efficiency, and therefore they are suitable cell sources for tissue engineering and cell therapy (Daphne L Hutton et al., 2012; Zuk et al., 2002). In addition, it has been observed that ASCs have higher differentiation efficiency, have higher resistance against apoptosis and have high oncogenic resistance than bone marrow mesenchymal stem cells (Ertaş et al., 2012; Meligy et al., 2012; Varma et al., 2007). ASCs can be obtained in high amounts and efficiency (AL-ASCs) from lipoaspirate which is a surgical waste of abdominal liposuction. It is determined that these cells have the ability to differentiate osteogenic (Hutton, Moore, Gimble, & Grayson, 2013), chondrogenic (L. Wu, Cai, Zhang,

Karperien, & Lin, 2013), vascular (D. L. Hutton et al., 2012), neuronal (Ashjian et al., 2003) and myogenic (Yilgor Huri et al., 2013).

2.4.2.1.2 Infrapatellar fat pad-derived adipose stem cells

Another important source of ASCs, especially for osteochondral tissue regeneration, is the infrapatellar fat pad, IPFP, which is found in the knee. IPFP is a highly vascularized extra synovial tissue located inside the anterior knee compartment. Besides its important role in knee biomechanics, it is a significant stem cell source that helps to heal knee injuries. IPFP-derived adipose stem cells, IPFP-ASCs show higher proliferation and differentiation capacity than other fat-derived stem cells (eg AL-ASCs isolated from abdominal lipoaspirate) (Khan, Adesida, Tew, Longo, & Hardingham, 2012). In addition, these cells show the differentiation capacity that does not decrease with age (Khan et al., 2012). IPFP-ASCs can be isolated from IPFP obtained as surgical waste in total knee replacement surgeries (Doner & Noyes, 2014). These cells demonstrate similar characteristic with mesenchymal stem cells when analyzed by flow cytometry (Wickham, Erickson, Gimble, Vail, & Guilak, 2003), show a chondrogenic, osteogenic and adipogenic differentiation when provided appropriate culture medium (Khan et al., 2012). Also, IPFP-ASCs represent age-independent differentiation potential when compared with other stem cells (Khan, Adesida, Tew, Andrew, & Hardingham, 2009; Mochizuki et al., 2006). The use of IPFP-ASC cells as a cell source in tissue engineering has not been studied in detail.

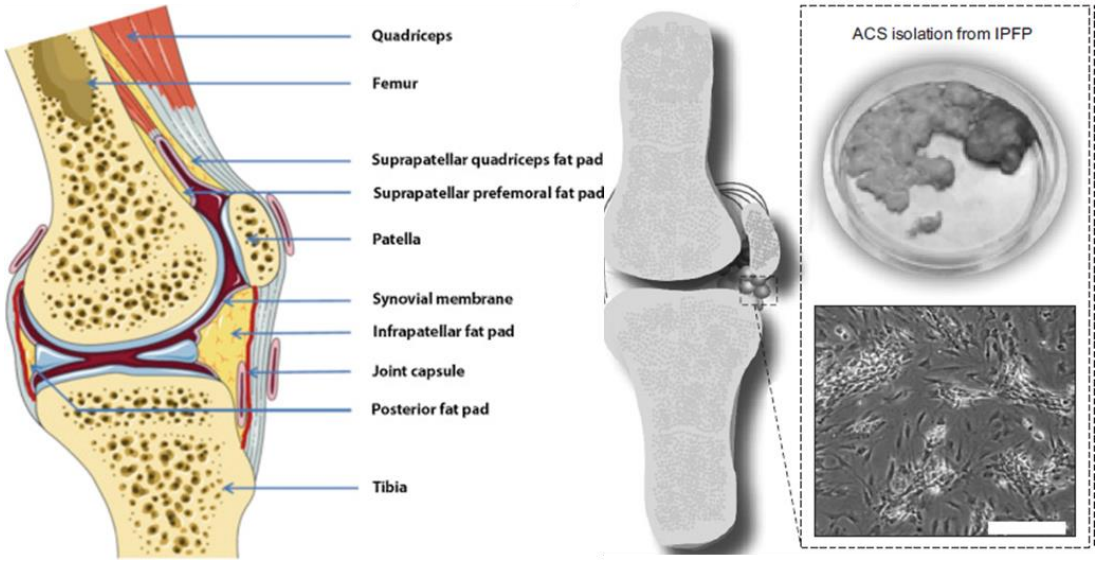

Figure 2. 7 The location of the infrapatellar fat pad (IPFP); ASCs isolated from IPFP (Huri, Hamsici, Ergene, Huri, & Doral, 2018)

Since IPFP is generally used as a surgical waste during the knee arthroplasty procedure of osteoarthritis patients the effect of the pathology on the differentiation of IPFP-ASCs was investigated in literature (Y. Liu, Buckley, Almeida, Mulhall, & Kelly, 2014). IPFP-ASC cells obtained from healthy donors by biopsy and IPFP-ASCs obtained from osteoarthritis patients were examined in terms of chondrogenic differentiation capacities and no significant change was observed. It was observed that the expression of specific genes that are responsible for chondrogenic and osteogenic differentiation have more activity according to the real-time polymerase chain reaction, in IPFP-ASCs when compared with AL-ASCs (Tangchitphisut et al., 2016). In addition, IPFP-ASC cells have been shown to have high chondrogenic (Buckley et al., 2010; Ye et al., 2014) and osteogenic differentiation ability in other studies (Tangchitphisut et al., 2016).

In the literature where IPFP-ASC cells were investigated with a tissue engineering approach, the chitosan scaffold was created by 3D printing and cartilage tissue formation was observed with the induction of TGF-β and BMP-6 (Felimban et al., 2014). Chondrogenic differentiation potential of IPFP-ASCs in poly (L-lactic acid-co-ε-caprolactone) scaffold was observed by 3D printing (Jurgens et al., 2009). In addition, fibrin hydrogel was used as a scaffold with the controlled release of the TGF-β1, and the chondrogenic potential of the IPFP-ASCs was examined (Ahearne, Buckley, & Kelly, 2011). In a pioneering study, IPFP-ASCs were shown to exhibit chondrogenic

differentiation with the use of chondrogenic culture medium and osteogenic differentiation with the use of BMP-2, in fibrin gels (Dragoo et al., 2003).

2.4.3 Biomaterials

Materials can be used in biological systems called biomaterials. They are used in medical applications to repair, regenerate and/or create tissues. Biomaterial that will be selected, should be decided based on the properties of the desired tissue. For a material to become a biomaterial, it must be in the body or on the surface of the body or contact with body fluids, and should treat, correct, or heal a disease, disorder or abnormality (Ratner, Hoffman, Schoen, & Lemons, 2004). Biomaterials must have some basic properties to be used in the body. For example, the biomaterials should be biodegradable, they should be degraded after a period of time remaining in the body. Products resulting from this degradation should not have a toxic effect for the body. In addition, the biomaterials must be biocompatible, they should not cause any undesirable conditions, for example, infection, chronic inflammation, or any carcinogenicity (J. Park & Lakes, 2007). In addition, biomaterials should have similar surface and mechanical properties, considering the natural properties of the desired tissue. Biomaterials' chemical and mechanical properties, surface structure, and interactions with protein and cells are the main criteria to choose them in the specific applications. In order to create the scaffold and use it in a living organism, it must be suitable for sterilization and fabrication.

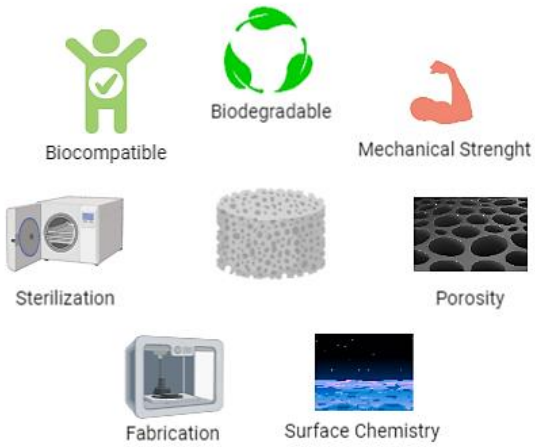

Figure 2. 8 Main requirements of biomaterials

Biomaterials are classified into three groups, metals, polymers and ceramics. Considering the advantages and disadvantages of them, polymers are highly utilized in tissue engineering applications than others. Because the metals are strong, they generally used in orthopaedic and dental applications. For example, titanium alloy is used for joint prostheses in the clinic. Ceramics are hard and quite brittle. They can be used in bone and dental applications. They have more resistance to degradation than metals. Due to their chemical and physical properties, polymers have wide applications areas such as contact lens vascular graft, suture, and artificial heart valves. Polymers classified into two main groups, synthetics, and natural polymers. Natural polymers are materials that consist of protein, polysaccharide, or extracellular matrix isolated from animals or plants (Ha, Quan, & Vu, 2013). They are non-toxic, biocompatible, biodegradable, and easy availability increases their usage in tissue engineering (KulkarniVishakha, ButteKishor, Sudha, & Mumbai, 2012). However, the fabrication and mechanical strength of natural polymers are limited. They include collagen, silk, starch, alginic acid, chitosan (chitosan); synthetic polymers include polylactic acid (PLA), polyglycolic acid (PGA), polycaprolactone (PCL) and polyurethane (PU) (Demirbag, Huri, Kose, Buyuksungur, & Hasirci, 2011). Synthetic polymers are biomaterials consisting of repeating units formed by chemical reactions in the laboratory environment (Reddy, Ponnamma, Choudhary, & Sadasivuni, 2021). The advantage of synthetic polymers is that they can be produced constantly with high quality and purity (Hacker, Krieghoff, & Mikos, 2019). Further, they are mechanically more durable than natural polymers. They have ability to tailor mechanical and degradation properties (Gunatillake & Adhikari, 2003). For this reason, their fabrications are carried out more easily, even if a complex structure is desired to be created. However, their usage is limited because of their poor biocompatibility and acidity of degradation products (Gunatillake & Adhikari, 2003).

2.4.3.1 Hydrogels

Hydrogels are cross-linkable polymers that contain hydrophilic polymer chains and plenty of water in their structures. They can take the gel form with chemical or physical crosslinking of hydrophilic polymer chains of them (Hennink & van Nostrum, 2002). They are naturally found in the extracellular matrix so; hydrogels are considered biocompatible. However, they have low mechanical strength and high degradation

profile. When crosslinking occurs, hydrogels become more stable form. The similarity with the natural extracellular matrix, their good biocompatibility, enabling cell and/or growth factors to embedded, and providing microenvironments for cell adhesion and proliferation enhance hydrogels usage in tissue engineering (K. Y. Lee & Mooney, 2001). Natural hydrogels are; collagen, gelatin, fibrin, alginate, agarose, and cellulose; synthetic hydrogels include poly(acrylic acid), poly(ethylene oxide), and their derivatives, poly(vinyl alcohol), and polypeptides (K. Y. Lee & Mooney, 2001).

2.4.4 Scaffold fabrications techniques

The scaffold fabrication method is of great importance, as well as the importance of biomaterial selection for tissue engineering. The attachment, proliferation, orientation, and differentiation of cells can vary depending on the geometry, shape, and porosity of the scaffold (Yilgor Huri et al., 2013). For this reason, different scaffold manufacturing methods have been developed. In traditional methods such as freeze-drying, solvent casting, and particle leaching, gas foaming, and thermally induced phase separation, the architecture and pore size of the scaffold cannot be produced in a fully controllable way (Subia, Kundu, & Kundu, 2010). Even though the electrospinning and wet-spinning techniques give slightly better results, again the architecture of the scaffold cannot be fully controlled. At this point, 3D printing technology has become an alternative option for creating scaffolds.

Table 2. 1 Hydrogels in tissue engineering, their crosslinker, specific applications, cell types and fabrication methods

Hydrogel	Crosslinker	Application	Cell	Fabrication	References
Agarose-Polydopamine (APG)	-	Skin Tissue Engineering	MRC-5, NIH3T3, and DPSC	Heating and Cooling	(Su et al., 2021)
N-Pentenyl Chitosan (PTL-CS)	UV Light (360-480 Nm)	Tissue Engineering	hMSCs	Freeze-Drying	(Ding et al., 2021)
Fibrin Alginate Dialdehyde (ADA) Gelatin	Thrombin	Liver Tissue Engineering	HepG2	Molding	(Rajalekshmi, Kaladevi Shaji, Joseph, & Bhatt, 2021)
Collagen	Genipin	Vascular Tissue Engineering	HepG2	Molding	(Justin et al., 2021)
Cellulose Chitosan	-	Bone Tissue Engineering	MC3T3-E1	Molding	(Maharjan et al., 2021)
Alginate Dialdehyde (ADA) Gelatin	-	Meniscus Tissue Engineering	Fibrochondrocytes	Molding	(Resmi, Parvathy, John, & Joseph, 2020)
Alginate-Methylcellulose (AlgMc)	100Mm $CaCl_2$	Osteochondral Tissue Engineering	hCh	3D Printing	(Kilian et al., 2020)

Table 2. 1 Hydrogels in tissue engineering, their crosslinker, specific applications, cell types and fabrication methods (continued)

Fibrinogen Collagen Type-I	EDC/NHS (1-Ethyl-3-(3–Dimethylaminopropyl) Carbo-Diimide/N-Hydroxysuccinimide)	Soft Tissue Engineering	C2C12	Freeze-Drying	(Shepherd, Bax, Best, & Cameron, 2017)
Gellan Gum (GG)	Bioamine	Neural Tissue Engineering	hIPSCs, hESCs	Molding	(Koivisto et al., 2017)
GelMa	UV Light (360-480 Nm)	Epidermal Tissue Engineering	HaCaT	Molding	(Zhao et al., 2016)
Alginate Gelatin Collagen	3% Calcium Chloride Solution	Tissue Engineering	HCEpC	3D Printing	(Z. Wu et al., 2016)
Chitosan and Gelatin	Glutaraldehyde	Liver Tissue Engineering	Hepatocytes	Stereolithography	(Jiankang et al., 2009)

MRC-5: Human fetal lung fibroblast; NIH/3T3: Mouse embryonic fibroblasts; DPSC: Dental pulp stem cells; HepG2: Human liver cancer cell; hMSCs: Human mesenchymal stem cells; MC3T3-E1: Mouse calvaria pre-osteoblast; hCh: Human chondrocytes; C2C12: Mouse myoblast cell line; hESCs: Human embryonic stem cells; hIPSCs: Human-induced pluripotent stem cells; HaCaT: Human immortalized keratinocyte; HCEpC: Human corneal epithelial cells

2.4.4.1 3D printing

3D printing, also referred to as additive manufacturing (AM), creates objects through layer-by-layer deposition based on the data from computer-aided design (CAD). It can be enabled to form objects in a reproducible manner with exactly the same architecture, size, and porosity as the intended structure. Biomedical applications of 3D printing technology, which has been utilized in various fields since the 1980s (Conner et al., 2014), have gained momentum in recent years (Tack, Victor, Gemmel, & Annemans, 2016). It is used in clinical applications in creating prosthetics and implants, preparing surgical models, surgical guides, and surgical planning materials (Yılgör Huri Et al., 2019). According to the magnetic resonance imaging (MRI) or computerized tomography (CT), scaffolds can be produced that can exactly match the damaged area. There are different technologies to fabricate 3-dimensional objects such as stereolithography (SLA), selective laser sintering (SLS), and fused deposition modeling (FDM). All methods have different working principles, but they aim to form objects based on digital images even if they have high complexity. Stereolithography or SLA, works with the laser system. There is a UV-cross-linkable photopolymer resin which is located bottom part. Laser head travels through the resin according to the computer data allowing to crosslink resin which produce object. Selective laser sintering or SLS, is the way to combine powder photopolymer with a laser system form 3 dimensional objects due to computational data. Powders are sintered with the high-power laser head. Both methods create objects in layer-by-layer manner. Fused deposition modelling or FDM, is the easy and often preferred 3D printing technology in which the filaments or biomaterials are melted with heat, or extruded high pressure to produce 3-dimensional objects according to the digital images. FDM can be applied in the production of customized graft in exactly the same shape as the defected site of the body. Metallic orthopaedic implants can be obtained easily by FDM with the desired shape. FDM is also frequently used in tissue engineering.

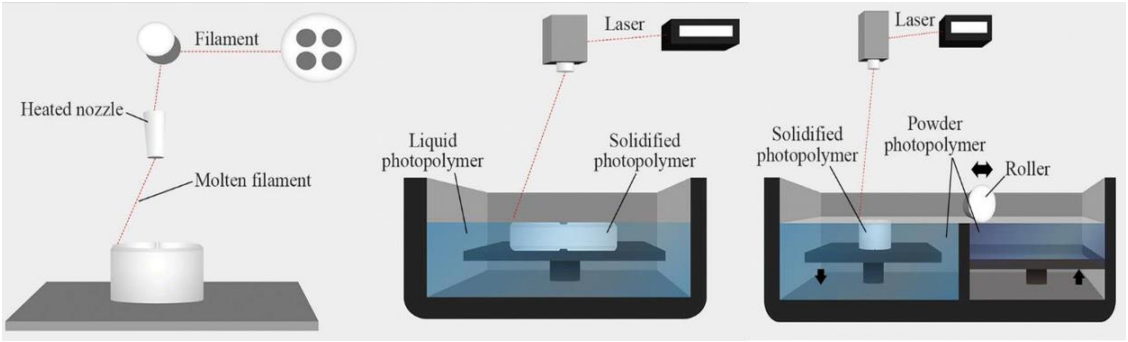

Figure 2. 9 Different kinds of printers; Fused Deposition Modelling (FDM), Stereolithography (SLA), and Selective Laser Sintering (SLS) (B. J. Park et al., 2019)

In tissue engineering, 3D printing can be applied with a cell-free or cell-containing biomaterial (bio-inks). The selected biomaterial as cell-containing or cell-free emerge from the syringe tip, form a filament, and construct scaffold by stacked in a layer-by-layer manner. In cell-free carriers, cells can be seeded later, however they cannot be effectively distributed. In cell-laden scaffold preparation, better cell distribution and proliferation are observed, and grafts that are more suitable for imitation of the natural tissue can be formed. 3D printers are used in the fields of bone (Kajave, Schmitt, Nguyen, Gaharwar, & Kishore, 2020), cartilage (Messaoudi et al., 2021), tendon (Bianchi et al., 2021), vascular (Savoji et al., 2020), cardiac (N. Liu et al., 2021), lung and tracheal (Mahfouzi, Safiabadi Tali, & Amoabediny, 2021) tissue engineering. Also, studies about 3D printing in osteochondral tissue engineering are compiled in the Table 2.2.

Table 2. 2 Osteochondral tissue engineering applications of 3D printing

Biomaterials	Cells	Structure of the Scaffold	Outcomes	References
Platelet-rich plasma (PRP)-Gelatin methacryloyl (GelMa)	Bone marrow mesenchymal stem cells (BMSCs)		The addition of PRP to GelMa was enhanced the osteochondral potential of the 3D printed scaffold when compared with pure GelMa hydrogel.	(Jiang et al., 2021)
Cartilage: alginate-methylcellulose (algMC) Calcified cartilage: algMC and calcium phosphate cement (CPC) Bone: CPC	Human chondrocytes (hCh)	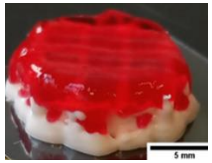	3D bioprinting of the novel multi-layered scaffold was carried out, and scaffold mineralization and chondrogenesis were observed after 3 weeks of culturing.	(Kilian et al., 2020)
Cartilage: sodium alginate and gelatin Bone: sodium alginate, gelatin, and hydroxyapatite (HA)	Rabbit BMSCs* *Cells were differentiated before printing	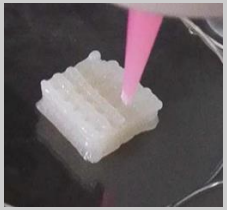	in vivo articular cartilage repair in the rabbit knee was observed according to the histological and biomechanical results.	(Y. Yang et al., 2020)
Cartilage: Silk fibroin and polyvinylpyrrolidone (PVP) Bone: Silk fibroin, PVP and nHA with doped or non-doped (Sr)	Porcine adipose derived stem cells (pASCs) *Cells were differentiated before printing		The incorporation of strontium doped nano-apatites with 3D printed silk-based scaffold was increased the osteochondral repair capacity.	(Moses, Saha, & Mandal, 2020)

Table 2. 2 Osteochondral tissue engineering applications of 3D printing (Continued)

Cartilage: decellularized bovine limbs Bone: Polylactic-co-glycolic acid (PLGA), and b-tricalcium phosphate (b-TCP)	Bovine Mesenchymal stem cells (MSCs)		3D printed multiphasic dECM, PLGA and b-TCP scaffold provided a suitable environment for the attachment of cells and showed the combination of alternative biomaterials that can be used in osteochondral tissue engineering.	(Z. Li et al., 2018)
Polycaprolactone (PCL) -HA	Co-culture of rabbit umbilical cord blood mesenchymal stem cells (UCB-MSCs) and chondrocytes		in vivo repair potential of the cell-seeded 3-D printed PCL-HA scaffolds was represented better results than non-seeded scaffold on the rabbit osteochondral defect.	(Zheng, Hu, Lou, & Tang, 2019)

2.4.5 Growth factors

Growth factors are biologically active molecules that regulate cellular events such as survival of the cell, proliferation, differentiation, inflammation. They are expressed based on the gene sequences and act as the ligand to bind to specific receptors, then start the cellular events with signalling pathways. Growth factors should be used, as they are critical for the induction of cellular differentiation.

Various growth factors are used to induce the differentiation of stem cells in tissue engineering applications. Depending on the tissue to be created and the cell source to be used, growth factors may be different and, affect the proliferation and differentiation of the cells. In order to achieve the desired tissue, suitable growth factor(s) must be added.

Growth factors can be directly distributed into the scaffold as well as carrier structures can also be used. They can be released with the help of the loaded- polymeric micro or nano capsules, polysaccharide- or lipid-based structures. They can lose their activity over time due to environmental and physical changes when directly distributed into the cell environment. Also, they have a short half-life, which means that the effect of them decreases rapidly (Caballero Aguilar, Silva, & Moulton, 2019). In addition, exposure to high doses leads toxic effects, while using low doses causes not reaching the desired goal (Z. Wang et al., 2017). Therefore, it is important to ensure controlled releases using a carrier system in order to achieve successful results.

Transforming growth factor beta-3 (TGF-β3) is the sub-member of the TGF-β superfamily that has a high ability to chondrogenesis (Augustyniak, Trzeciak, Richter, Kaczmarczyk, & Suchorska, 2015; Mueller et al., 2010). Also, bone morphogenetic proteins-2 (BMP-2) is a member of the BMP-2 family that plays a role in osteogenesis (J. Yang et al., 2014). There are studies in the literature that stimulate bone and cartilage tissue differentiation using BMP-2 and TGF-β in osteochondral tissue engineering (Mohan et al., 2011; Saha et al., 2013; Z. Wang et al., 2017).

2.5 Scope and Novelty of the Study

It is aimed to produce osteochondral tissue that contains a single cell source and osteochondral differentiation is achieved by local induction. It is intended to analyze the use of IPFP-ASCs in the production of osteochondral grafts in comparison with AL-ASC cells. Differentiation potential of IPFP- and AL-ASCs isolated from two different patient populations, young and mature was evaluated with Alizarin Red and Alcian Blue staining. It is aimed to produce osteochondral grafts having two distinct parts in the bone section cells were printed with alginate/ gelatin/ carboxymethylcellulose (CMC)/ HA bioinks, and in the cartilage part of the graft were prepared with alginate/gelatin/CMC bioinks. The osteogenic and chondrogenic differentiation of cells were induced by the controlled release of site-specific growth factors. PCL capsules loaded with BMP-2 and TGF-β were utilized to site specific differentiation induction. Osteogenic and chondrogenic differentiation of cells in the osteochondral graft were examined.

There is no study in the literature regarding the application of IPFP-ASC cells, which have an important potential to be excellent cell source for cell therapy and tissue engineering applications due to their age-independent proliferation and differentiation ability, in bilayered osteochondral scaffold with 3D bioprinting. Also, the osteogenic and chondrogenic differentiation potential of IPFP-ASC and AL-ASC cells in osteochondral grafts, which were created by 3D bioprinting, were compared for the first time.

3. MATERIAL AND METHODS

3.1 Materials

Based on the ethics committee approval of Ankara University Faculty of Medicine Clinical Research Ethics Committee dated 28 January 2019 and numbered 02-115-19, adipose-derived stem cells were isolated from lipoaspirate and infrapatellar fat pad. Liposuction surgery was performed by Assoc. Dr. Burak Kaya at Ankara University Plastic, Reconstructive, and Aesthetic Surgery. The infrapatellar fat pad was provided by Prof Dr. Gazi Huri member of the Hacettepe University Orthopedics and Traumatology faculty. Adipose-derived stem cells were isolated from these fat tissues and, cells were grown by culturing.

Fetal bovine serum (FBS) (Biological Industries penicillin streptomycin (P/S) (Biological Industries), fibroblast growth factor-2 (FGF-2) (Sigma-Aldrich) in Dulbecco's Modified Eagle Medium (DMEM) (high glucose) (Biological Industries) was used as the extension media for adipose-derived stem cells. The media used for the induction of chondrogenic differentiation are as follows; FBS, P/S, ITS Universal Culture Supplement Premix (Corning), dexamethasone (Merck), sodium pyruvate (Serva), L-ascorbic acid-2-phosphate (Serva), proline (Serva) in high glucose DMEM.

FBS, P/S, β-glycerophosphate (Serva), dexamethason, L-ascorbic acid-2-phosphate in low glucose DMEM (Biological Industries) were used as osteogenic media.

Other chemicals used in cell culture are as follows, Trypsin (Biological Industries), Dimethyl Sulfoxide (DMSO) (Sigma-Aldrich), Triton X100 (Merck).

Cell viability was determined by the Alamar Blue test (Thermo Fisher). In addition to cell viability, fluorescence staining DAPI/Alexa Fluor™ 488 Phalloidin (Thermo Fisher), staining the nucleus and actin filament, and Live/Dead™ Viability/Cytotoxicity Kit (Thermo Fisher) was applied. Alcian Blue (Sigma) was used to determine the chondrogenic differentiation of the cells, and Alizarin red (Sigma) was used to determine the osteogenic differentiation. Paraformaldehyde (PFA) (Merck) was used to fix the fluorescent staining samples.

The materials used in the production of scaffold are as follows; Alginate (Sigma, USA), gelatin (Merck), carboxymethyl cellulose (Sigma), methacrylate gelatin (Collagen). Autoclaved water was used as solvent. $CaCl_2$ (Sigma, USA) was used as the crosslink agent after 3D printing.

Polycaprolactone (PCL) (Perstorp AB), bovine serum albumin (BSA) (Sigma-Aldrich), polyvinyl alcohol (PVA) (Sigma Aldrich), dichloromethane (DCM) (Sigma Aldrich), Trizma base (Merck), recombinant human BMP-2 (BioLegend), and recombinant human TGF-β (BioLegend) were used during capsule formation steps. For the determination of release kinetics, Coomassie (Bradford) Protein Assay Kit (Thermo Fisher) was utilized.

3.2 Cell Isolation

3.2.1 IPFP-ASC isolation

After the knee replacement surgery performed by Hacettepe University Orthopedics and Traumatology faculty member Assoc. Dr. Gazi Huri, normally discarded IPFP was taken under sterile conditions and it was brought to Biomedical Engineering Department Laboratories at Ankara University (Ethics committee approval was obtained, in appendix 4). For isolation, IPFP was provided from two different patient populations, 25-40 and 50-65 years old. After mechanical and enzymatic fragmentation, cells were grown in culture medium containing 10% fetal bovine serum (FBS), 1% penicillin/streptomycin (P/S), 1 ng/mL FGF-2 in high glucose DMEM. 24-48 hours, the medium in the flask was replaced with a new one and the media change repeated every two days until the cells are 80-90% confluent. Finally, the cells were separated from flasks by tripinizing and stored in a liquid nitrogen tank in a freezing solution containing 10% DMSO, 50% DMEM and 40% FBS (D. L. Hutton et al., 2012; Yilgor Huri et al., 2013).

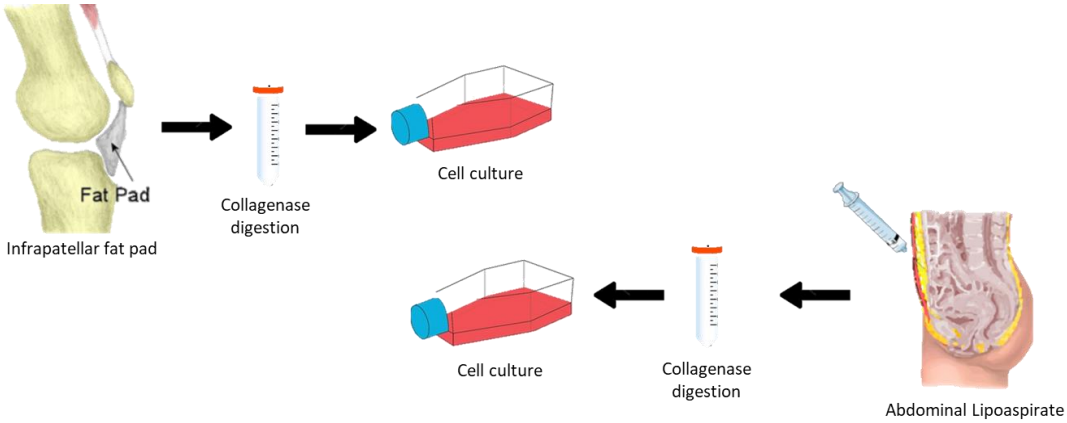

Figure 3. 1 Schematic illustration of the isolation of IPFP- and AL-ASCs

3.2.2 AL-ASC isolation

After the liposuction surgery performed by Ankara University Plastic, Reconstructive, and Aesthetic Surgery faculty member Assoc. Burak Kaya, normally discarded lipoaspirate was taken under sterile conditions and it was brought to Biomedical Engineering Department Laboratories at Ankara University (Ethics committee approval was obtained; in appendix 4). For isolation, lipoaspirate was provided from two different patient populations, 25-40 years old and 50-65 years old. Following the enzymatic breakup, cell isolation was performed as described above (Section 3.2.1).

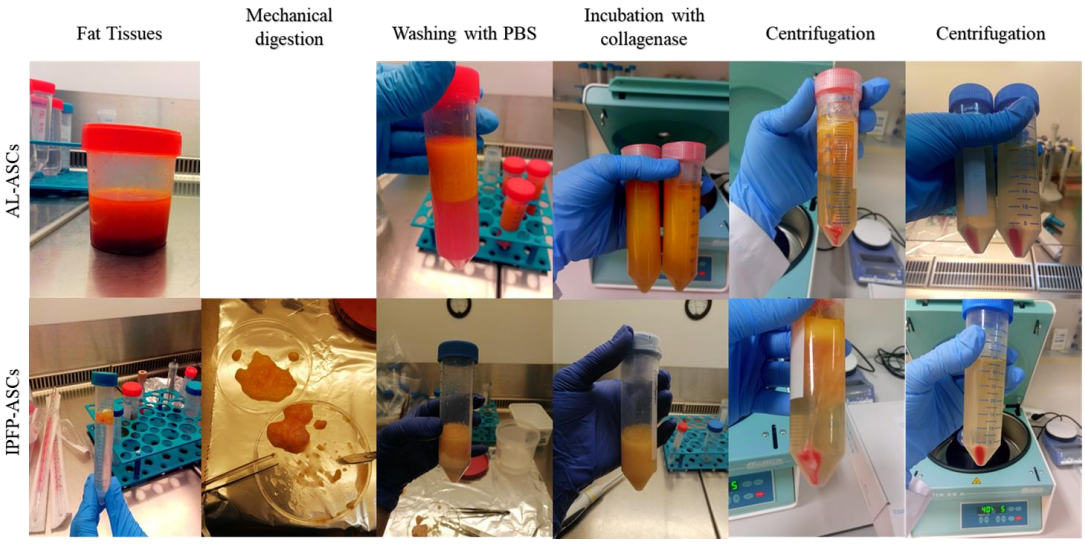

Figure 3. 2 Step-by-step isolation of adipose-derived stem cells

3.3 Characterization of Cells

3.3.1 Flow cytometry

Flow cytometry was performed to prove that the cells isolated from the infrapatellar fat pad and abdominal lipoaspirate were mesenchymal stem cells. Cells (P-3) were stained with Alexa Fluor 488 labelled antibodies specific for isotype control CD31, CD73, and CD105 surface markers. Mouse IgG1κ antibodies were utilized to define potential non-specific binding that cells may show against the mouse antibodies used. Analyses were performed using the BD AccuriC6 Flow Cytometer device. The results obtained will be evaluated by comparison with the signal acquired from unstained cells. Cells that give positive signals to more than 50% of the population were evaluated as positive for that surface marker.

3.3.2 Cell viability/ Alamar Blue assay

The number of viable cells were determined by the Alamar Blue cell viability test. The feature of this test is that metabolic activity can be determined without affecting cell viability and metabolism. The medium was discarded from the well plate where the cells found. Cells were washed with PBS, then a 10% concentration of Alamar Blue solution prepared with colorless DMEM was incubated with the cells. One-hour incubation protected from light in 37°C and 5% CO_2 conditions was carried out. Then, the dye solution from the well plate where the cells found was taken and absorbance values were measured at 570 and 595 nm wavelengths in a microplate reader. After measurement, cells were washed with PBS, and culture medium was added to continue to cell growth. Cell viability was determined by repeating this test on days 1, 7, 14, and 21 of the culture. The reduction amount determined by the absorbance values of the Alamar Blue dye was converted to the number of live cells based on calibration curve (in appendix 1-2).

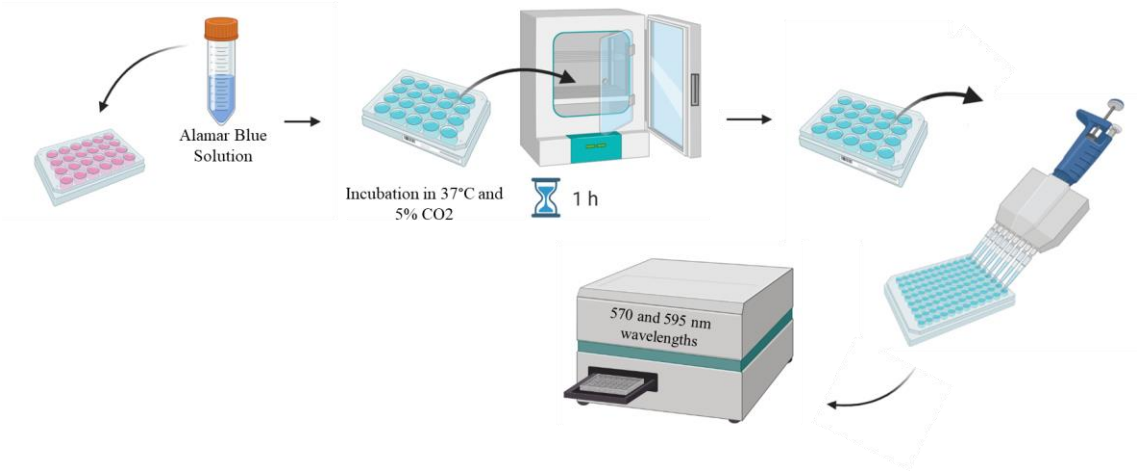

Figure 3. 3 Schematic representation of Alamar Blue Assay

3.3.3 DAPI/Phalloidin staining

Evaluation of the F-actin distribution within the cells was done with phalloidin staining. On days 1, 7, 14, and 21, the medium was disposed from the well plate where cells were found and washed with PBS. Cells were fixed with 3.7% paraformaldehyde (PFA) for 30 min. After washing with PBS, Triton-1X was added for the permeabilization of the cell membrane and kept for 5 minutes. Then, PBS washing was applied, and BSA at a concentration of 1% (w/v) was added and kept for 15 minutes. After removing BSA, Phalloidin dye (1:200) was added to the samples and incubated for 1 hour at 37°C protected from light. Afterward, washing with PBS was done and DAPI dye (1:1000) was added to label cell nuclei and it was kept for 10 minutes at room temperature. The dye was removed, the samples were washed with PBS. Imaging was performed with a fluorescent microscope. The values excitation/emission for Phalloidin; 495/518 nm for DAPI: 340/488 nm.

3.4 Differentiation Studies

3.4.1 Chondrogenic induction

In order to induce chondrogenic differentiation on monolayer, adipose-derived stem cells were cultured containing 10% FBS, 1% P/S, 1% ITS Universal Culture Supplement

Premix Corning, 10^{-7} M dexamethasone, 100 μg/ml sodium pyruvate, 50 μg/ml L-ascorbic acid-2-phosphate, 40 μg/ml proline in high glucose DMEM (Sasaki et al., 2018).

3.4.2 Alcian Blue staining

Alcian blue was carried out to observe the chondrogenic potential of the cells. It detects the presence of glycoproteins; sulfated and carboxylated polysaccharides. Alcian Blue dye was added to the fixed samples and incubated for 30 minutes. At the end of the period, washing with PBS was done. This process was continued until the liquid became clear. Samples were examined with a light microscope. Samples with blue intensity will indicate higher chondrogenic differentiation (J. Y. Park et al., 2014).

3.4.3 Osteogenic induction

For osteogenic differentiation on monolayer, adipose-derived stem cells were cultured containing 10% FBS, 1% P/S, 10 mM β-glycerophosphate, 10^{-7} M dexamethasone, 50 μM L-ascorbic acid-2-phosphate in low glucose DMEM (Temple et al., 2014).

3.4.4 Alizarin Red staining

Alizarin Red staining was carried out to investigate the osteogenic differentiation potential of the cells. It stains calcium and carbonate minerals. Alizarin red dye was added to the fixed samples and after 30 minutes of incubation, the dye was removed and washed with PBS. This process was continued until the liquid became clear. Samples were examined with a light microscope. The resulting red color intensity and the high number of dark spots indicate mineral accumulation and hence higher osteogenic differentiation (Zhang et al., 2018).

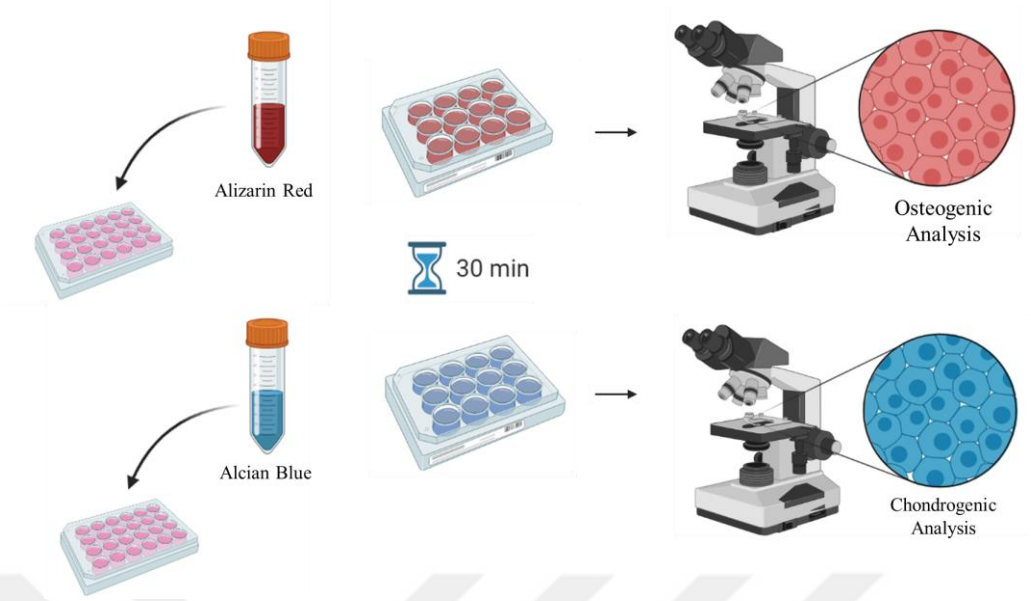

Figure 3. 4 Detection of the chondrogenesis and osteogenesis with Alcian Blue and Alizarin Red staining, respectively

3.5 BMP-2 and TGF-β Encapsulation with PCL Capsules

Capsules were prepared using the double emulsion method to achieve the controlled release of growth factors (Pinar Yilgor, Tuzlakoglu, Reis, Hasirci, & Hasirci, 2009). For this, polycaprolactone (PCL) (5%, 10%, and 20%) was used to create capsules (M_w=37000 g/mol). First, the model protein bovine serum albumin (BSA) or growth factors TGF-β and BMP-2 were dissolved in distilled water, and probe sonication was performed (8 W for 60 s) by adding it into PCL dissolved in dichloromethane (DCM). The prepared solution was added to 4% polyvinyl alcohol (PVA) and sonicated again. Then the solution was transferred into 0.3% PVA and kept overnight on the stirrer. After evaporation of the solvent, washing with Tris-HCL (pH 7.4) solution was performed and then solution was poured into a petri dish and freeze-dried to collect the capsules (Figure 3.5).

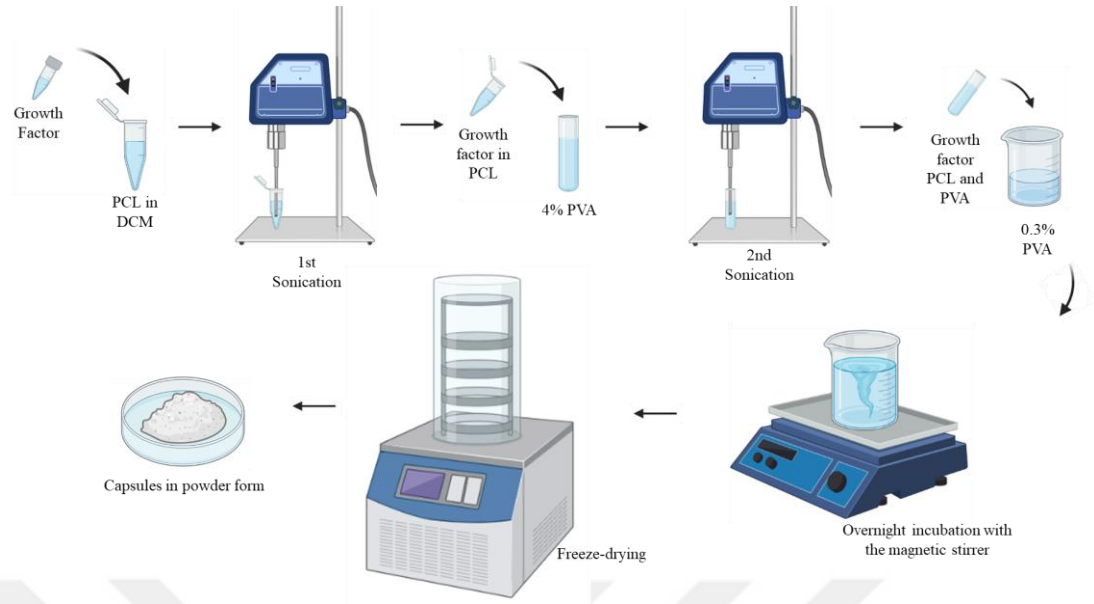

Figure 3. 5 Production of growth factor encapsulation with PCL

3.5.1 SEM morphological examination of capsules

SEM imaging was performed to investigate morphological and structural features of capsules at METU Central Laboratory. Prepared capsules were washed with distilled water to get rid of salt crystals and possible contamination. SEM images were taken after overnight drying and coating with the gold-palladium conductor.

3.5.2 Encapsulation efficiency

5%, 10%, and 20% PCL carriers were evaluated based on their efficiency. For this, 5 mg of capsules prepared in different concentrations were taken and transferred to glass test tubes, and DCM added to them. After the capsules were dissolved in DCM, the same amount of distilled water was added to the test tubes and vortexed for 60 seconds. After the vortex, a period of time waited for phase separation to occur. The water phase was collected from the tubes and the protein concentration was determined according to the Bradford Assay protocol.

3.5.3 Release kinetics of capsules

Determination of release kinetics from PCL capsules was performed using BSA as the model protein (Pinar Yilgor et al., 2009). 5mg of capsules containing BSA was taken into

eppendorf tubes and incubated at 37°C in 1 mL of PBS (pH 7.4). At various incubation times (1, 3, 7, 14, and 21 days), samples were centrifuged to collect the supernatant, and the incubation was continued by adding fresh PBS in eppendorf tubes. BSA determination in the supernatant was performed by the Bradford assay. Accordingly, 150 µL of the supernatant sample was taken into a 96-well culture dish and 150 µL of Bradford solution was added on it (Coomassie Plus Bradford Assay; Pierce, USA). The change in wavelength created by the Coomassie dye-binding with protein was determined by absorbance reading at 595 nm with the micro-plate reader at the end of a 10-minute incubation period. The correlation between absorbance and protein concentration was calculated based on the Beer-Lambert equation.

The Beer-Lambert equation;

$$A = \varepsilon L C$$

A; absorbance at 595 nm,

L; optical length (equation constant),

Ɛ; being the molar absorption coefficient (come from the calibration curve).

The determination of the release kinetics of the capsules embedded in the scaffold was similarly examined. It was aimed to print scaffolds containing 5 mg BSA loaded capsule per scaffold. The effect of hydrogel structure on growth factor release was investigated (n=4).

3.6 Optimization of 3D Printed Osteochondral Scaffold

The osteochondral scaffold having bi-layer, cartilage, and subchondral bone, was designed (Figure 3.6). The internal designs of the subchondral bone and cartilage parts of the graft were prepared differently to imitate native bone and cartilage. Before deciding on the hydrogel concentration used, optimization studies were carried out first.

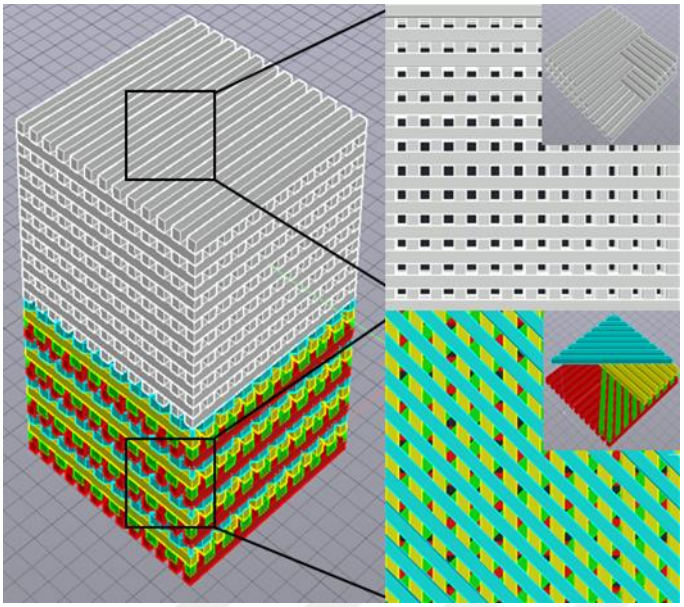

Figure 3. 6 CAD design of bi-layered osteochondral scaffold

Printing parameters such as pressure and speed were also tested to gain successful print. After optimization studies, the concentration of hydrogels to be used was determined. HA, which is added to the bio-ink in the bone part of the graft, was used for its osteoinductive effect and its contribution increase mechanical strength.

The hydrogels were dissolved in sterile distilled water at 50°C and loaded into the syringe, and 3D printing was performed with a low-temperature print head with 3D bioplotter device (Envisiontec GmbH, Germany). Crosslinking of alginate was achieved by treatment with 0.5M $CaCl_2$ after printing. With the use of single-cell source osteochondral printing was performed (additional HA in the bone part).

Table 3. 1 Optimization values for hydrogel concentration

Hydrogels in different concentrations tested for 3D printing		
Alginate	Carboxymethyl cellulose	Gelatin
3%	9% medium viscous	-
	9% high viscous	-
		5%
		10%
5%	4% medium viscous	-
	4% high viscous	-

For the bioactive cell-laden scaffold bioprinting, the bioink prepared with Alginate/GelMa were printed with an Axolotl Biosystems 3D bioprinter. Before printing, GelMa prepared with triethanolamine (TEA) and N-vinyl-2-pyrrolidinone (V-2-P) and autoclaved water. After that Eosin Y was added to the solution to complete GelMa modification. Then alginate was added to GelMa solution to form bioink. Alginate was crosslinked with 0.5M CaCl2, while GelMa was crosslinked with blue light (380-500 nm) exposure for 10 seconds.

3.6.1 Characterization studies for scaffold

3.6.1.1 Compression test

The mechanical properties of the printed scaffolds were evaluated with the compression test. After the scaffolds were printed, they were kept in PBS until the compression test was started. In the test applied to compare the mechanical strength of different hydrogel combinations, the linear pre-load was set as 50kN and the compression speed as 200µm / min. 3 samples were tested for each experimental group. Images of a sample taken during the compression test are presented (Figure 3.7).

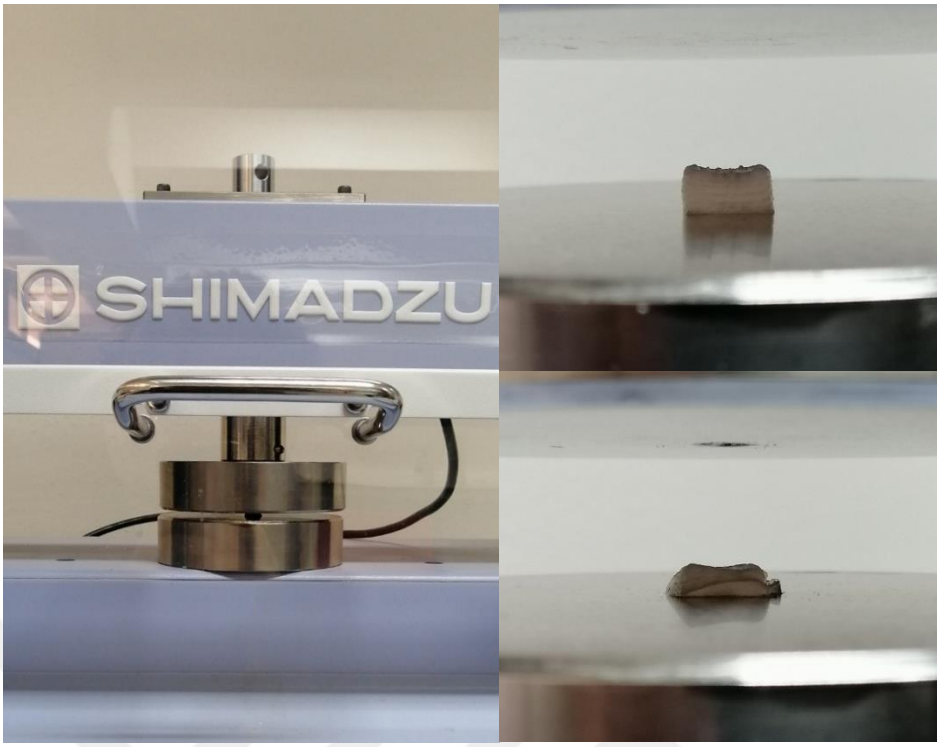

Figure 3. 7 The images of the scaffold during the compression test

3.6.1.2 FTIR analysis

In order to analyze the chemical structures of optimized bone and cartilage scaffold hydrogels dried in a lyophilizer, FTIR-ATR analyzes were performed at 4 cm-1 resolution at 4000-400 cm^{-1} wavelength range using 32 scans in ATR mode at Hünitek Lab (FT-IR Nicolet IS50). The presence of specific peaks of chemical bonds of hydrogels within the scaffold was determined.

3.6.1.3 SEM analysis

The morphological features of optimized bone and cartilage scaffolds were evaluated by SEM examination to be performed in the METU Central Laboratory. The fixed samples were placed on carbon tapes adhered to SEM sample holders (stub). After the sputter coating with gold, the samples were viewed with the Quanta 400F Field Emission SEM device by the expert personnel of the METU Central Laboratory.

3.6.2 3D Bioprinting of hydrogel scaffold

The cells, which were isolated as previously described and kept in the nitrogen tank, were resuspended for the purpose of cell seeding on the scaffold. Cells were thawed in culture medium quick and gently. Centrifugation was applied to collect cells for 5 minutes at 3500 rpm. After, cells were seeded on the cell culture flask for expansion. When cells on the flask become confluent, trypsinization was applied. When the desired cell number was reached, cells were seeded on the scaffold or added into bioink for bioprinting. The number of cells to be loaded per scaffold and the amount of cell solution to be used during loading were determined by calculating according to the number of total cells and the volume of a scaffold. Both cell seeding on scaffolds and cell-laden printing of scaffolds was studied.

3.6.2.1 3D printing of cell-seeded and cell-laden alginate-CMC- gelatin scaffold

Firstly, cell seeding on the scaffold were performed with AL-ASCs. 30000 cells were seeded on a scaffold printed as 5mm x 5mm x 1.5mm using 8µL of cell solution. 3D bioplotter, Envisiontec, was used in the cell seeding part of the printing. The cell-seeded printing parameters were as follows; layer thickness 0.300mm, speed 2 mm/s, pressure 2.4 bar, temperature 37°C. 21 Ga needle tip was used during printing.

Also, cell-laden bioprinting of scaffold was carried out. During this, as the same with previous study, 300000 cells were used per scaffold (10 mm x 10 mm x 1 mm). The cell-laden printing parameters were as follows; layer thickness 0.287mm, speed 5 mm/s, pressure 14 msi, temperature 37°C. Axolotl Biosystem printer was used for cell-laden printing. 22Ga plastic needle tip was used during printing.

The remaining cells were frozen with the freezing solution and incubated at -20 C in Mr. Frosty and overnight. Then it was taken to the nitrogen tank for long-term preservation. Freezing media was prepared with 50% DMEM, 40% FBS and 10% dimethyl sulfoxide (DMSO). Cell-seeded and cell-laden scaffolds were preserved for one day in the expansion medium. The site-specific differentiation of cells were induced by the spatiotemporal release of the respective growth factors as well as environmental cues such as HA loaded bioink and denser/looser 3D printed patterns. After first day of culturing differentiation mediums were added to scaffolds for 21 days.

3.6.2.2 3D bioprinting of cell-laden and bioactive Alginate/GelMa scaffold

Cell-laden Alginate/GelMa and encapsulated TGF-β for chondrogenic and encapsulated BMP-2 for osteogenic induction were printed. The local induction of osteogenic and chondrogenic differentiation, Alginate/GelMa containing BMP-2 and TGF-β loaded capsules were prepared.

Cell-laden and capsule-containing bioprinting of scaffold was carried out by using 300000 cells and capsules per scaffold (10 mm x 10 mm x 1 mm). The Alginate/GelMa scaffold printing parameters were as follows; layer thickness 0.156mm, speed 5 mm/s, pressure 10 msi, temperature 37°C. 25Ga plastic needle tip was used during printing. In order to do this Axolotl Biosystem printer was used.

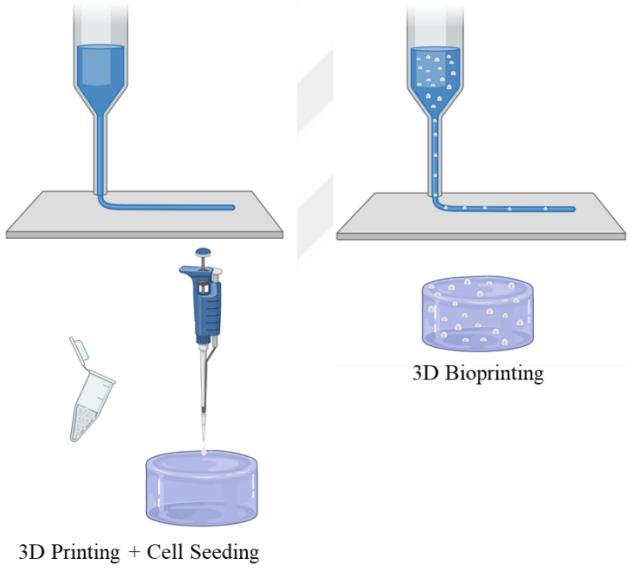

Figure 3. 8 Schematic representation of 3D printing and 3D Bioprinting

3.6.2.3 Live/Dead staining for 3D printed hydrogel scaffold

Live/Dead Kit staining was performed in order to display live and dead cells and to monitor cell morphology in the 3D printed scaffold. Live and dead cells were labelled with Calcein-AM and Ethidium Homodimer-1 (EthD-1), respectively. The composition of the staining solution was prepared as follows: 2 µM Calcein and 4 µM EthD-1 in 10 mL of PBS. Samples to be stained were transferred to clean wells and washed with PBS. Staining solution was added to them and incubation was carried out for 20 minutes at

37°C, protected from light. At the end of the incubation period, the staining solution was washed off with PBS and visualized with a laser scanning confocal microscope (Leica) without waiting. Lasers with wavelengths of 488 nm and 528 nm, respectively, were used in a confocal microscope to visualize cells labelled with calcein and EthD-1.

3.6.2.4 Cryogenic and paraffin embedded sectioning for 3D printed hydrogel scaffold

Scaffolds were fixed using formaldehyde for 4 hours at 4°C under gentle agitation, were then washed with PBS. After fixation, the samples were frozen by embedding in OCT. Then, 10 μm thick sections were taken from the samples embedded in OCT using a cryomicrotome at -20 C. Sections taken were collected on slide.

3.6.2.5 Differentiation analysis for 3DpPrinted hydrogel scaffold

Fixed cell-loaded scaffolds were stained as previously described in the "3.4.2 Alcian Blue Staining" and "3.4.4 Alizarin Red Staining". However, as stated in the result and discussion part section "4.3.3 Alcian Blue and Alizarin Red Staining for Scaffolds" these two dyes were not found suitable for use with cell-loaded scaffold since they stain scaffold.

3.6.2.6 Phalloidin/ DAPI staining for 3D printed hydrogel scaffold

Before staining, scaffolds were fixed with PFA for 4 hours at 4°C, then washed with PBS. Staining was performed on cell-loaded scaffolds as previously mentioned in the section "3.3.3. Phalloidin /DAPI Staining".

3.7 Statistical Analysis

In order to have rational data, laboratory experiments will be conducted on all samples at least 4 times and the results will be stated with mean ± standard deviation (n=4). In pursue of having meaningful data $p < 0.05$, one-way analysis of variance (ANOVA) test and Tukey's post-hoc test will be conducted to evaluate the results. The results that are below $p \leq 0.05$ will be accepted statistically.

4. RESULTS AND DISCUSSION

4.1 IPFP- and AL-ASCs Isolation

Adipose-derived stem cells were isolated successfully from IPFP tissue and lipoaspirate. The morphological structures of cells on passage 0 were examined with a light microscope on the 3rd day of the culture. According to morphological examination, the cells were determined to have a fibroblast-like character and spindle shape like being other MSCs (Figure 4.1) (Grzesiak, Krzysztof, Karol, & Joanna, 2011).

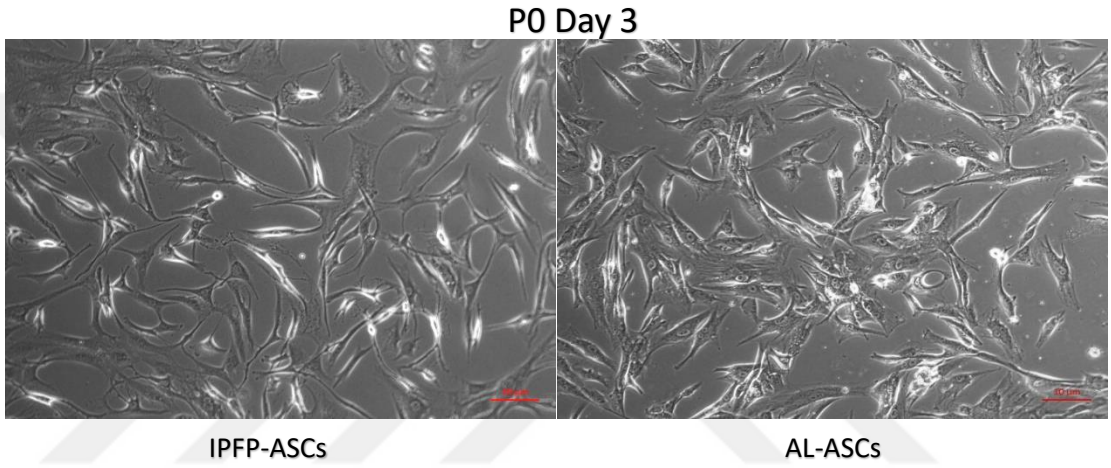

Figure 4. 1 Investigation of IPFP- and AL-ASCs with light microscope (Scale bar: 10μm)

4.1.1 Characterization of cells

4.1.1.1 Flow cytometry

Mesenchymal stem cells are known to synthesize the surface proteins CD105 (endoglin) and CD73 (ecto-5'-nucleotidase) (C. S. Lin, Xin, Dai, & Lue, 2013). CD31 (Platelet endothelial cell adhesion molecule (PECAM-1)) is found in platelet, monocyte-macrophage, and endothelial cells, and is not synthesized in mesenchymal stem cells.

Characterization of IPFP- and AL-ASCs were performed by flow cytometry to confirm the isolation success. Based on the results, it was determined that both cell populations didn't show non-specific binding with the antibodies used. Isolated IPFP- and AL-ASC cells were found to be negative for the CD31 surface marker. While AL-ASC cells were positive for CD105 and CD73 markers, IPFP-ASCs were positive for CD 73 but only

44% of the population received a positive signal for CD105. In the literature, studies represented that CD105 protein synthesis was low in mesenchymal stem cells newly isolated from adipose tissue, but its positivity increases in future passages (Varma et al., 2007; Yoshimura et al., 2006)). Flow cytometry revealed that IPFP- and AL-ASCs expressed CD 73 and CD 105 but do not CD 31, like the other mesenchymal stem cells. In addition, about the effect of age on cell characteristics, which constitutes the main idea of the thesis; It was observed that the surface markers were not affected by aging. (Huri et al., 2018)

Table 4.1 Results of flow cytometry analysis of IPFP- and AL-ASCs against isotype control, CD31, CD105, and CD73 surface markers. The curves in black represent the signals received from unstained cells.

Surface Marker	IPFP-ASCs	AL-ASCs
Mouse IgG1 κ	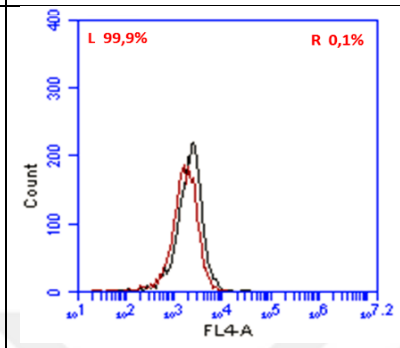	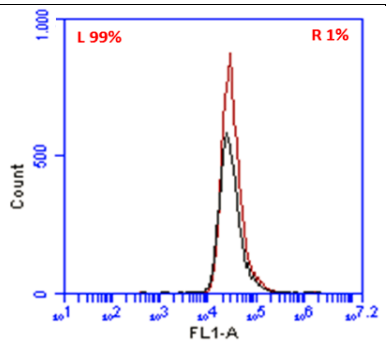
CD 105 (+)	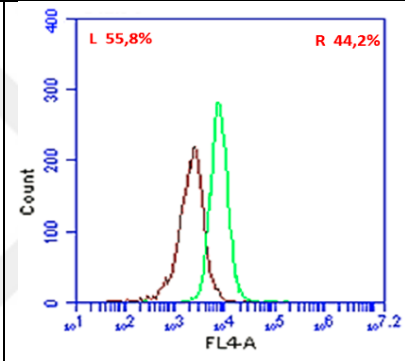	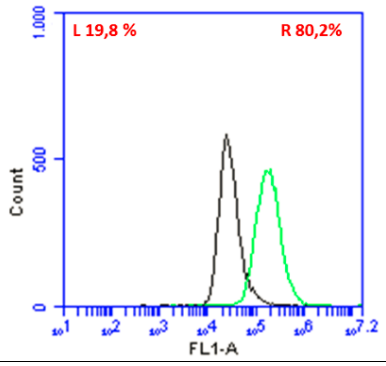
CD 73 (+)	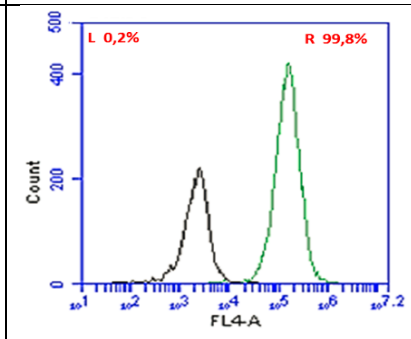	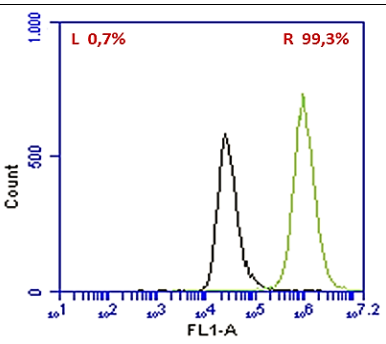
CD 31 (-)	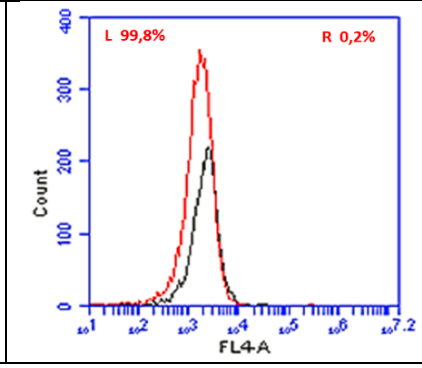	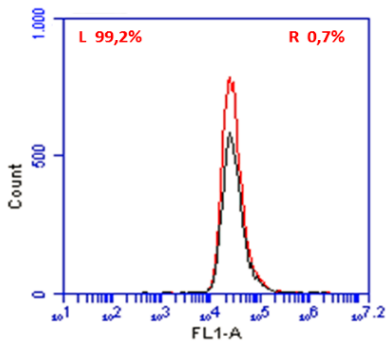

4.1.1.2 Alamar Blue assay

Investigation and comparison of the viability of IPFP- and AL-ASCs cells isolated from patients of different age groups (young 25-40, and mature 50-65) were performed with the Alamar Blue assay. On days 1, 7, 14, and 21 of culture, cells were incubated in osteogenic and chondrogenic differentiation, and expansion media (including FGF-2). Effects of different mediums on cell viability were examined.

According to the results of Alamar blue assay, chondrogenic differentiation enhanced cell proliferation, while induction for osteogenesis decreased the proliferation rate of cell for both age groups. Chondrogenic induction increased mature IPFP-ASCs viability nearly 4 times whereas osteogenic induction decreased viability in half according to the control group. When the young IPFP-ASCs group was examined, it was observed that the chondrogenic media had almost the same viability as the control media. AL-ASCs in both age groups, especially mature group, were showed more proliferation in chondrogenic induction medium. In osteogenic media, the viability was decreased compared to control and chondrogenic media. While osteogenic media increased cell viability in the younger AL-ASCs group, it decreased in the mature group when compared with expansion medium (control group). AL-ASCs demonstrated more proliferation than IPFP-ASCs.

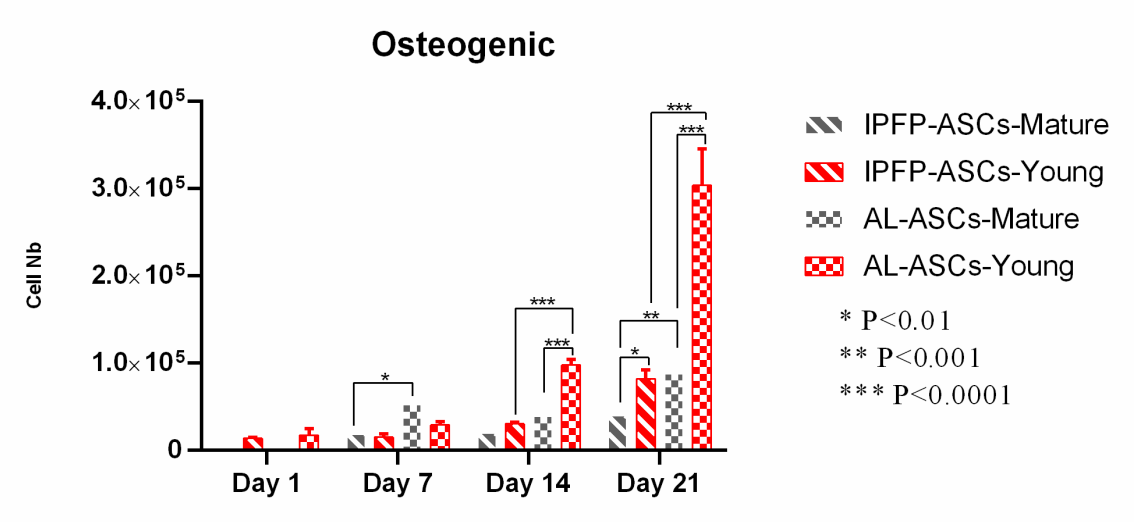

Figure 4. 2 The effect of osteogenic differentiation medium on cell viability of IPFP- and AL-ASCs from mature and young patients.

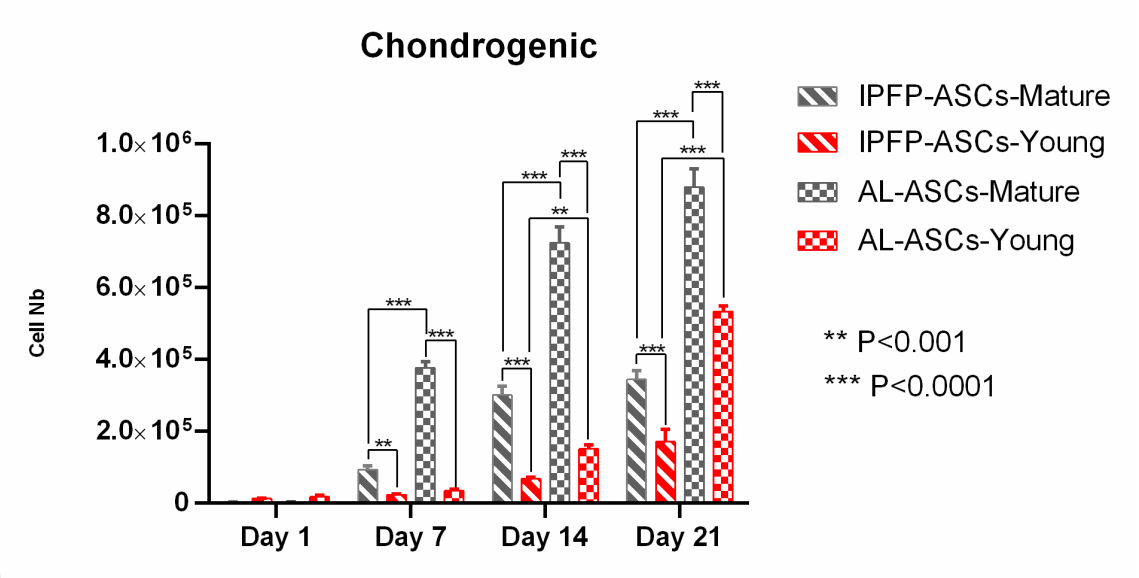

Figure 4. 3 The effect of chondrogenic differentiation medium on cell viability of IPFP- and AL-ASCs from mature and young patients.

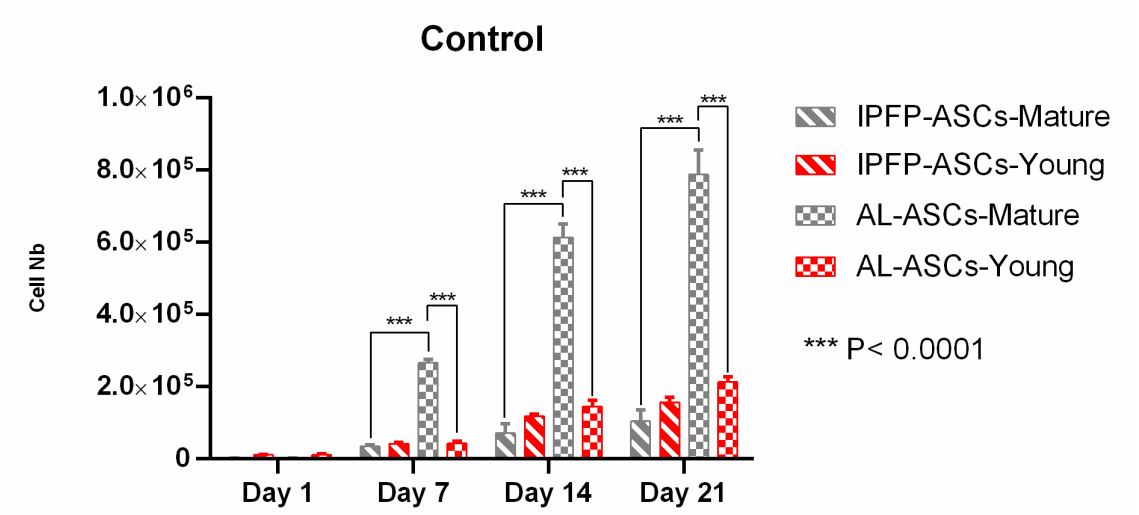

Figure 4. 4 The effect of control medium on cell viability of IPFP- and AL-ASCs from mature and young patients.

4.1.1.3 DAPI /Phalloidin staining

IPFP- and AL-ASCs were stained with Phalloidin/DAPI to indicate the actin filament (cytoskeletons) and cell nucleus. On days 1, 7, 14, and 21 of the culture, the cells were fixed and stained on cell culture plate. The images of the results are presented in the Figure 4.5 and Figure 4.6. Cell nuclei are stained blue and actin filaments green (Prabha

et al., 2019). DAPI/Phalloidin staining of the cell showed densely packed cell mass from Day 1 to Day 21. In parallel with the Alamar Blue assay results, AL-ASCs showed better proliferation than IPFP-ASCs.

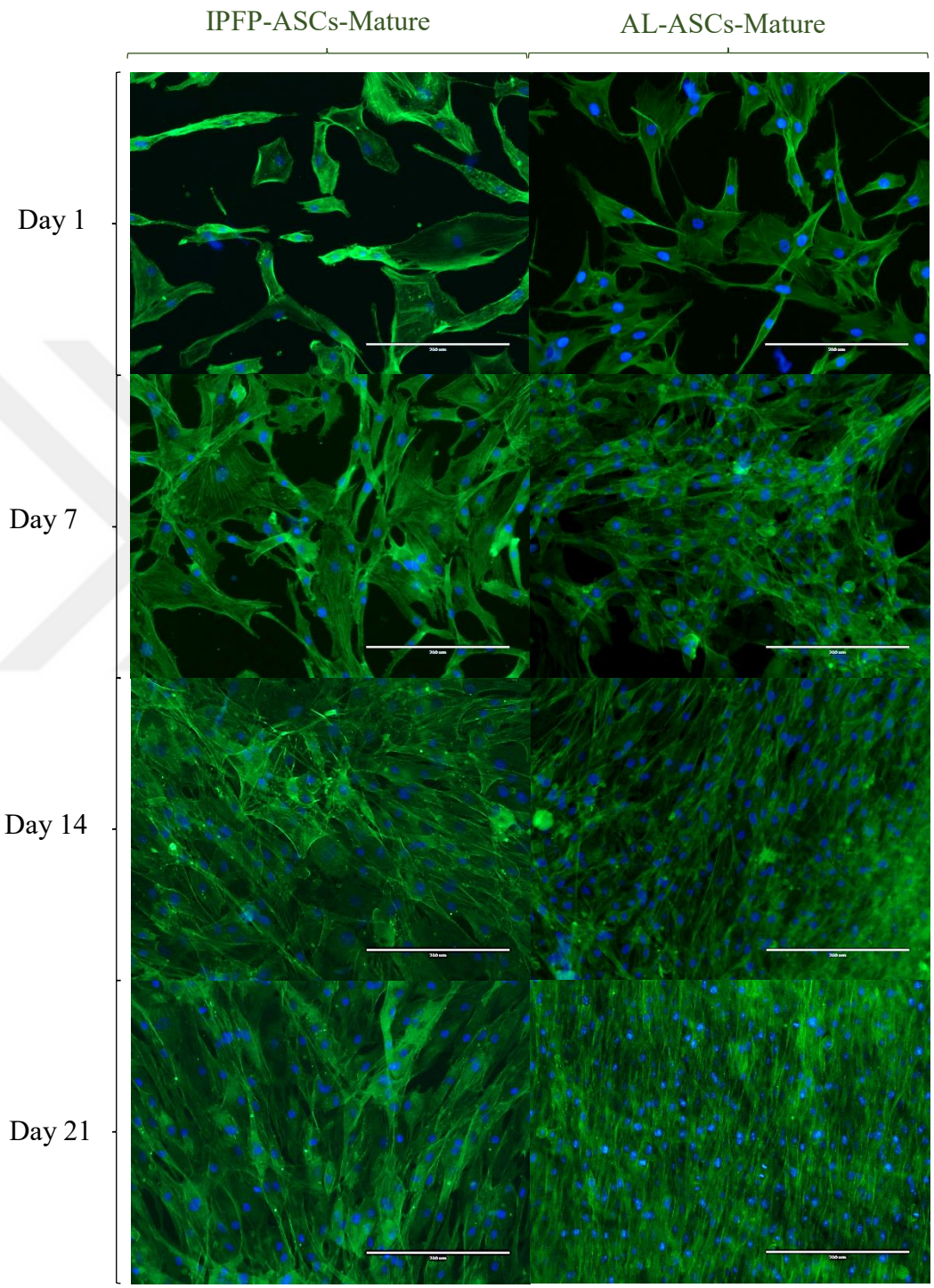

Figure 4. 5 Phalloidin/DAPI staining of IPFP- and AL-ASCs from mature patients (Scale bar: 200µm, 20x magnification)

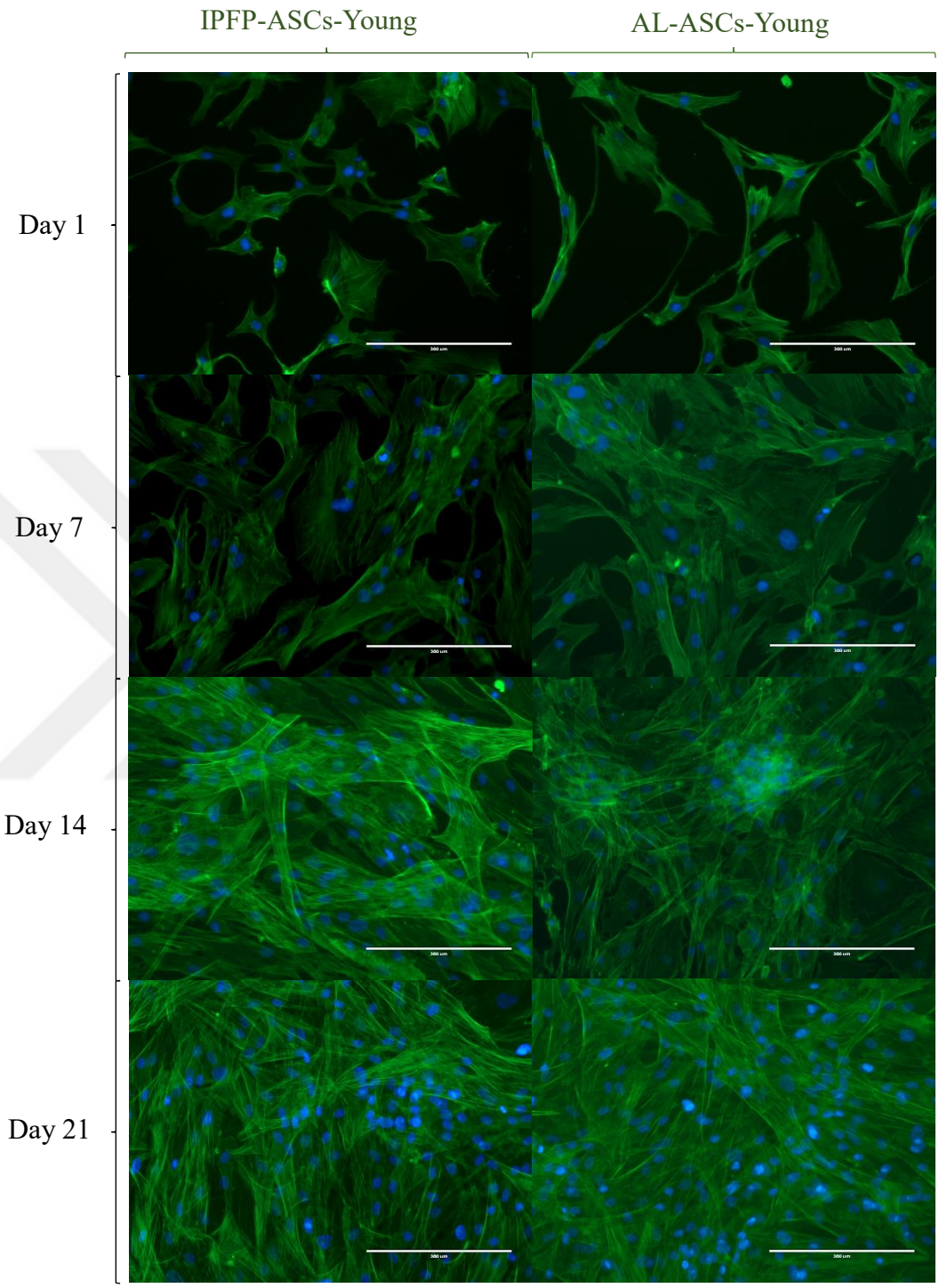

Figure 4. 6 Phalloidin/DAPI staining of IPFP- and AL-ASCs from young patients (Scale bar: 200µm, 20x magnification)

4.1.2 Differentiation analysis

The osteogenic and chondrogenic differentiation potentials of the cells were examined by alizarin red and alcian blue staining, respectively. On days 7, 14, and 21 of culture, cells were fixed with PFA, then stained. According to the results, chondrogenic and osteogenic induction with culture conditions (differentiation media) were successfully carried out.

There were no significant differences observed in IPFP- and AL-ASCs. More intense staining was observed in the mature population for alcian blue and alizarin red staining. It was observed that IPFP-ASCs stained more when compared to other groups, especially when the Day 21 data were examined, more intense staining was observed in the mature group.

IPFP-ASCs possess trilineage and age-independent differentiation potential. In literature, there are several studies investigating the potential of IPFP-ASCs. Especially chondrogenic genes (COL2A1 and SOX-9 etc.) expression was found significantly higher (Congcong et al., 2021; C.-C. Wang, Chen, Yang, Chen, & Yang, 2021). Even though IPFP-ASCs have high passage, they do not lose their differentiation and proliferation potential due to telomerase activity and telomere integrity (Khan et al., 2012; Neri, Guidotti, Lilli, Cattini, & Mariani, 2017; Zhong, Wang, Han, & Wen, 2020). As stated in the literature, besides age-independent capacity of them, chondrogenic, osteogenic and adipogenic potential make IPFP-ASCs an important alternative cell source.

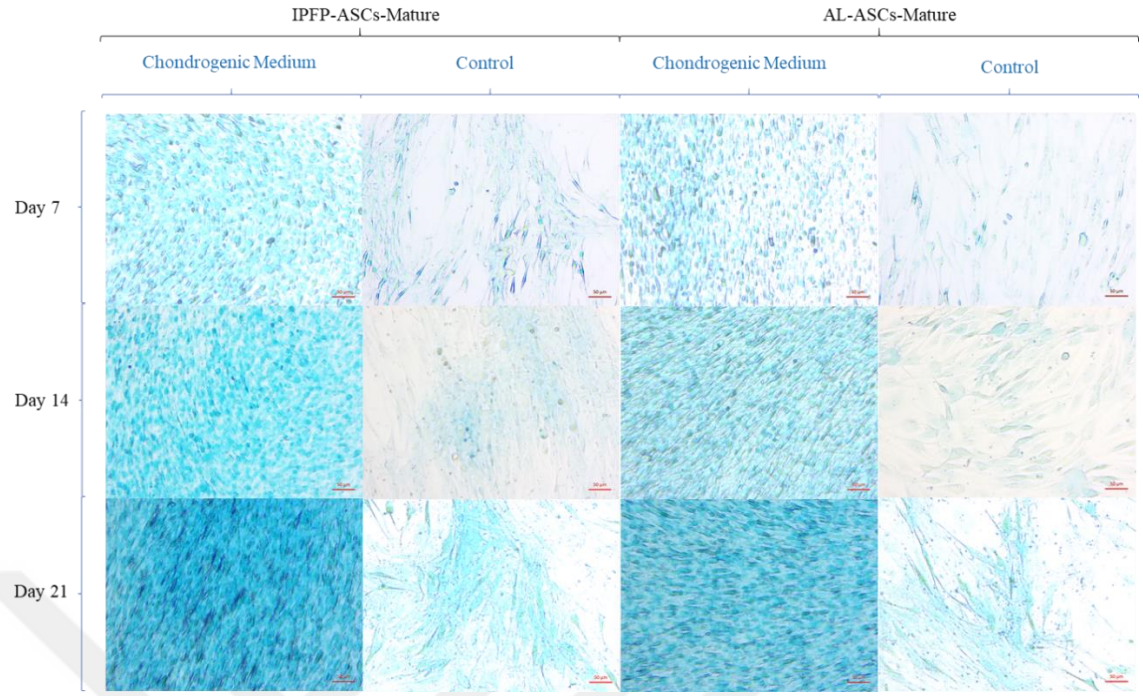

Figure 4. 7 Alcian Blue staining to investigate chondrogenic differentiation potential of IPFP- and AL-ASCs from mature patients (Scale bar: 50µm)

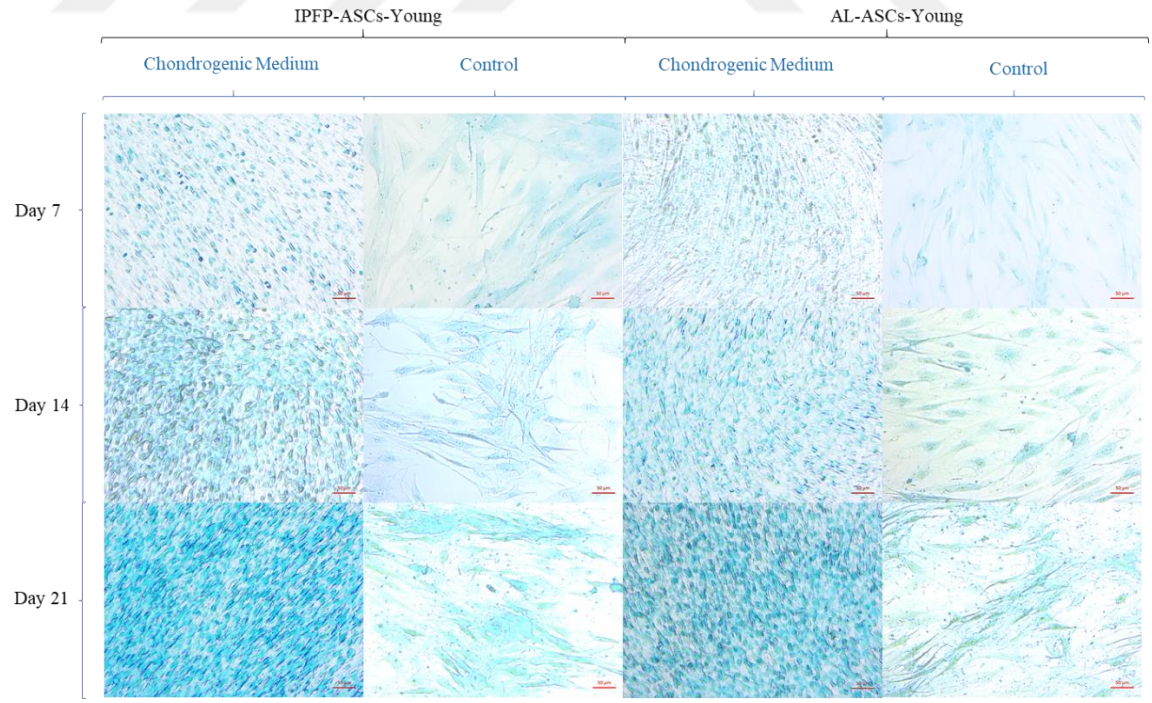

Figure 4. 8 Alcian Blue staining to investigate chondrogenic differentiation potential of IPFP- and AL-ASCs from young patients (Scale bar: 50µm)

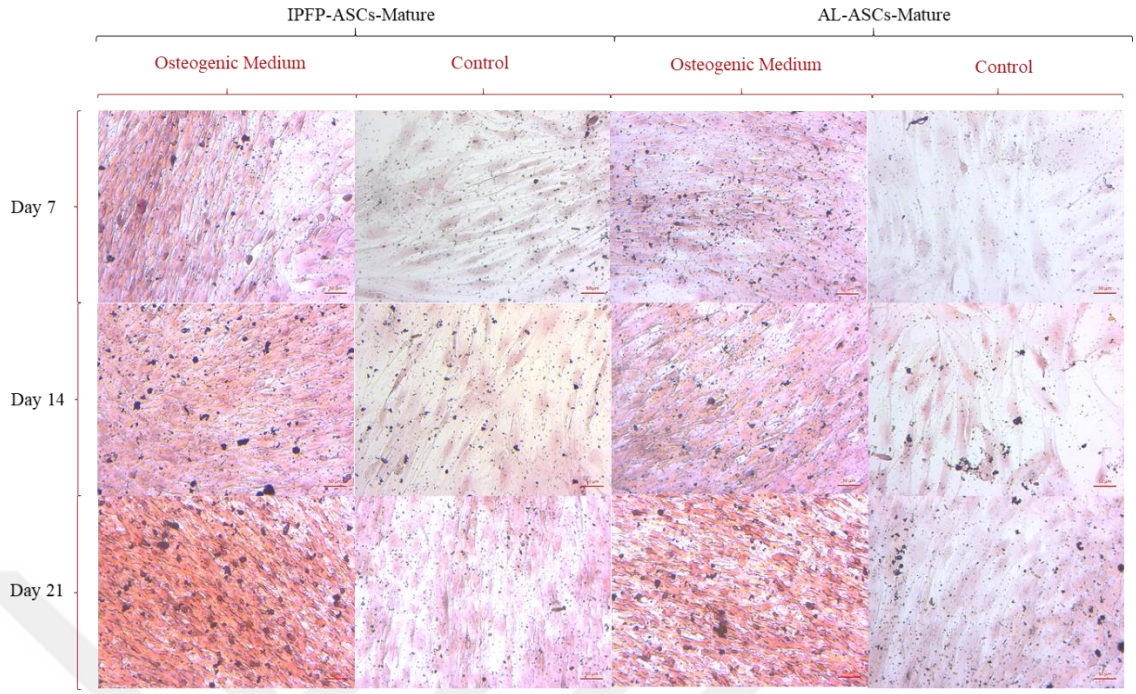

Figure 4. 9 Alizarin Red staining to investigate osteogenic differentiation potential of IPFP- and AL-ASCs from mature patients (Scale bar: 50µm)

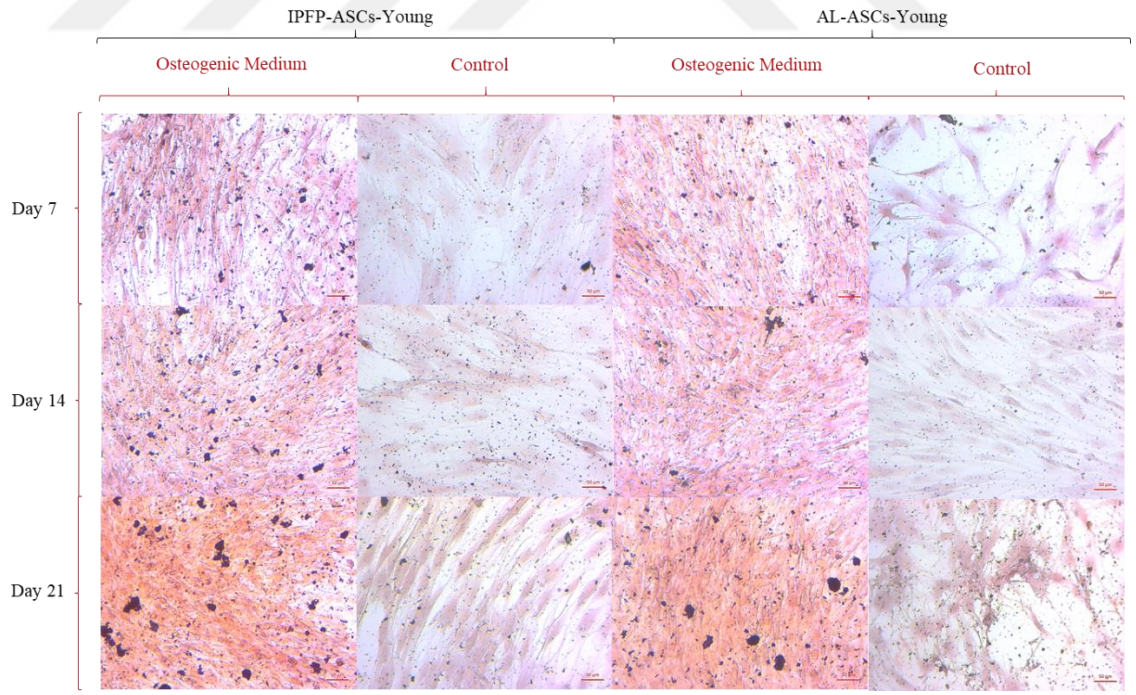

Figure 4. 10 Alizarin Red staining to investigate osteogenic differentiation potential of IPFP- and AL-ASCs from young patients (Scale bar: 50µm)

Considering the hypothesis based on the proliferation and differentiation potential of IPFP-ASCs that do not decrease with age, it was aimed to examine the IPFP-ASCs in comparison with AL-ASCs in the scope of this thesis. Based on the results from both the Alamar blue, Alcian blue and Alizarin red assays, it was not concluded that IPFP-ASCs have superior potential for differentiation and viability. In this case, it was decided to continue the in vitro studies of the thesis by using AL-ASCs, since no result could be reached to support the hypothesis about IPFP-ASCs and much more ASCs from abdominal lipoaspirate were obtained.

4.2 Growth Factors Encapsulation with PCL Capsules

The morphologies of the PCL capsules created in 5, 10, and 20% were examined by SEM imaging. Capsule production was successfully carried out in all groups based on the structural investigation. Larger diameter of capsules was observed in the group containing 20% PCL compared to the other two groups. High concentration of polymers used for encapsulation agents leads to high particle size capsules (Lamprecht et al., 2000). Increasing the number of polymers causes an increased viscosity of the first emulsion. So larger size occurs at the end of the second emulsion step. The sticky PCL capsules are thought to be due to the remaining not evaporated PVA (Fong, 1990).

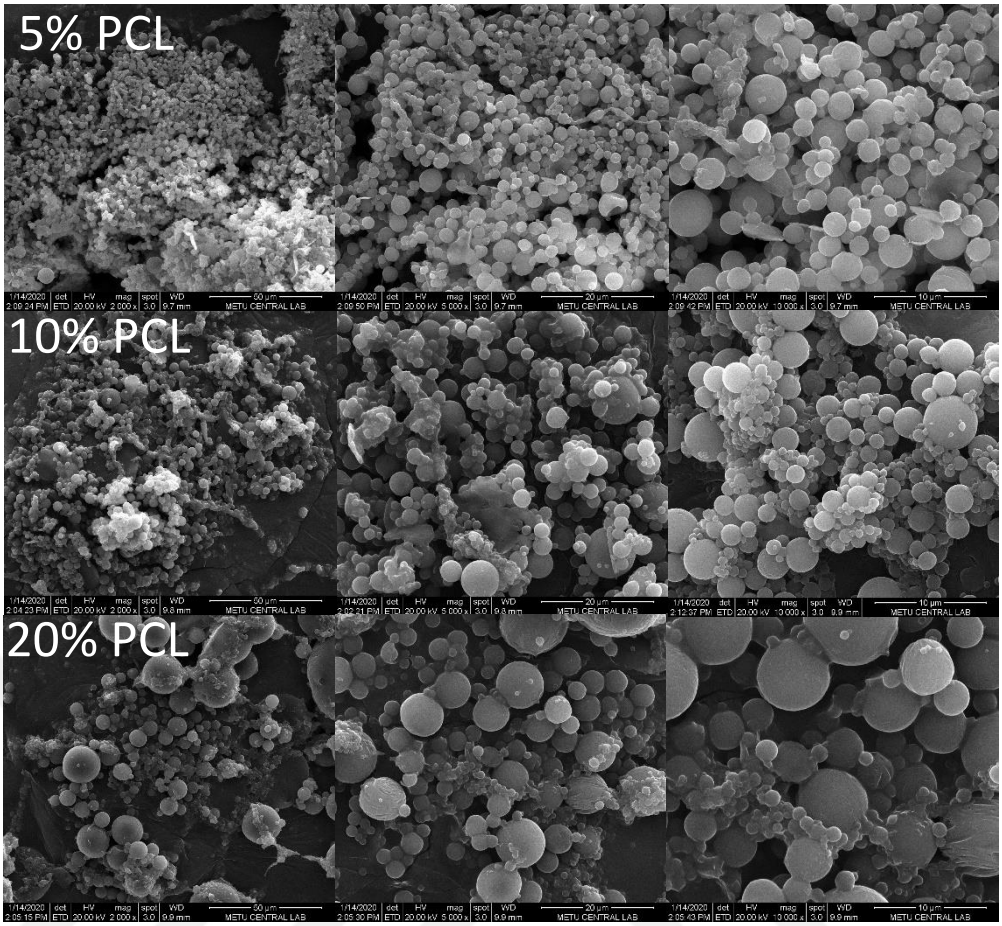

Figure 4. 11 SEM images of the PCL capsules (5, 10 and 20%) 2000x, 5000x and 10000x magnifications (Scale bar: 50µm, 20µm and 10µm, respectively)

4.2.1 Analysis of particle size and distribution

Particle size analysis of the capsules was evaluated using the ImageJ program. For this, 4 SEM images were taken from each test group and their diameter lengths were measured. The frequency distribution graph of the obtained results was plotted using Origin Lab.

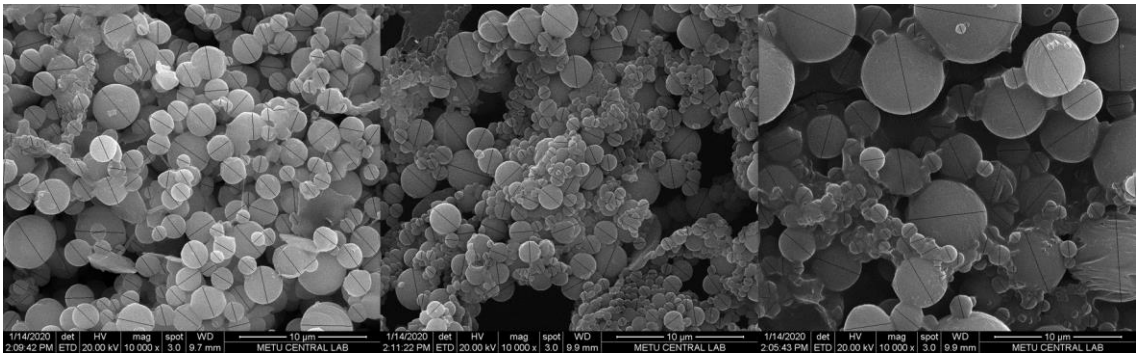

Figure 4. 12 Particle size and distribution of PCL capsules were analyzed by using Origin Lab with SEM images 10000x magnification (Scale bar: 10µm)

When the data were examined, it was observed that the particle size varies in the range of 97-19000 nm, and distribution graphs were shown in Figure 4.13, Figure 4.14 and Figure 4.15. In the group prepared with 5% PCL, capsules were determined to be between 220 and 4300 nm in size. Nearly 75% of particle size distribution of 5%PCL was observed in 220 to 2000nm. More than 50% of the particle size was in the range of 1000-2000nm. In the capsule group prepared with 10% PCL, 40% of the distribution was particle size between 500-1000 nm, more than 30% was in the 1000-2000 nm range, and nearly 15% was in 270-500 nm. The distribution of particles in this group varies between 270-5500 nm. In the group prepared with 20% PCL, it was determined that the smallest diameter of the capsules was 221 nm and the largest diameter was 19800 nm (Since few capsules above 10000 nm were observed, they were ignored in the graphic drawing). The distribution between 221-2000 nm accounts for about 70% of the capsules. For the 20% PCL group, capsules with a diameter less than 1000 nm are about 45% of the total.

Sonication power, exposure time, amplitude, amount of encapsulation agent, and evaporation rate of the solvent significantly affect nanoparticle size and morphology (Iqbal, Valour, Fessi, & Elaissari, 2015; Jafari, He, & Bhandari, 2007; Maia, Santana, & Ré, 2004). Smaller size particles can be obtained at higher amplitude of ultrasound, increasing PVA concentration and small size PCL.

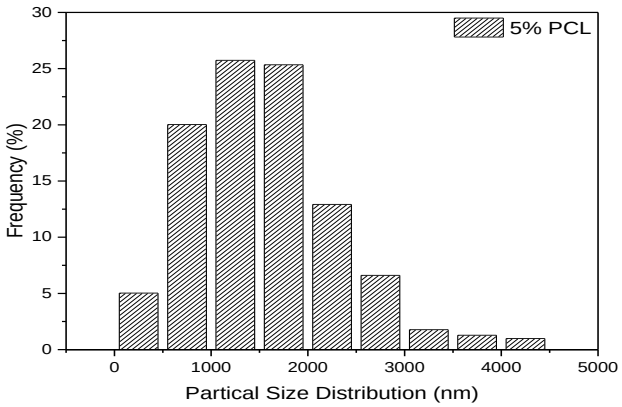

Figure 4. 13 Particle size distribution of the 5% PCL capsules

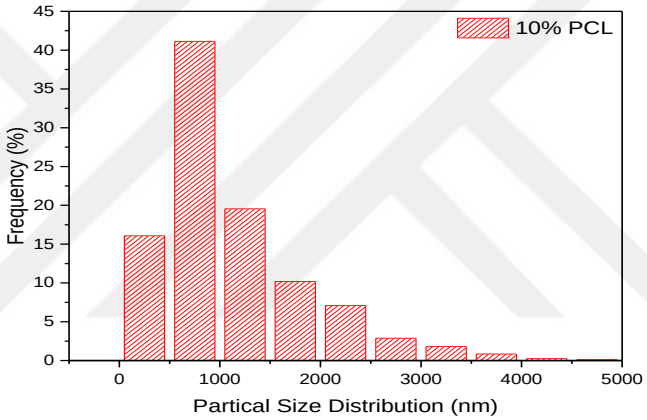

Figure 4. 14 Particle size distribution of the 10% PCL capsules

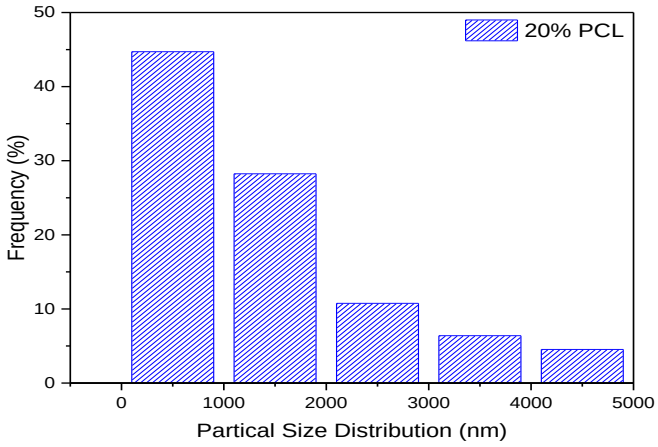

Figure 4. 15 Particle size distribution of the 20% PCL capsules

When the average diameter was investigated, 5%, 10%, 20% PCL capsules were found to be 1600, 1100, 1700 nm, respectively (Figure 4.16).

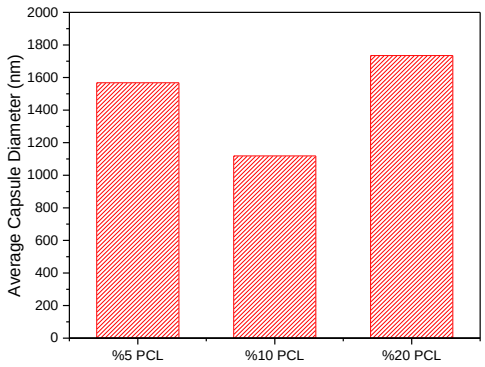

Figure 4. 16 Average diameters of 5, 10, 20% PCL capsules which analysed by using Origin Lab with SEM images.

4.2.2 Encapsulation efficiency

The encapsulation efficiency of capsules prepared with 5, 10 and 20% PCL were calculated. Accordingly, efficiency was found the highest in the group prepared with 20% PCL, while low efficiency was observed in the group containing 5% PCL. High concentration of polymers used for encapsulation agent causes high encapsulation efficiency. Byun et al., enhanced PCL concentration from 3 to 5 g, and observed that encapsulation efficiency increased (Byun et al., 2011).

Efficiency% = BSA amount measured with Bradford Assay/Amount of BSA used when producing the capsule * 100

Table 4. 2 Encapsulation efficiency of 5, 10 and 20% PCL capsules loaded with BSA

Encapsulation Efficiency %	
5% PCL	14.56 ± 3.2
10% PCL	32.32 ± 2.5
20% PCL	70.18 ± 2.4

4.2.3 Release kinetics

In order to investigate the release profile of capsules in 5, 10 and 20% PCL containing model protein BSA, micro-scale Bradford assay were applied. When the release kinetics of the capsules were examined, the highest release was observed at 17% in the group prepared with 5% PCL. The lowest release was seen in the 20% PCL group at 6%, and release in 10% PCL at 9% (Figure 4.18). According to the literature, the large diameter of polymeric capsules shows slow release (Chen, Palazzo, Hennink, & Kok, 2017; Siepmann, Faisant, Akiki, Richard, & Benoit, 2004). The slowest release was observed in encapsulation with 20% PCL. A result parallel to the literature was obtained. It is also shown in the table 4.5 that the most efficient encapsulation occurs at the highest concentration. The 20% group with the best encapsulation efficiency and the slowest release was determined as the ideal group.

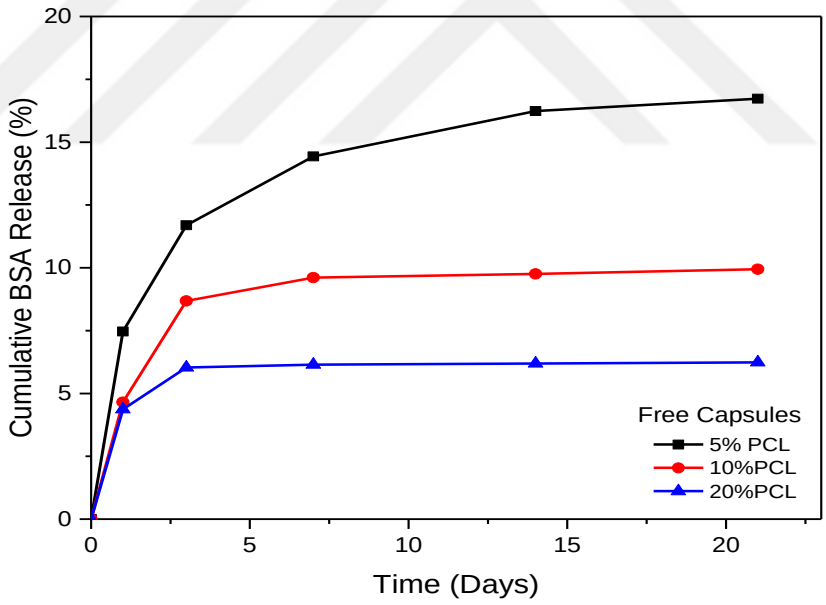

Figure 4. 17 Release profiles of free capsules

In addition to the reviews so far, the release of capsules from scaffolds was also tested. Capsules were printed with hydrogels used as bone and cartilage scaffolds, and their release determination was examined with Bradford assay (Figure 4.19). Almost similar results were obtained with free capsule release. While the slowest release was observed at 20% PCL, the fastest release was observed in the 5% PCL group within the two groups.

In the 20% PCL group, nearly 4% release was observed in the cartilage scaffold and 5% in the bone scaffold.

The release kinetics from capsules depends on the crosslinking density of the scaffold (H. Wang et al., 2013). When crosslink density of scaffold increased, degradation rate and diffusion ability of the factors encapsulated decreased (Holloway, Ma, Rai, & Burdick, 2014). In this study, the crosslink density of the cartilage scaffold is higher than the bone scaffold. So, bone scaffold caused more release in release kinetics measurement.

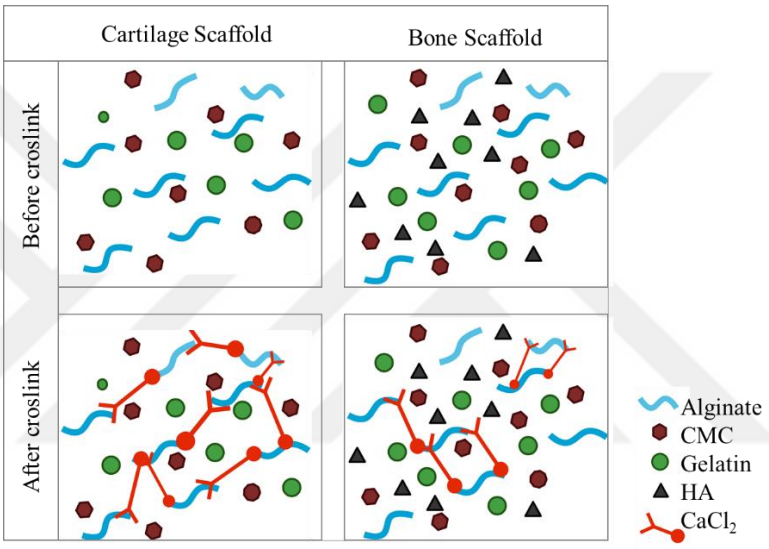

Figure 4. 18 Illustrations for representing the crosslink density of cartilage and bone scaffolds

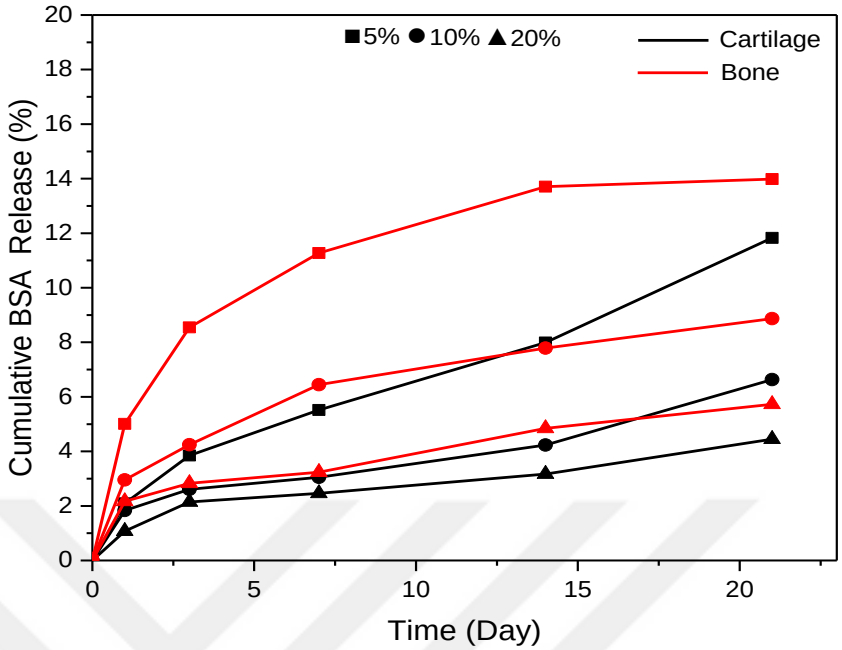

Figure 4. 19 Release profiles of capsules on cartilage and bone scaffolds.

According to the whole steps in capsule formation part; as the concentration of the polymer used for encapsulation increases, capsule size increased, release kinetics decreased, encapsulation efficiency increased. Considering all these results, the 20% w/v group showed the best results and was decided to be the optimal concentration for encapsulation of TGF-β and BMP-2. BMP-2 concentration was utilized as 40ng/mL whereas TGF-β concentration was utilized 10ng/mL (Henning Madry, Rey-Rico, Venkatesan, Johnstone, & Cucchiarini, 2014; Pinar Yilgor et al., 2009)

4.3 3D Printing of Hydrogel Scaffold

4.3.1 Optimization studies for 3D printed hydrogel scaffold

In order to create a hydrogel-based scaffold, first of all, biomaterial optimization was performed. 3D printing of alginate and CMC hydrogels at different concentrations were carried out. Alginate is a commonly used biomaterial with basic properties such as water-soluble viscosity, being biocompatible, and biodegradable. There are several studies in the literature showing the usability of alginate in cartilage tissue engineering (Farokhi, Jonidi Shariatzadeh, Solouk, & Mirzadeh, 2020). CMC is a polysaccharide-based biomaterial derived from cellulose and supports cell attachment. It is used in tissue engineering applications with 3D printers, because it increases printability (Habib, Sathish, Mallik, & Khoda, 2018).

5% (w/v) alginate and 4% (w/v) CMC (medium viscous) were used to prepare bilayered scaffold. In order to form bilayered osteochondral scaffold printing at least more than five layers of scaffold printing was aimed. With the combination of 5% (w/v) alginate and 4% (w/v) CMC (medium viscous) five-layer scaffold was not constructed. Therefore, high viscosity CMC was used with the same combination, but again, no successful results were obtained.

3D printing was performed using 3% (w/v) alginate and 9% (w/v) CMC (medium and high viscous). Ten and even twenty layers were successfully printed with the 3-9% (w/v) alginate-CMC hydrogel concentration used.

After printing, scaffolds were incubated in cell culture medium and their mechanical stability was observed. According to the incubation results, 3-9% (w / v) alginate-CMC (high viscous) was chosen as the osteochondral scaffold biomaterial. The images of the printed scaffolds before and after the incubation and the printing parameters were presented in the table 4.3.

In order to increase the cell interaction with scaffold, gelatin to which the cells adhere better was also added to the hydrogel combination. Gelatin positively affects the adhesion and proliferation of cells due to the fact that it is a derivative of collagen (Bello, Kim, Kim, Park, & Lee, 2020). The scaffolds containing 5 and 10 percent gelatin were incubated in cell culture medium for 21 days to determine the gelatin concentration. Considering the incubation results, it was decided to use a scaffold containing 5% gelatin.

Combination of osteochondral scaffold was determined as follows;

- ✓ cartilage part: 3% (w/v) alginate / 9% (w/v) CMC/ 5% (w/v) gelatin in a grid pattern
- ✓ bone part: 3% (w/v) alginate / 9% (w/v) CMC/ 5% (w/v) gelatin/ 3% (w/v) HA in a snowflake pattern.

Table 4. 3 Optimization parameters for alginate and CMC printing

Alginate (%)	CMC (%)	Printing Parameters	Images	
			After printing	After Incubation
3	9 Medium Viscous	• Pressure: 3.7 • Speed: 1.5 • DBS: 1.20 • DFC: 0.25	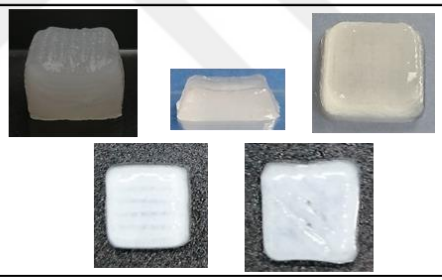	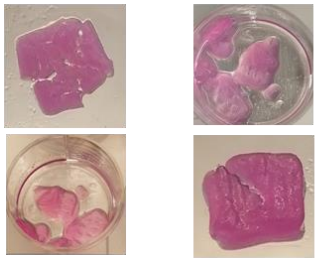
3	9 High Viscous	• Pressure: 2.6 • Speed: 1.2 • DBS: 1.20 • DFC: 0.25	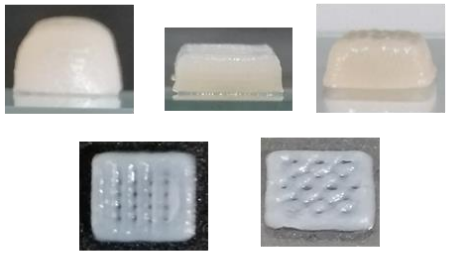	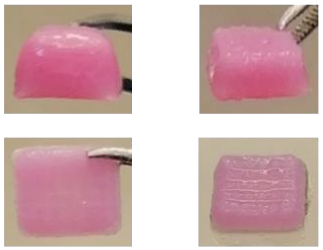
5	4 Medium Viscous	• Pressure: 2.5 • Speed: 1.0 • DBS: 1.10 • DFC: 0.25		
5	4 High Viscous	• Pressure: 2.0 • Speed: 2.5 • DBS: 1.20 • DFC: 0.25		

Table 4. 4 Optimization parameters for gelatin and alginate/CMC printing

Alginate (%)	CMC (%)	Gelatin (%)	Printing Parameters	Pictures		
				After printing	After Incubation	After 21 days incubation
3	9 High Viscous		• Pressure: 3.7 • Speed: 1.5 • DBS: 1.20 • DFC: 0.25	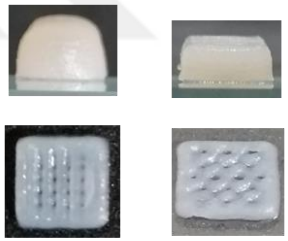	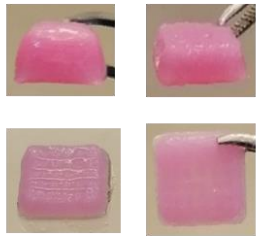	
3	9 High Viscous	5	• Pressure: 2.6 • Speed: 1.0 • DBS: 1.20 • DFC: 0.25	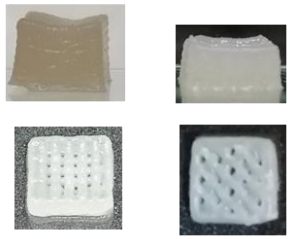	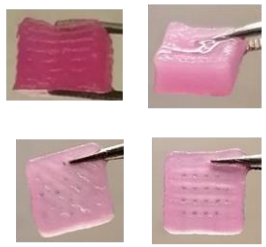	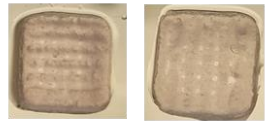
3	9 High Viscous	10	• Pressure: 2.9 • Speed: 1.5 • DBS: 1.20 • DFC: 0. 25	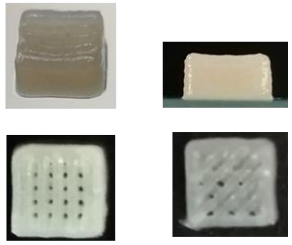	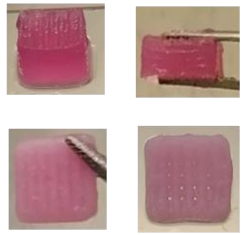	

The importance of scaffold architecture in cell attachment, migration even differentiation has been determined by various studies (M. Lee, Wu, & Dunn, 2008; P. Yilgor, Sousa, Reis, Hasirci, & Hasirci, 2010). According to the native tissue morphology, cartilage and bone scaffolds in grid and snowflake patterns respectively were printed separately with optimized hydrogels (Figure 4.20). The bone scaffold was printed with snowflake pattern along with HA to enhance the mechanical strength and stimulate cell spread with natural tissue.

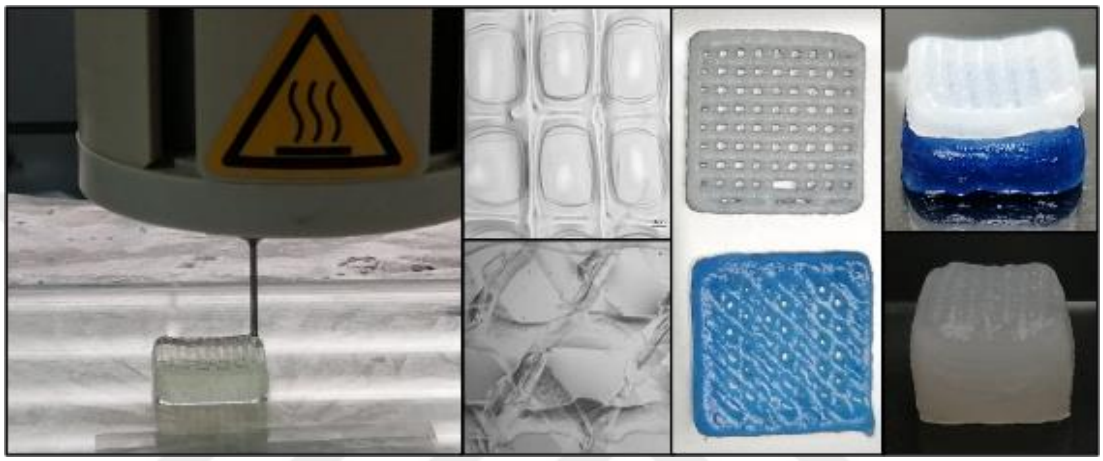

Figure 4. 20 3D printing of cartilage and bone scaffold in grid and snowflake pattern, respectively.

Printing parameters were optimized to create 3D bilayer scaffold (Figure 4.21). The osteochondral scaffold was printed using a 0.51 Gauge needle tip in 357um layer thickness. Cartilage part was prepared with 3.8 bar pressure and 1 speed whereas bone part with 4.6 bar pressure and 0.9 speed. As a result of the optimization studies, bilayer osteochondral scaffold was also obtained. Up to 20 layers were printed with the hydrogel concentration used.

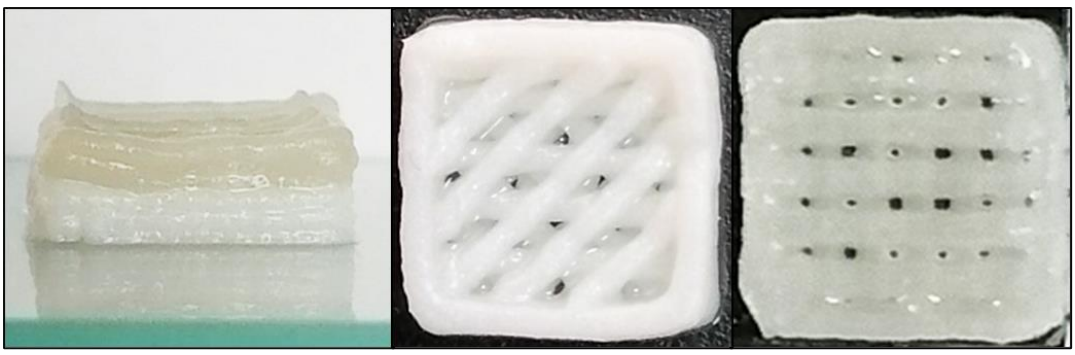

Figure 4. 21 3D printing of bilayer osteochondral scaffold

4.3.2 Characterization of scaffold

4.3.2.1 Compression test

Compression test was applied to scaffolds to examine the mechanical strength. Compression modulus for each hydrogel was measured by the slope of the stress-strain graphs. While the highest compression modulus was observed in alginate-CMC, the lowest was observed in alginate-CMC-5% gelatin scaffold. Adding gelatin to hydrogel combination reduced the compression modulus. However, adding 10% gelatin was created a higher compression modulus than 5% and a lower than alginate-CMC. HA added for bone scaffold was increased the compression modulus. The compression module of the bilayer osteochondral scaffold prepared with cartilage and bone scaffold was observed to be lower than bone and more than cartilage.

The increase in HA concentration causes an increase in the compression modulus (Yannan Liu, Gu, & Fan, 2020). Furthermore, the addition of the gelatin to alginate decreases the compression modulus (Chung et al., 2013). Based on the results of compression modulus in Table 4.5, the addition of gelatin at a high rate caused an increase in less (10 % Gelatin 14.3±4.81; 5 % Gelatin 10.8±3.46).

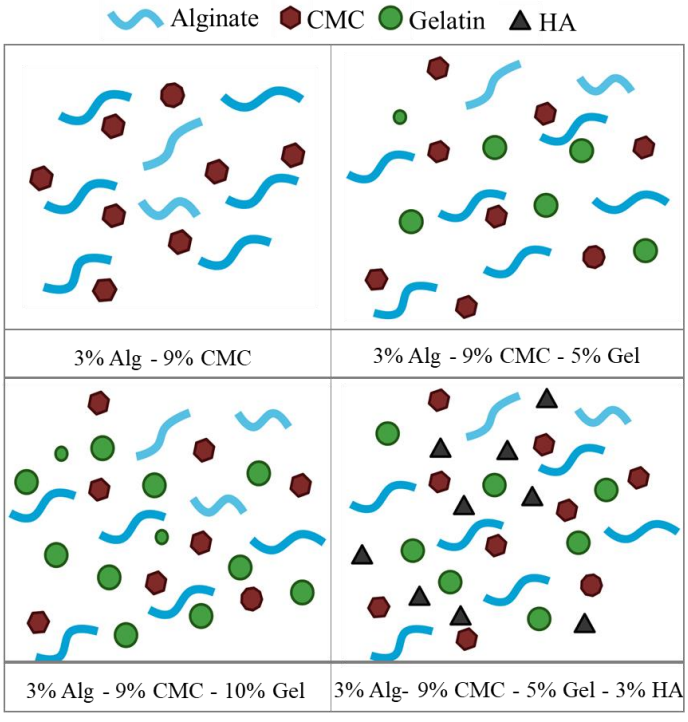

Figure 4. 22 Schematic illustrations for different hydrogel combinations

Table 4. 5 Results of the compression test on scaffolds

Hydrogels	Compression Modulus (kPa)
3%Alginate-9%CMC	21.5±7.07
3%Alginate-9%CMC-5%Gelatin-3%Hap (Bone Scaffold)	19.3±7.51
Osteochondral Scaffold (Cartilage + Bone Scaffold)	15.2±1.08
3%Alginate-9%CMC-10%Gelatin	14.3±4.81
3%Alginate-9%CMC-5%Gelatin (Cartilage Scaffold)	10.8±3.46

4.3.2.2 FTIR analysis

Chemical analysis of hydrogel combinations used to create cartilage and bone scaffold was investigated by FTIR analysis. FTIR spectra of alginate, CMC, gelatin, and HA biomaterials were given in the Figure 4.23. For alginate and CMC, the peak observed at 3300 cm^{-1} wavelength indicates the hydroxyl group (O-H bond), 2930 cm^{-1} wavelength C-H group, and 1590 cm^{-1} wavelength carbonyl group (C=O) (Asl, Mousavi, & Labbafi, 2017; Ramos et al., 2018; Riaz et al., 2018; Thomas-Busani et al., 2020). The characteristic peaks of vegetable hydrolysable tannins and Amide-III N-H belonging to gelatin were observed at the wavelengths of 1330 and 1240 cm^{-1}, respectively (Ramos et al., 2018; Vichi, Eliazyan, & Kazarian, 2018). The characteristic peak of ether group (-O-) for CMC at 1202 cm^{-1} wavelength were attributed (Asl et al., 2017). Glycosidic (C–O–C) bonds vibration belonging to alginate occurred in the peaks observed at 1030 and 815 cm^{-1} wavelengths (Jejurikar et al., 2012). It was concluded that there was PO4, P-O and OH vibration at 1080, 960 and 630 cm^{-1} wavelengths, respectively in HA doped bone scaffold (Khallok et al., 2021; Montazeri, Jahandideh, & Biazar, 2011).

When the bone and cartilage scaffold were compared, the difference between them was the HA content of the bone scaffold. While peaks were observed at 1080, 960 and 630

cm^{-1} wavelengths in the bone scaffold, there was no peak at these values in the cartilage scaffold (Figure 4.24).

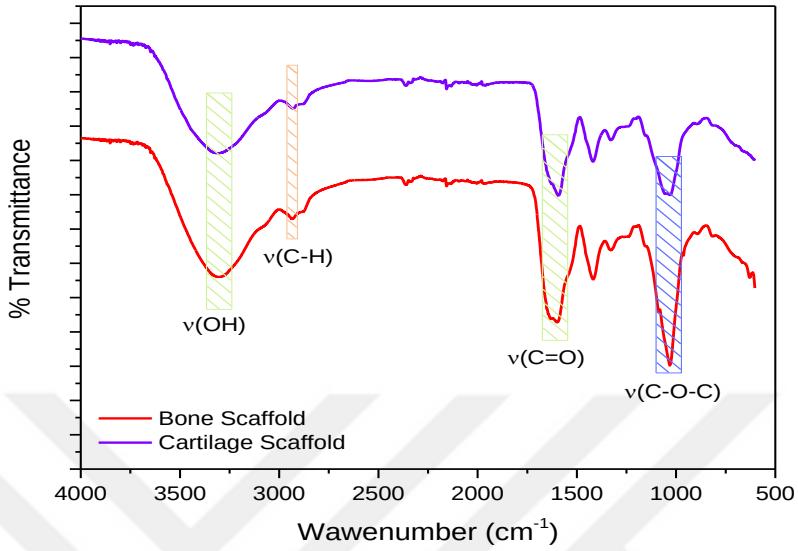

Figure 4. 23 FTIR analysis of cartilage and bone scaffold

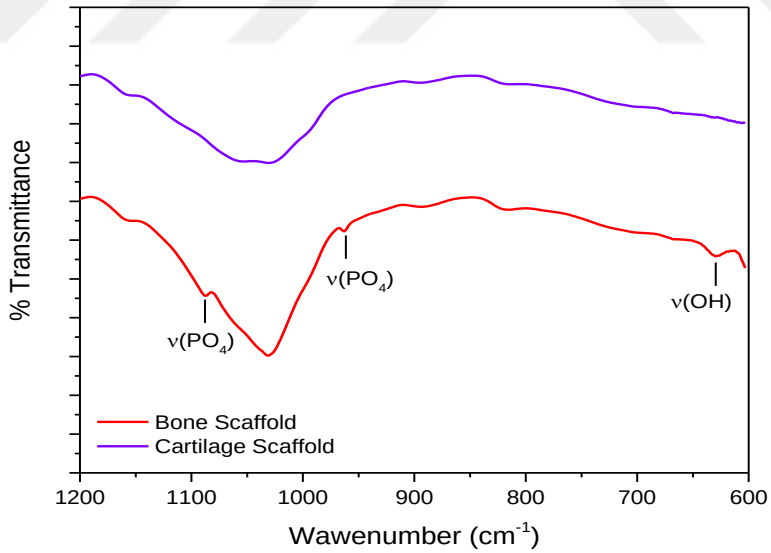

Figure 4. 24 FTIR results of PO4 OH vibrations between 1080, 960 and 630 cm^{-1} wavelengths caused by HA found in bone scaffold.

4.3.2.3 SEM images of 3D printed hydrogel scaffold

Cartilage scaffold in grid pattern and bone scaffold in snowflake pattern were examined with SEM. In addition, the morphological analysis of the osteochondral scaffold, that upper part is grid and lower part is snowflake, was also carried out with SEM. Images taken with different magnification values (50x, 100x and 250x) prove that 3D printing of scaffold was successfully accomplished.

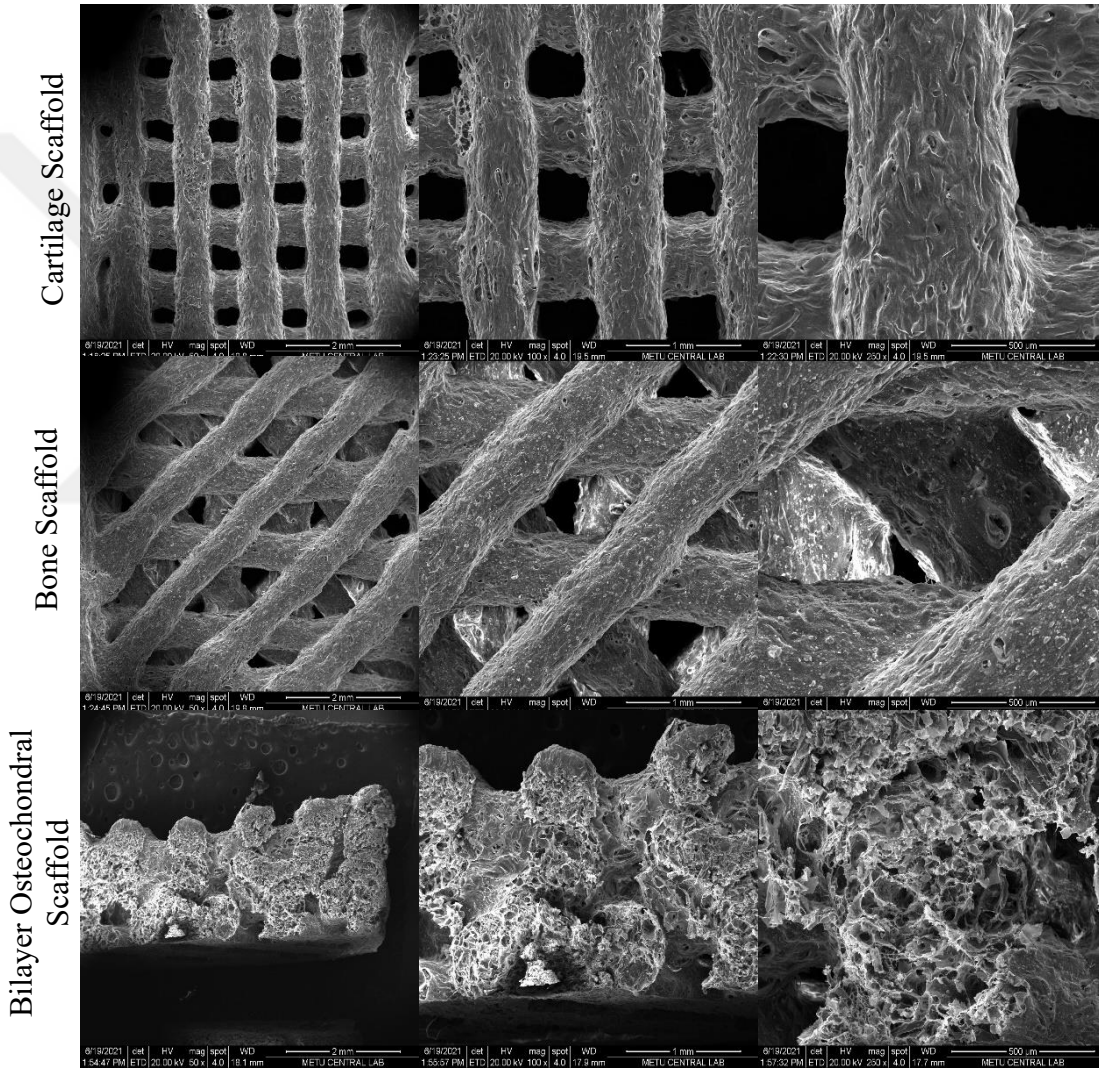

Figure 4. 25 SEM images of 3D printed cartilage, bone, and bilayer osteochondral scaffolds 50x, 100x and 250x magnifications (Scale bar: 2mm, 1mm and 500µm, respectively)

4.4 in vitro Studies

4.4.1 Alamar Blue assay for hydrogel scaffolds

The viability of the cells in the cell-seeded cartilage (Alginate-CMC-Gelatin) and bone scaffolds (Alginate-CMC-Gelatin-HA) was examined by Alamar blue assay. Cell seeding was performed in all groups and cell viability and proliferation were observed. Osteogenic media and bone scaffold were act like control groups; they showed the same graphical increase. However, cell proliferation on cartilage scaffolds in chondrogenic media was less observed from day 1 to 7 (Figure 4.26).

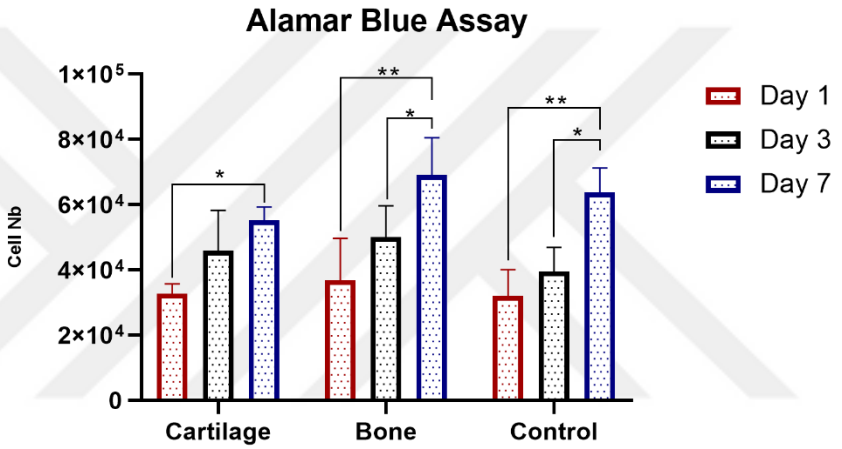

Figure 4. 26 Alamar blue assay of cartilage and bone scaffolds

4.4.2 Live/Dead staining for hydrogel scaffolds

Live/dead staining was applied to the scaffolds on the first day of culture following cell-loaded hydrogel printing. Since the used alginate-CMC- gelatin bioink rapidly degrades in the cell culture medium, only the first day's imaging could be obtained. A successful result could not be observed in this figure.

According to the literature, post-printing cell viability depends on the needle diameter, flow rate, applied pressure, and viscosity of bioink. During the experiment, 300000 cells were loaded into the syringe and mixed with bioink. Based on the data (Figure 4. 26) the cell seeded Alamar blue results, only 12% of cells adhered to the scaffold and proliferated. Even when this ratio is taken into account, it was concluded that the number of cells stained with L/D was much less (Figure 4.27).

After L/D staining was done many times and tried in different staining and techniques, it was decided that this material could not be continued in the culture medium. Bioink obstacled viability of cells or rapidly degraded in cell culture that did not allow to examine the interaction of cell and biomaterial.

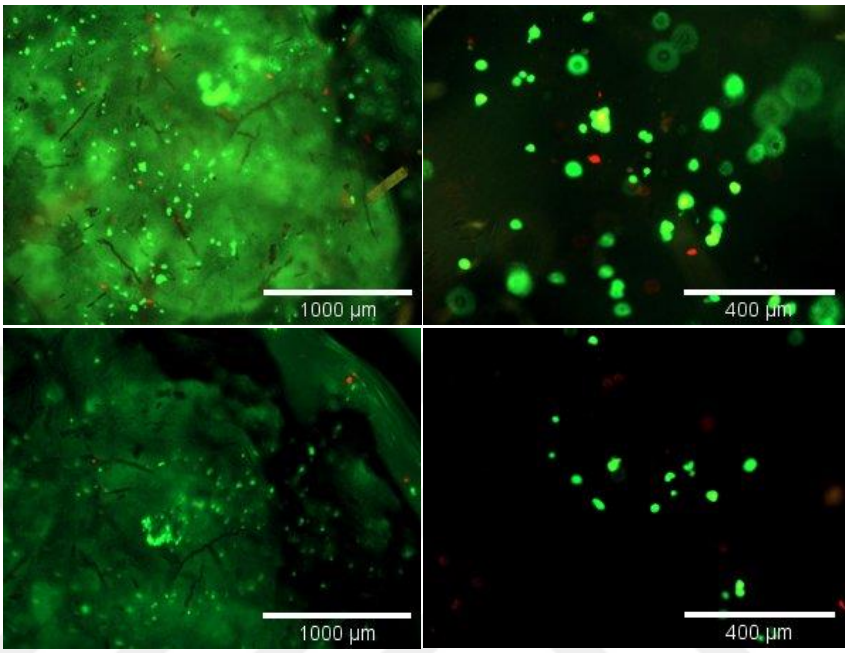

Figure 4. 27 AL-ASCs-laden scaffold L/D staining D0

4.4.3 Alcian Blue and Alizarin Red staining for hydrogel scaffolds

Alcian blue and alizarin red staining were applied according to the sections "3.4.2. Alcian Blue Staining" and "3.4.4. Alizarin Red Staining". As can be seen in Figure 4.28, the dyes completely colored the scaffolds (cartilage (alginate-CMC-gelatin) and bone scaffolds (alginate-CMC-gelatin-HA)). All groups, including the control groups without cells, were stained. As mentioned previously, Alizarin red stains calcium and carbonate minerals whereas Alcian blue detects the presence of glycoproteins; sulfated and carboxylated polysaccharides. So, when alginate-gelatin-carboxymethylcellulose-hydroxy apatite (just for bone) used as scaffold, dyes stained scaffold due characteristic interactions between dyes and scaffolds.

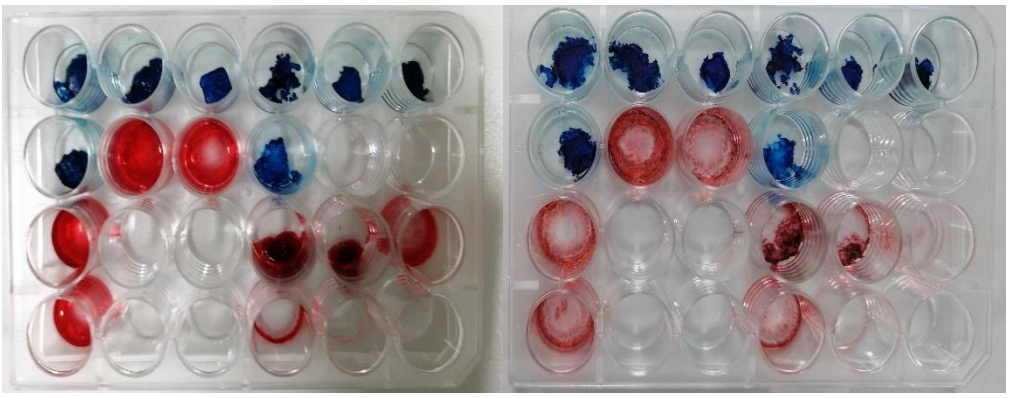

Figure 4. 28 Alcian blue and Alizarin red staining of cartilage and bone scaffolds (Upper figure; wet scaffolds, bottom figure; dry version of scaffolds)

4.4.4 Cryogenic and paraffin-embedded sectioning for scaffolds

Sectioning was taken to analyse the scaffolds by fluorescence staining and to perform differentiation analyses. For this purpose, both paraffin-embedded sectioning and cryogenic sectioning were tried. Since the structure of the alginate-gelatin-CMC hydrogel used became extremely sensitive when cultured, no results could be obtained from the paraffin embedding process due to having the high-temperature structure of paraffin. Cryogenic sectioning was performed successfully (Figure 4.29). However, successful results could not be obtained with the subsequent dyeing studies. No cell staining could be distinguished with Alcian Blue and Alizarin Red staining. The presence of cells could not be detected when the sections taken on the slide were stained with DAPI/Phalloidin due to the instability of scaffold when culturing. The presence of only 1 cell colony was observed (Figure 4.29).

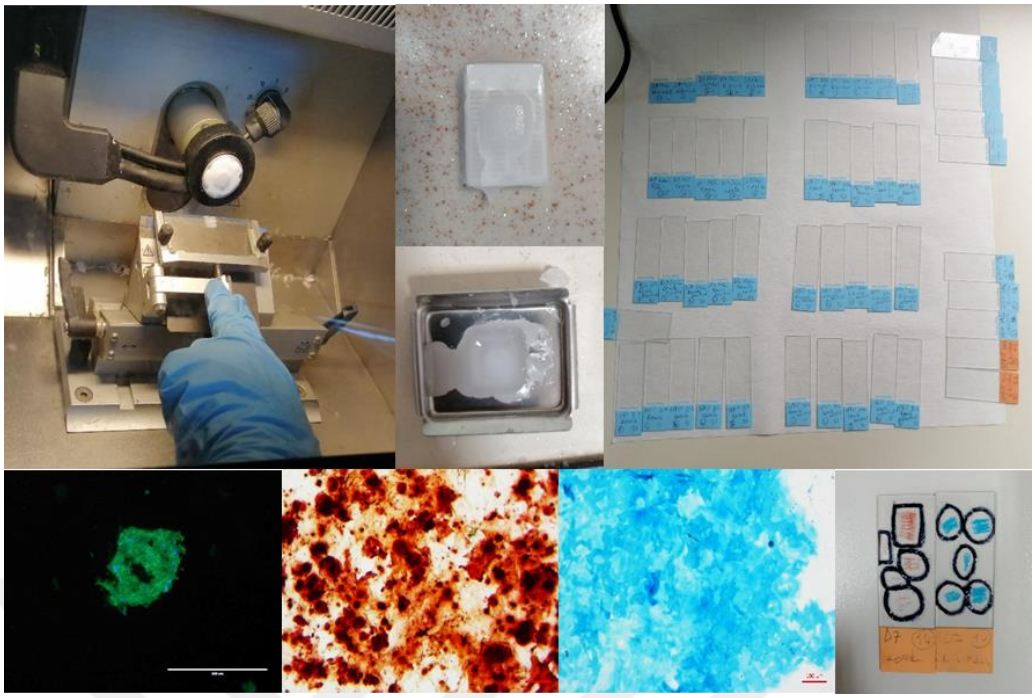

Figure 4. 29 Cell-seeded cartilage and bone scaffolds cryogenic and paraffin-embedded sectioning and D/P, alizarin red and alcian blue staining.

Additional experiments were conducted due to the instability of the CMC-based scaffold during cell culture. It was aimed to create a more stable scaffold by crosslinking the CMC. Firstly, the CMC crosslink was tested using citric acid. No successful results were obtained in the experiment with 10% 20% citric acid. It has been concluded that the success achieved in the reference article depends on the high temperature (Ghorpade et al., 2018). However, the high-temperature application does not constitute a suitable alternative for cell-laden printing. As a second option, crosslinking of CMC was targeted using glutaraldehyde (Siswanta, Wahyuni, & Mudasir, 2020). Although limited amount of crosslink was obtained, it was decided not to use glutaraldehyde because it causes the cytotoxic effect (Fürst & Banerjee, 2005). Finally, CMC crosslink was targeted by using methylenebisacrylamide (MBAAm) crosslink agent with ammonium persulfate (APS) and tetramethyl ethylene diamine (Temed) initiators. In studies using different ratios of BIS, APS and Temed, the CMC crosslink could not be successfully optimized (Figure 4.30). It is foreseen that appropriate optimization can be achieved by continuing the studies on crosslinking CMC with MBAAm, which has the potential to be a new thesis topic.

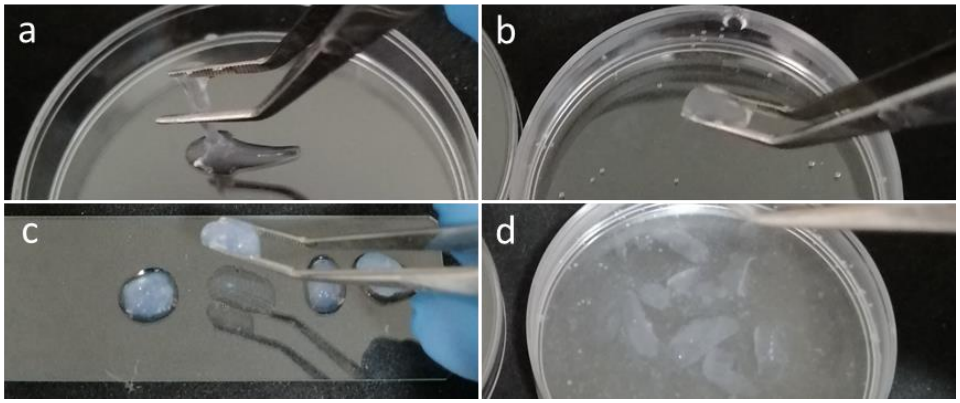

Figure 4. 30 Crosslinking trials of CMC with MBAAm; a) Before crosslink, b) After crosslink with using 6.75mg BIS, c) After crosslink with using 20mg BIS, d) All attempts resulted in degradation

4.4.5 SEM images of capsule loaded bioactive scaffold

In order to perform bioactive scaffold printing, alginate and GelMa bioinks were used. GelMa was dissolved autoclaved water, and V-2-P, TEA and Eosin Y were added to water for modification step. After GelMa modification, alginate was added solution and magnetic stirred until dissolved. The capsules were calculated at 5 mg/scaffold, then distributed to Alginate-GelMa solution. After mixing well, the bioink was loaded into the printing syringe. The Alginate/GelMa scaffold printing parameters were as follows; layer thickness 0.156mm, speed 5 mm/s, pressure 10 msi, temperature 37°C. 25Ga plastic needle tip was used during printing.

Bioactive scaffold printing was carried out successfully with the Alginate-GelMa bioink. Growth factor-loaded PCL capsules were distributed to bioink, then 3D printing of them was performed. SEM morphology analysis was applied to examine the distribution of capsules (Figure 4.31). Incorporation of capsules in cartilage and bone scaffold was successfully obtained. In addition to the capsule, HA particles were distributed homogeneously into the bone scaffold.

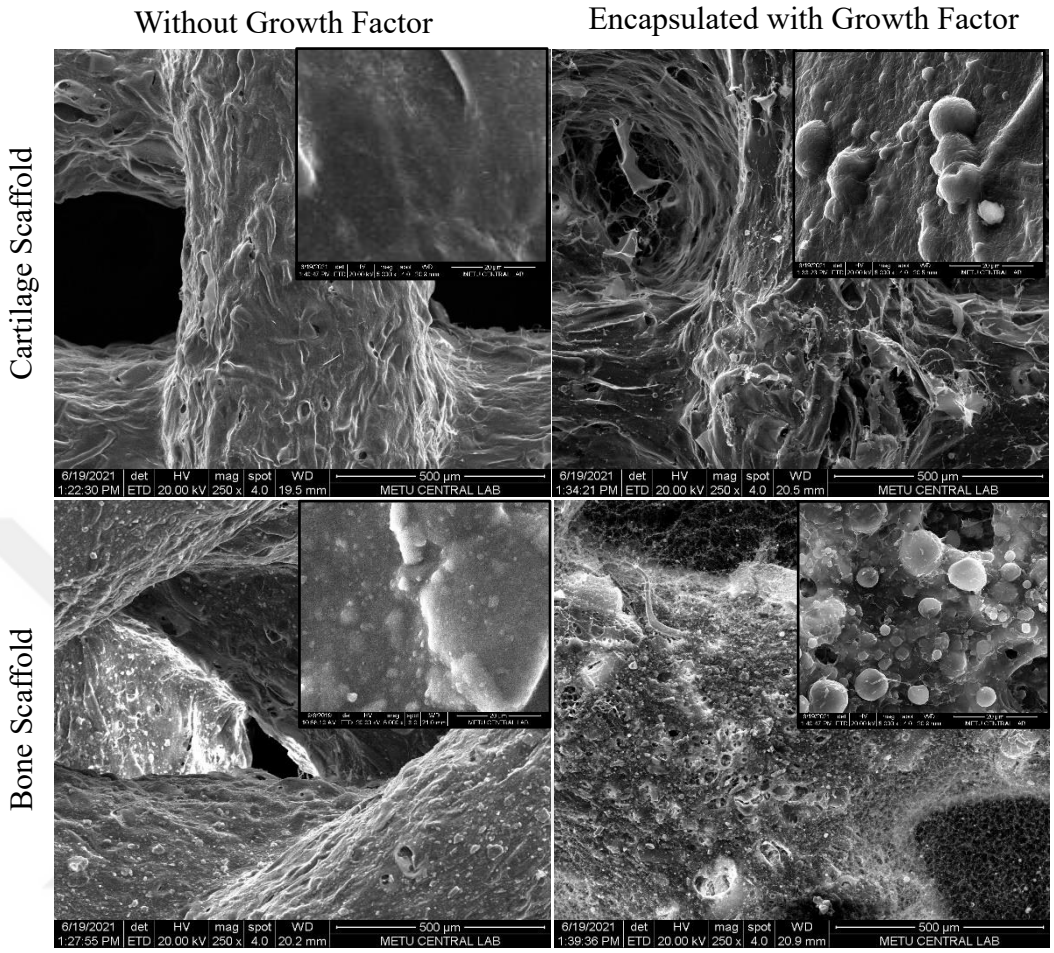

Figure 4. 31 The morphological examination of cartilage and bone scaffold surface and distribution of capsules in scaffolds 250x and 5000x magnifications (Scale bar: 500µm and 20µm)

4.4.6 DAPI/Phalloidin staining of Alginate/GelMa (bioactive) scaffold

DAPI/Phalloidin staining of Alginate-GelMa scaffold was successfully obtained. With the staining performed in D3-7-10 and 14, the nucleus and actin filaments of the cells were indicated. Cells continued to proliferate within the scaffold and spread by forming actin filament extensions (Figure4.32 100µm magnification; Figure 4.33 50µm magnification).

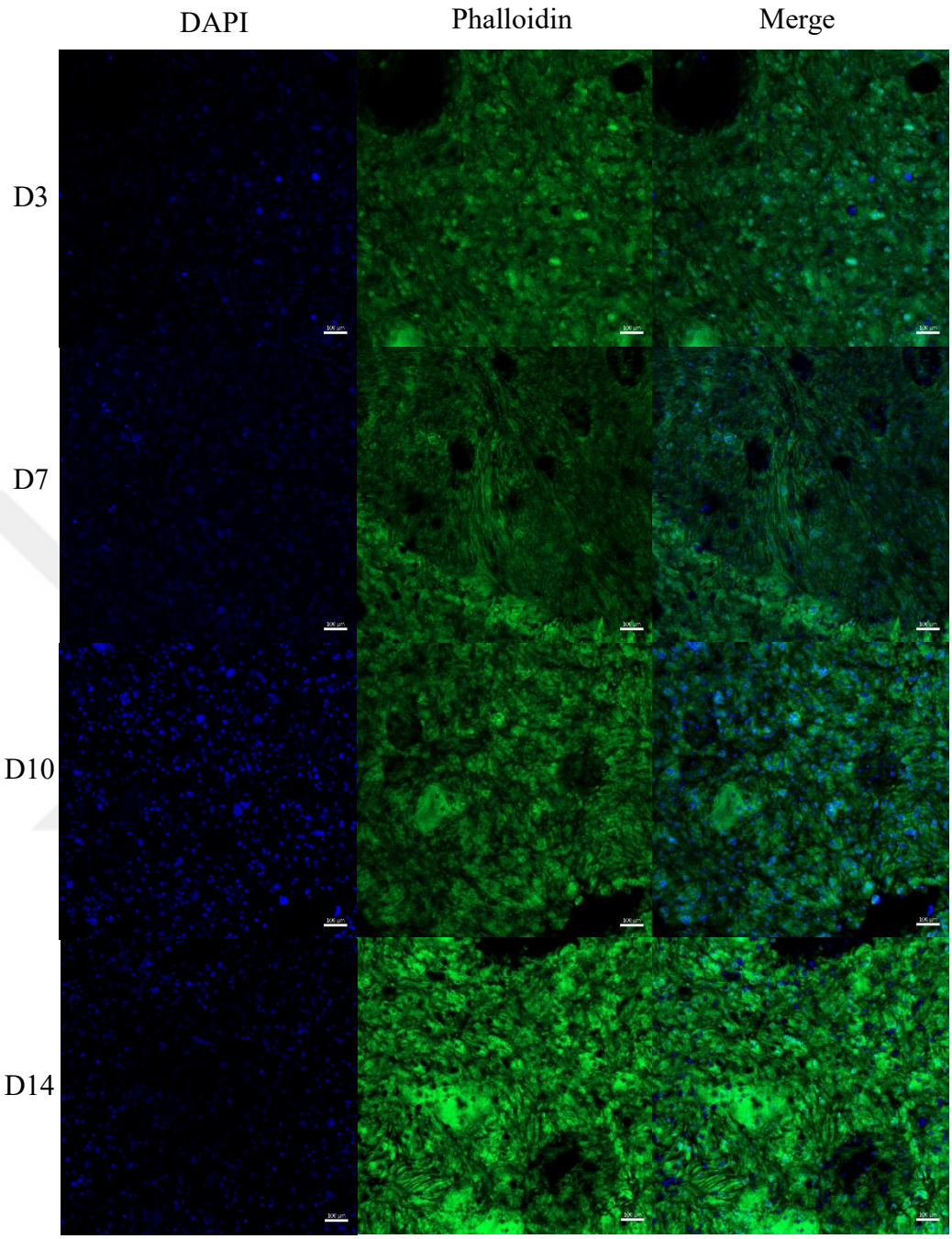

Figure 4. 32 ASCs-laden Alginate-GelMa (5x-100um magnification)

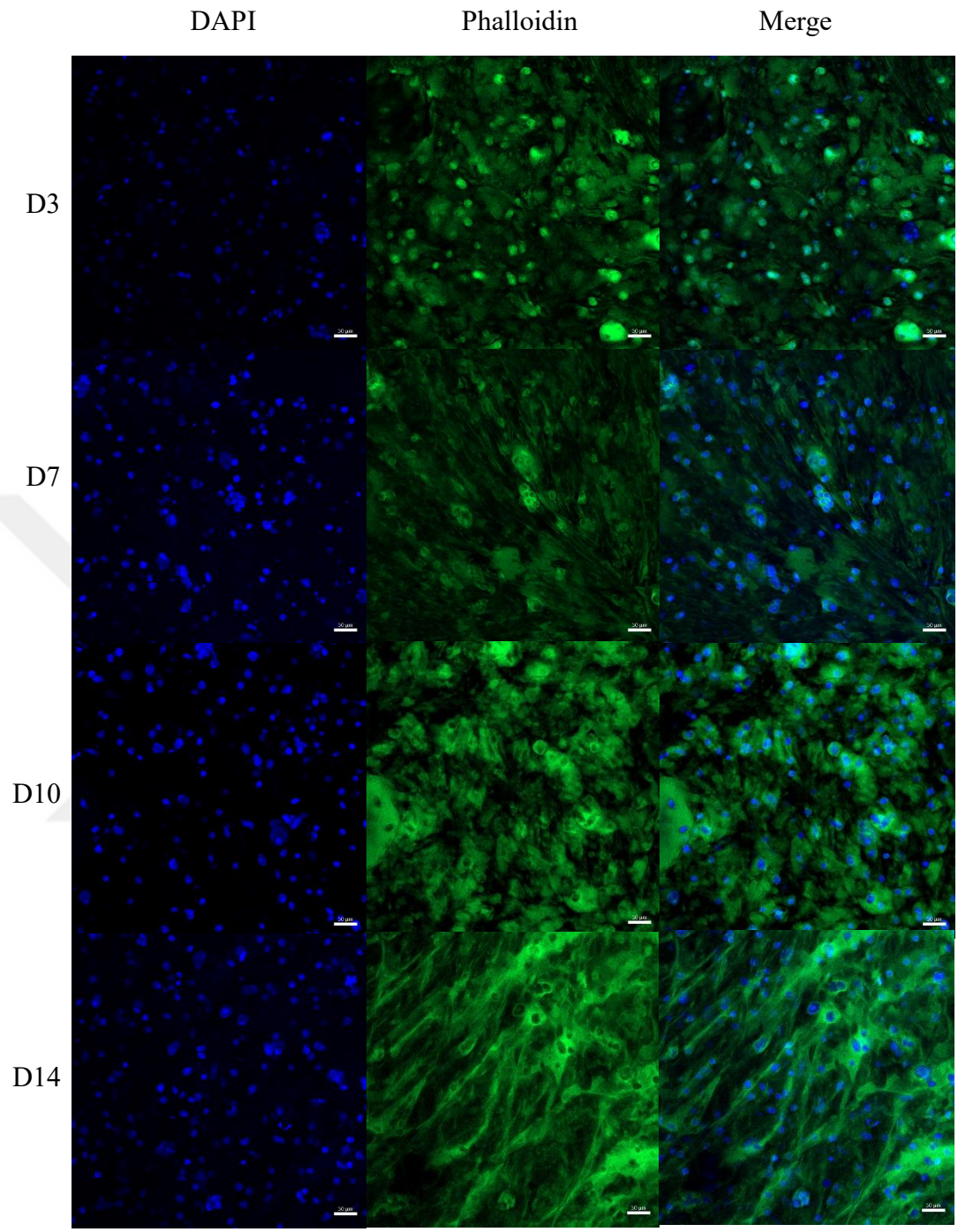

Figure 4. 33 ASCs-laden Alginate-GelMa (10x-50um magnification)

Ongoing studies about the last part of the thesis are continuing. Differentiation analysis of scaffolds created with growth factor loaded capsules and cell-loaded 3D printing are ongoing. The results will be compiled as soon as possible and added to the thesis article.

5. CONCLUSION

More than 2 million arthroscopic knee surgeries are performed worldwide annually and 60% of these surgeries are performed because of osteochondral tissue damage. Due to its nerve-free and avascular structure, the damage can progress and cause subchondral bone tissue damage in addition to cartilage tissue damage over time. Since there is no effective drug treatment that induces cartilage tissue healing, osteochondral tissue regeneration can only be achieved by surgical operation. In order to produce a solution to this need, studies on the production of osteochondral grafts have gained speed with a tissue engineering approach by using cells, biomaterials, and bioactive molecules. Also, stem cells are widely used in tissue engineering due to the difficulties in the isolation and culture of primary cells. Especially mesenchymal stem cells are frequently preferred. The isolation of the adipose-derived stem cells (ASCs) is carried out easily and is obtained a high number of cells due to the abundance of the fat tissue. Another important source of ASCs, especially for osteochondral tissue regeneration, is the infrapatellar fat pad, IPFP. IPFP-ASCs show higher proliferation and differentiation capacity than other stem cells. Also, IPFP-ASCs possess age-independent differentiation capacity as compared to other stem cells.

With this study, it was aimed to investigate osteogenic and chondrogenic differentiation of IPFP- and AL-ASCs with Alizarin Red and Alcian Blue staining. The osteogenic and chondrogenic differentiation capacities of IPFP- and AL-ASCs isolated from two different patient populations, young and mature were evaluated. It was aimed to produce bioactive grafts having two distinct parts in which the osteogenic and chondrogenic differentiation of cells are induced by the spatiotemporal release of site-specific growth factors. The site-specific differentiation of cells was induced by the release of the respective growth factors as well as environmental cues such as HA loaded bioink and denser/looser (snowflake/grid) 3D printed patterns.

According to the results, cell differentiation was successfully carried out by differentiation media. It was concluded that IPFP-ASCs was not shown superior potential for differentiation and viability unlike the hypothesis in the literature. Subsequently, AL-ASCs was utilized as cell source to investigate the cellular interaction of scaffold. The selected bioink could not be cultured in cell media. Although a very well printable bioink

could be obtained with alginate-CMC-gelatin biomaterials, their interaction with the cell could not be investigated due to their highly degradable characteristics in cell culture. Therefore, bioactive and cell-loaded scaffold production was carried out successfully by changing the biomaterial from alginate-CMC-gelatin to alginate-GelMa. Cell proliferation and differentiation assays in alginate-GelMa scaffolds were successfully carried out.

REFERENCES

Ahearne, M., Buckley, C. T., & Kelly, D. J. (2011). A growth factor delivery system for chondrogenic induction of infrapatellar fat pad-derived stem cells in fibrin hydrogels. *Biotechnol Appl Biochem, 58*(5), 345-352. doi:10.1002/bab.45

Altinörs, M. N. (2020). Future Prospects of Organ Transplantation. In *Organ Donation and Transplantation*: IntechOpen.

Ashjian, P. H., Elbarbary, A. S., Edmonds, B., DeUgarte, D., Zhu, M., Zuk, P. A., . . . Hedrick, M. H. (2003). In vitro differentiation of human processed lipoaspirate cells into early neural progenitors. *Plast Reconstr Surg, 111*(6), 1922-1931. doi:10.1097/01.Prs.0000055043.62589.05

Asl, S. A., Mousavi, M., & Labbafi, M. (2017). Synthesis and characterization of carboxymethyl cellulose from sugarcane bagasse. *Journal of Food Processing and Technology, 8*(8).

Augat, P., & Schorlemmer, S. (2006). The role of cortical bone and its microstructure in bone strength. *Age Ageing, 35 Suppl 2*, ii27-ii31. doi:10.1093/ageing/afl081

Augustyniak, E., Trzeciak, T., Richter, M., Kaczmarczyk, J., & Suchorska, W. (2015). The role of growth factors in stem cell-directed chondrogenesis: a real hope for damaged cartilage regeneration. *International Orthopaedics, 39*(5), 995-1003. doi:10.1007/s00264-014-2619-0

Baranova, J. (2018). Lentiviral Vectors for Sustained Inducible Transgene Expression in Human Adipose Tissue Derived Mesenchymal Stem Cells.

Bedi, A., Feeley, B. T., & Williams, R. J. (2010). Management of articular cartilage defects of the knee. *The Journal of bone and joint surgery. American volume, 92*(4), 994-1009. doi:10.2106/jbjs.i.00895

Bello, A. B., Kim, D., Kim, D., Park, H., & Lee, S.-H. (2020). Engineering and functionalization of gelatin biomaterials: From cell culture to medical applications. *Tissue Engineering Part B: Reviews, 26*(2), 164-180.

Benjamin, M., & Evans, E. (1990). Fibrocartilage. *Journal of anatomy, 171*, 1.

Bernhardt, A., Paul, B., & Gelinsky, M. (2018). Biphasic scaffolds from marine collagens for regeneration of osteochondral defects. *Marine drugs, 16*(3), 91.

Bianchi, E., Ruggeri, M., Rossi, S., Vigani, B., Miele, D., Bonferoni, M. C., . . . Ferrari, F. (2021). Innovative Strategies in Tendon Tissue Engineering. *Pharmaceutics, 13*(1), 89. Retrieved from https://www.mdpi.com/1999-4923/13/1/89

Buckley, C. T., Vinardell, T., Thorpe, S. D., Haugh, M. G., Jones, E., McGonagle, D., & Kelly, D. J. (2010). Functional properties of cartilaginous tissues engineered from infrapatellar fat pad-derived mesenchymal stem cells. *J Biomech, 43*(5), 920-926. doi:10.1016/j.jbiomech.2009.11.005

Byun, Y., Hwang, J. B., Bang, S. H., Darby, D., Cooksey, K., Dawson, P. L., . . . Whiteside, S. (2011). Formulation and characterization of α-tocopherol loaded poly ε-caprolactone (PCL) nanoparticles. *Lwt-food science and technology, 44*(1), 24-28.

Caballero Aguilar, L. M., Silva, S. M., & Moulton, S. E. (2019). Growth factor delivery: Defining the next generation platforms for tissue engineering. *J Control Release, 306*, 40-58. doi:10.1016/j.jconrel.2019.05.028

CHANG, C.-H., LIN, C.-C., CHOU, C.-H., LIN, F.-H., & LIU, H.-C. (2005). NOVEL BIOREACTORS FOR OSTEOCHONDRAL TISSUE ENGINEERING. *Biomedical Engineering: Applications, Basis and Communications, 17*(01), 38-43. doi:10.4015/s101623720500007x

Chen, W., Palazzo, A., Hennink, W. E., & Kok, R. J. (2017). Effect of particle size on drug loading and release kinetics of gefitinib-loaded PLGA microspheres. *Molecular pharmaceutics, 14*(2), 459-467.

Chung, J. H., Naficy, S., Yue, Z., Kapsa, R., Quigley, A., Moulton, S. E., & Wallace, G. G. (2013). Bio-ink properties and printability for extrusion printing living cells. *Biomaterials Science, 1*(7), 763-773.

Congcong, L., Nan, Y., Dane, H., Min, S., Sha, P., Anan, L., . . . Wengang, L. (2021). Identification and chondrogenic differentiation of human infrapatellar fat pad derived stem cells. *Chinese Journal of Tissue Engineering Research, 25*(19), 2976.

Conner, B. P., Manogharan, G. P., Martof, A. N., Rodomsky, L. M., Rodomsky, C. M., Jordan, D. C., & Limperos, J. W. (2014). Making sense of 3-D printing: Creating a map of additive manufacturing products and services. *Additive Manufacturing, 1-4*, 64-76. doi:https://doi.org/10.1016/j.addma.2014.08.005

Correia, S. I., Pereira, H., Silva-Correia, J., Van Dijk, C. N., Espregueira-Mendes, J., Oliveira, J. M., & Reis, R. L. (2013). Current concepts: tissue engineering and regenerative medicine applications in the ankle joint. *Journal of the Royal Society, Interface, 11*(92), 20130784-20130784. doi:10.1098/rsif.2013.0784

Cowin, S., & Telega, J. (2003). Bone mechanics handbook. *Appl. Mech. Rev., 56*(4), B61-B63.

Demirbag, B., Huri, P. Y., Kose, G. T., Buyuksungur, A., & Hasirci, V. (2011). Advanced cell therapies with and without scaffolds. *Biotechnology Journal, 6*(12), 1437-1453. doi:https://doi.org/10.1002/biot.201100261

Ding, H., Li, B., Liu, Z., Liu, G., Pu, S., Feng, Y., . . . Zhou, Y. (2021). Nonswelling injectable chitosan hydrogel via UV crosslinking induced hydrophobic effect for minimally invasive tissue engineering. *Carbohydr Polym, 252*, 117143. doi:10.1016/j.carbpol.2020.117143

Doner, G. P., & Noyes, F. R. (2014). Arthroscopic Resection of Fat Pad Lesions and Infrapatellar Contractures. *Arthroscopy Techniques, 3*(3), e413-e416. doi:https://doi.org/10.1016/j.eats.2014.04.002

Dragoo, J. L., Choi, J. Y., Lieberman, J. R., Huang, J., Zuk, P. A., Zhang, J., . . . Benhaim, P. (2003). Bone induction by BMP-2 transduced stem cells derived from human fat. *Journal of Orthopaedic Research, 21*(4), 622-629.

Eggenschwiler, R., & Cantz, T. (2009). Induced pluripotent stem cells generated without viral integration. *Hepatology, 49*(3), 1048-1049. doi:https://doi.org/10.1002/hep.22827

Ertaş, G., Ural, E., Ural, D., Aksoy, A., Kozdağ, G., Gacar, G., & Karaöz, E. (2012). Comparative analysis of apoptotic resistance of mesenchymal stem cells isolated from human bone marrow and adipose tissue. *ScientificWorldJournal, 2012*, 105698. doi:10.1100/2012/105698

Farokhi, M., Jonidi Shariatzadeh, F., Solouk, A., & Mirzadeh, H. (2020). Alginate based scaffolds for cartilage tissue engineering: a review. *International Journal of Polymeric Materials and Polymeric Biomaterials, 69*(4), 230-247.

Felimban, R., Ye, K., Traianedes, K., Di Bella, C., Crook, J., Wallace, G. G., . . . Myers, D. E. (2014). Differentiation of stem cells from human infrapatellar fat pad: characterization of cells undergoing chondrogenesis. *Tissue Eng Part A, 20*(15-16), 2213-2223. doi:10.1089/ten.tea.2013.0657

Fong, J. W. (1990). Process for preparation of microspheres. In: Google Patents.

Fürst, W., & Banerjee, A. (2005). Release of Glutaraldehyde From an Albumin-Glutaraldehyde Tissue Adhesive Causes Significant In Vitro and In Vivo Toxicity. *The Annals of Thoracic Surgery, 79*(5), 1522-1528. doi:https://doi.org/10.1016/j.athoracsur.2004.11.054

Gadjanski, I., & Vunjak-Novakovic, G. (2015). Challenges in engineering osteochondral tissue grafts with hierarchical structures. *Expert Opin Biol Ther, 15*(11), 1583-1599. doi:10.1517/14712598.2015.1070825

Gelse, K., Pöschl, E., & Aigner, T. (2003). Collagens--structure, function, and biosynthesis. *Adv Drug Deliv Rev, 55*(12), 1531-1546. doi:10.1016/j.addr.2003.08.002

Ghorpade, V. S., Yadav, A. V., Dias, R. J., Mali, K. K., Pargaonkar, S. S., Shinde, P. V., & Dhane, N. S. (2018). Citric acid crosslinked carboxymethylcellulose-poly(ethylene glycol) hydrogel films for delivery of poorly soluble drugs. *Int J Biol Macromol, 118*(Pt A), 783-791. doi:10.1016/j.ijbiomac.2018.06.142

Gillogly, S. D., Voight, M., & Blackburn, T. (1998). Treatment of articular cartilage defects of the knee with autologous chondrocyte implantation. *J Orthop Sports Phys Ther, 28*(4), 241-251. doi:10.2519/jospt.1998.28.4.241

Grzesiak, J., Krzysztof, M., Karol, W., & Joanna, C. (2011). Isolation and morphological characterisation of ovine adipose-derived mesenchymal stem cells in culture. *Int J Stem Cells, 4*(2), 99-104. doi:10.15283/ijsc.2011.4.2.99

Gunatillake, P. A., & Adhikari, R. (2003). Biodegradable synthetic polymers for tissue engineering. *Eur Cell Mater, 5*, 1-16; discussion 16. doi:10.22203/ecm.v005a01

Ha, T. L. B., Quan, T. M., & Vu, D. N. (2013). Naturally derived biomaterials: preparation and application. In *Regenerative medicine and tissue engineering*: IntechOpen.

Habib, A., Sathish, V., Mallik, S., & Khoda, B. (2018). 3D printability of alginate-carboxymethyl cellulose hydrogel. *Materials, 11*(3), 454.

Hacker, M. C., Krieghoff, J., & Mikos, A. G. (2019). Synthetic polymers. In *Principles of regenerative medicine* (pp. 559-590): Elsevier.

Hennink, W. E., & van Nostrum, C. F. (2002). Novel crosslinking methods to design hydrogels. *Adv Drug Deliv Rev, 54*(1), 13-36. doi:10.1016/s0169-409x(01)00240-x

Hoemann, C. D. (2004). Molecular and biochemical assays of cartilage components. *Methods Mol Med, 101*, 127-156. doi:10.1385/1-59259-821-8:127

Holloway, J. L., Ma, H., Rai, R., & Burdick, J. A. (2014). Modulating hydrogel crosslink density and degradation to control bone morphogenetic protein delivery and in vivo bone formation. *Journal of Controlled Release, 191*, 63-70.

Hu, X., Xu, J., Li, W., Li, L., Parungao, R., Wang, Y., . . . Song, K. (2020). Therapeutic "Tool" in Reconstruction and Regeneration of Tissue Engineering for Osteochondral Repair. *Appl Biochem Biotechnol, 191*(2), 785-809. doi:10.1007/s12010-019-03214-8

Hunziker, E. B. (1999). Biologic repair of articular cartilage. Defect models in experimental animals and matrix requirements. *Clin Orthop Relat Res*(367 Suppl), S135-146.

Hunziker, E. B. (2002). Articular cartilage repair: basic science and clinical progress. A review of the current status and prospects. *Osteoarthritis Cartilage, 10*(6), 432-463. doi:10.1053/joca.2002.0801

Hunziker, E. B., Lippuner, K., & Shintani, N. (2014). How best to preserve and reveal the structural intricacies of cartilaginous tissue. *Matrix Biology, 39*, 33-43. doi:https://doi.org/10.1016/j.matbio.2014.08.010

Huri, P. Y., Hamsici, S., Ergene, E., Huri, G., & Doral, M. N. (2018). Infrapatellar Fat Pad-Derived Stem Cell-Based Regenerative Strategies in Orthopedic Surgery. *Knee surgery & related research, 30*(3), 179-186. doi:10.5792/ksrr.17.061

Hutton, D. L., Logsdon, E. A., Moore, E. M., Gabhann, F. M., Gimble, J. M., & Grayson, W. L. (2012). Vascular morphogenesis of adipose-derived stem cells is mediated by heterotypic cell-cell interactions. *Tissue Engineering Part A, 18*(15-16), 1729-1740.

Hutton, D. L., Logsdon, E. A., Moore, E. M., Mac Gabhann, F., Gimble, J. M., & Grayson, W. L. (2012). Vascular morphogenesis of adipose-derived stem cells is mediated by heterotypic cell-cell interactions. *Tissue Eng Part A, 18*(15-16), 1729-1740. doi:10.1089/ten.tea.2011.0599

Hutton, D. L., Moore, E. M., Gimble, J. M., & Grayson, W. L. (2013). Platelet-derived growth factor and spatiotemporal cues induce development of vascularized bone tissue by adipose-derived stem cells. *Tissue Eng Part A, 19*(17-18), 2076-2086. doi:10.1089/ten.TEA.2012.0752

Iqbal, M., Valour, J.-P., Fessi, H., & Elaissari, A. (2015). Preparation of biodegradable PCL particles via double emulsion evaporation method using ultrasound technique. *Colloid and Polymer Science, 293*(3), 861-873.

Jafari, S. M., He, Y., & Bhandari, B. (2007). Production of sub-micron emulsions by ultrasound and microfluidization techniques. *Journal of Food Engineering, 82*(4), 478-488.

Jejurikar, A., Seow, X. T., Lawrie, G., Martin, D., Jayakrishnan, A., & Grøndahl, L. (2012). Degradable alginate hydrogels crosslinked by the macromolecular crosslinker alginate dialdehyde. *Journal of Materials Chemistry, 22*(19), 9751-9758.

Jiang, G., Li, S., Yu, K., He, B., Hong, J., Xu, T., . . . Yan, R. (2021). A 3D-printed PRP-GelMA hydrogel promotes osteochondral regeneration through M2 macrophage polarization in a rabbit model. *Acta Biomater*. doi:10.1016/j.actbio.2021.04.010

Jiankang, H., Dichen, L., Yaxiong, L., Bo, Y., Hanxiang, Z., Qin, L., . . . Yi, L. (2009). Preparation of chitosan-gelatin hybrid scaffolds with well-organized microstructures for hepatic tissue engineering. *Acta Biomater, 5*(1), 453-461. doi:10.1016/j.actbio.2008.07.002

Jurgens, W. J., van Dijk, A., Doulabi, B. Z., Niessen, F. B., Ritt, M. J., van Milligen, F. J., & Helder, M. N. (2009). Freshly isolated stromal cells from the infrapatellar fat pad are suitable for a one-step surgical procedure to regenerate cartilage tissue. *Cytotherapy, 11*(8), 1052-1064. doi:10.3109/14653240903219122

Justin, A. W., Burgess, S., Ong, J., Jacob, A. G., Sinha, S., & Markaki, A. E. (2021). Densified Collagen Tubular Grafts for Human Tissue Replacement and Disease Modelling Applications. *bioRxiv*, 2021.2002.2005.429744. doi:10.1101/2021.02.05.429744

Kajave, N. S., Schmitt, T., Nguyen, T. U., Gaharwar, A. K., & Kishore, V. (2020). Bioglass incorporated methacrylated collagen bioactive ink for 3D printing of bone tissue. *Biomed Mater*. doi:10.1088/1748-605X/abc744

Khallok, H., Zbair, M., Ojala, S., Ainassaari, K., Brahmi, R., Keiski, R. L., & Hatim, Z. (2021). Ceramic hydroxyapatite foam as a new material for Bisphenol A removal from contaminated water. *Environmental Science and Pollution Research, 28*(14), 17739-17751.

Khan, W. S., Adesida, A. B., Tew, S. R., Andrew, J. G., & Hardingham, T. E. (2009). The epitope characterisation and the osteogenic differentiation potential of human fat pad-derived stem cells is maintained with ageing in later life. *Injury, 40*(2), 150-157. doi:10.1016/j.injury.2008.05.029

Khan, W. S., Adesida, A. B., Tew, S. R., Longo, U. G., & Hardingham, T. E. (2012). Fat pad-derived mesenchymal stem cells as a potential source for cell-based adipose tissue repair strategies. *Cell Prolif, 45*(2), 111-120. doi:10.1111/j.1365-2184.2011.00804.x

Kheir, E., & Shaw, D. (2009). Hyaline articular cartilage. *Orthopaedics and Trauma, 23*(6), 450-455. doi:https://doi.org/10.1016/j.mporth.2009.01.003

Kilian, D., Ahlfeld, T., Akkineni, A. R., Bernhardt, A., Gelinsky, M., & Lode, A. (2020). 3D Bioprinting of osteochondral tissue substitutes – in vitro-chondrogenesis in multi-layered mineralized constructs. *Scientific Reports, 10*(1), 8277. doi:10.1038/s41598-020-65050-9

Koivisto, J. T., Joki, T., Parraga, J. E., Pääkkönen, R., Ylä-Outinen, L., Salonen, L., . . . Kellomäki, M. (2017). Bioamine-crosslinked gellan gum hydrogel for neural

tissue engineering. *Biomed Mater, 12*(2), 025014. doi:10.1088/1748-605X/aa62b0

KulkarniVishakha, S., ButteKishor, D., Sudha, S., & Mumbai, N. (2012). *Natural Polymers - A Comprehensive Review*.

Kwon, H., Brown, W. E., Lee, C. A., Wang, D., Paschos, N., Hu, J. C., & Athanasiou, K. A. (2019). Surgical and tissue engineering strategies for articular cartilage and meniscus repair. *Nat Rev Rheumatol, 15*(9), 550-570. doi:10.1038/s41584-019-0255-1

Lamprecht, A., Ubrich, N., Pérez, M. H., Lehr, C.-M., Hoffman, M., & Maincent, P. (2000). Influences of process parameters on nanoparticle preparation performed by a double emulsion pressure homogenization technique. *International journal of pharmaceutics, 196*(2), 177-182.

Lee, C. H., Kim, J. H., Lee, H. J., Jeon, K., Lim, H., Choi, H., . . . Cho, S. G. (2011). The generation of iPS cells using non-viral magnetic nanoparticle based transfection. *Biomaterials, 32*(28), 6683-6691. doi:10.1016/j.biomaterials.2011.05.070

Lee, K. Y., & Mooney, D. J. (2001). Hydrogels for tissue engineering. *Chemical reviews, 101*(7), 1869-1880.

Lee, M., Wu, B. M., & Dunn, J. C. (2008). Effect of scaffold architecture and pore size on smooth muscle cell growth. *Journal of Biomedical Materials Research Part A: An Official Journal of The Society for Biomaterials, The Japanese Society for Biomaterials, and The Australian Society for Biomaterials and the Korean Society for Biomaterials, 87*(4), 1010-1016.

Levingstone, T. J., Thompson, E., Matsiko, A., Schepens, A., Gleeson, J. P., & O'Brien, F. J. (2016). Multi-layered collagen-based scaffolds for osteochondral defect repair in rabbits. *Acta Biomater, 32*, 149-160. doi:10.1016/j.actbio.2015.12.034

Li, G., Yin, J., Gao, J., Cheng, T. S., Pavlos, N. J., Zhang, C., & Zheng, M. H. (2013). Subchondral bone in osteoarthritis: insight into risk factors and microstructural changes. *Arthritis Res Ther, 15*(6), 223. doi:10.1186/ar4405

Li, Z., Jia, S., Xiong, Z., Long, Q., Yan, S., Hao, F., . . . Yuan, Z. (2018). 3D-printed scaffolds with calcified layer for osteochondral tissue engineering. *J Biosci Bioeng, 126*(3), 389-396. doi:10.1016/j.jbiosc.2018.03.014

Lin, C. S., Xin, Z. C., Dai, J., & Lue, T. F. (2013). Commonly used mesenchymal stem cell markers and tracking labels: Limitations and challenges. *Histol Histopathol, 28*(9), 1109-1116. doi:10.14670/hh-28.1109

Lin, X., Patil, S., Gao, Y. G., & Qian, A. (2020). The Bone Extracellular Matrix in Bone Formation and Regeneration. *Front Pharmacol, 11*, 757. doi:10.3389/fphar.2020.00757

Liu, N., Ye, X., Yao, B., Zhao, M., Wu, P., Liu, G., . . . Zhu, P. (2021). Advances in 3D bioprinting technology for cardiac tissue engineering and regeneration. *Bioactive Materials, 6*(5), 1388-1401. doi:https://doi.org/10.1016/j.bioactmat.2020.10.021

Liu, Y., Buckley, C. T., Almeida, H. V., Mulhall, K. J., & Kelly, D. J. (2014). Infrapatellar fat pad-derived stem cells maintain their chondrogenic capacity in disease and can

be used to engineer cartilaginous grafts of clinically relevant dimensions. *Tissue Eng Part A, 20*(21-22), 3050-3062. doi:10.1089/ten.TEA.2014.0035

Liu, Y., Gu, J., & Fan, D. (2020). Fabrication of high-strength and porous hybrid scaffolds based on nano-hydroxyapatite and human-like collagen for bone tissue regeneration. *Polymers, 12*(1), 61.

Madry, H., Rey-Rico, A., Venkatesan, J. K., Johnstone, B., & Cucchiarini, M. (2014). Transforming growth factor beta-releasing scaffolds for cartilage tissue engineering. *Tissue Engineering Part B: Reviews, 20*(2), 106-125.

Madry, H., van Dijk, C. N., & Mueller-Gerbl, M. (2010). The basic science of the subchondral bone. *Knee Surg Sports Traumatol Arthrosc, 18*(4), 419-433. doi:10.1007/s00167-010-1054-z

Maharjan, B., Park, J., Kaliannagounder, V. K., Awasthi, G. P., Joshi, M. K., Park, C. H., & Kim, C. S. (2021). Regenerated cellulose nanofiber reinforced chitosan hydrogel scaffolds for bone tissue engineering. *Carbohydr Polym, 251*, 117023. doi:10.1016/j.carbpol.2020.117023

Mahfouzi, S. H., Safiabadi Tali, S. H., & Amoabediny, G. (2021). 3D bioprinting for lung and tracheal tissue engineering: Criteria, advances, challenges, and future directions. *Bioprinting, 21*, e00124. doi:https://doi.org/10.1016/j.bprint.2020.e00124

Maia, J., Santana, M., & Ré, M. (2004). The effect of some processing conditions on the characteristics of biodegradable microspheres obtained by an emulsion solvent evaporation process. *Brazilian Journal of Chemical Engineering, 21*(1), 01-12.

Martin, I., Miot, S., Barbero, A., Jakob, M., & Wendt, D. (2007). Osteochondral tissue engineering. *J Biomech, 40*(4), 750-765. doi:10.1016/j.jbiomech.2006.03.008

Meligy, F. Y., Shigemura, K., Behnsawy, H. M., Fujisawa, M., Kawabata, M., & Shirakawa, T. (2012). The efficiency of in vitro isolation and myogenic differentiation of MSCs derived from adipose connective tissue, bone marrow, and skeletal muscle tissue. *In Vitro Cellular & Developmental Biology - Animal, 48*(4), 203-215. doi:10.1007/s11626-012-9488-x

Messaoudi, O., Henrionnet, C., Bourge, K., Loeuille, D., Gillet, P., & Pinzano, A. (2021). Stem Cells and Extrusion 3D Printing for Hyaline Cartilage Engineering. *Cells, 10*(1), 2. Retrieved from https://www.mdpi.com/2073-4409/10/1/2

Mitchell, N., & Shepard, N. (1976). The resurfacing of adult rabbit articular cartilage by multiple perforations through the subchondral bone. *J Bone Joint Surg Am, 58*(2), 230-233.

Mochizuki, T., Muneta, T., Sakaguchi, Y., Nimura, A., Yokoyama, A., Koga, H., & Sekiya, I. (2006). Higher chondrogenic potential of fibrous synovium- and adipose synovium-derived cells compared with subcutaneous fat-derived cells: distinguishing properties of mesenchymal stem cells in humans. *Arthritis Rheum, 54*(3), 843-853. doi:10.1002/art.21651

Mohan, N., Dormer, N. H., Caldwell, K. L., Key, V. H., Berkland, C. J., & Detamore, M. S. (2011). Continuous gradients of material composition and growth factors for

effective regeneration of the osteochondral interface. *Tissue Engineering Part A, 17*(21-22), 2845-2855.

Montazeri, N., Jahandideh, R., & Biazar, E. (2011). Synthesis of fluorapatite–hydroxyapatite nanoparticles and toxicity investigations. *International journal of nanomedicine, 6*, 197.

Moses, J. C., Saha, T., & Mandal, B. B. (2020). Chondroprotective and osteogenic effects of silk-based bioinks in developing 3D bioprinted osteochondral interface. *Bioprinting, 17*, e00067. doi:https://doi.org/10.1016/j.bprint.2019.e00067

Mueller, M. B., Fischer, M., Zellner, J., Berner, A., Dienstknecht, T., Prantl, L., . . . Angele, P. (2010). Hypertrophy in mesenchymal stem cell chondrogenesis: effect of TGF-β isoforms and chondrogenic conditioning. *Cells Tissues Organs, 192*(3), 158-166.

Neri, S., Guidotti, S., Lilli, N. L., Cattini, L., & Mariani, E. (2017). Infrapatellar fat pad-derived mesenchymal stromal cells from osteoarthritis patients: In vitro genetic stability and replicative senescence. *Journal of Orthopaedic Research, 35*(5), 1029-1037.

Nukavarapu, S. P., & Dorcemus, D. L. (2013). Osteochondral tissue engineering: current strategies and challenges. *Biotechnol Adv, 31*(5), 706-721. doi:10.1016/j.biotechadv.2012.11.004

Okita, K., Nakagawa, M., Hyenjong, H., Ichisaka, T., & Yamanaka, S. (2008). Generation of mouse induced pluripotent stem cells without viral vectors. *Science, 322*(5903), 949-953. doi:10.1126/science.1164270

Panseri, S., Russo, A., Cunha, C., Bondi, A., Di Martino, A., Patella, S., & Kon, E. (2012). Osteochondral tissue engineering approaches for articular cartilage and subchondral bone regeneration. *Knee Surg Sports Traumatol Arthrosc, 20*(6), 1182-1191. doi:10.1007/s00167-011-1655-1

Park, B. J., Choi, H. J., Moon, S. J., Kim, S. J., Bajracharya, R., Min, J. Y., & Han, H.-K. (2019). Pharmaceutical applications of 3D printing technology: Current understanding and future perspectives. *Journal of Pharmaceutical Investigation, 49*(6), 575-585.

Park, H. Y., Noh, E. H., Chung, H.-M., Kang, M.-J., Kim, E. Y., & Park, S. P. (2012). Efficient Generation of Virus-Free iPS Cells Using Liposomal Magnetofection. *PLOS ONE, 7*(9), e45812. doi:10.1371/journal.pone.0045812

Park, J., & Lakes, R. S. (2007). *Biomaterials: an introduction*: Springer Science & Business Media.

Park, J. Y., Choi, J. C., Shim, J. H., Lee, J. S., Park, H., Kim, S. W., . . . Cho, D. W. (2014). A comparative study on collagen type I and hyaluronic acid dependent cell behavior for osteochondral tissue bioprinting. *Biofabrication, 6*(3), 035004. doi:10.1088/1758-5082/6/3/035004

Parsons, J. (1998). Cartilage. In *Handbook of biomaterial properties* (pp. 40-47): Springer.

Prabha, R. D., Nair, B. P., Ditzel, N., Kjems, J., Nair, P. D., & Kassem, M. (2019). Strontium functionalized scaffold for bone tissue engineering. *Materials Science and Engineering: C, 94*, 509-515.

Rajalekshmi, R., Kaladevi Shaji, A., Joseph, R., & Bhatt, A. (2021). Scaffold for liver tissue engineering: Exploring the potential of fibrin incorporated alginate dialdehyde-gelatin hydrogel. *Int J Biol Macromol, 166*, 999-1008. doi:10.1016/j.ijbiomac.2020.10.256

Ramos, P. E., Silva, P., Alario, M. M., Pastrana, L. M., Teixeira, J. A., Cerqueira, M. A., & Vicente, A. A. (2018). Effect of alginate molecular weight and M/G ratio in beads properties foreseeing the protection of probiotics. *Food Hydrocolloids, 77*, 8-16.

Ratner, B. D., Hoffman, A. S., Schoen, F. J., & Lemons, J. E. (2004). *Biomaterials science: an introduction to materials in medicine*: Elsevier.

Reddy, M. S. B., Ponnamma, D., Choudhary, R., & Sadasivuni, K. K. (2021). A Comparative Review of Natural and Synthetic Biopolymer Composite Scaffolds. *Polymers, 13*(7), 1105. doi:10.3390/polym13071105

Resmi, R., Parvathy, J., John, A., & Joseph, R. (2020). Injectable self-crosslinking hydrogels for meniscal repair: A study with oxidized alginate and gelatin. *Carbohydrate polymers, 234*, 115902. doi:10.1016/j.carbpol.2020.115902

Rho, J. Y., Kuhn-Spearing, L., & Zioupos, P. (1998). Mechanical properties and the hierarchical structure of bone. *Med Eng Phys, 20*(2), 92-102. doi:10.1016/s1350-4533(98)00007-1

Riaz, T., Zeeshan, R., Zarif, F., Ilyas, K., Muhammad, N., Safi, S. Z., . . . Rehman, I. U. (2018). FTIR analysis of natural and synthetic collagen. *Applied Spectroscopy Reviews, 53*(9), 703-746.

Robey, P. G. (2002). Chapter 14 - Bone Matrix Proteoglycans and Glycoproteins. In J. P. Bilezikian, L. G. Raisz, & G. A. Rodan (Eds.), *Principles of Bone Biology (Second Edition)* (pp. 225-237). San Diego: Academic Press.

Saha, S., Kundu, B., Kirkham, J., Wood, D., Kundu, S. C., & Yang, X. B. (2013). Osteochondral tissue engineering in vivo: a comparative study using layered silk fibroin scaffolds from mulberry and nonmulberry silkworms. *PLoS One, 8*(11), e80004. doi:10.1371/journal.pone.0080004

Sasaki, A., Mizuno, M., Ozeki, N., Katano, H., Otabe, K., Tsuji, K., . . . Sekiya, I. (2018). Canine mesenchymal stem cells from synovium have a higher chondrogenic potential than those from infrapatellar fat pad, adipose tissue, and bone marrow. *PLoS One, 13*(8), e0202922. doi:10.1371/journal.pone.0202922

Savoji, H., Davenport Huyer, L., Mohammadi, M. H., Lun Lai, B. F., Rafatian, N., Bannerman, D., . . . Radisic, M. (2020). 3D Printing of Vascular Tubes Using Bioelastomer Prepolymers by Freeform Reversible Embedding. *ACS Biomaterials Science & Engineering, 6*(3), 1333-1343. doi:10.1021/acsbiomaterials.9b00676

Seo, S. J., Mahapatra, C., Singh, R. K., Knowles, J. C., & Kim, H. W. (2014). Strategies for osteochondral repair: Focus on scaffolds. *J Tissue Eng, 5*, 2041731414541850. doi:10.1177/2041731414541850

Sharma, C., Gautam, S., Dinda, A. K., & Mishra, N. C. (2011). Cartilage tissue engineering: current scenario and challenges. *Adv Mater Lett, 2*(2), 90-99.

Shepherd, J., Bax, D., Best, S., & Cameron, R. (2017). Collagen-Fibrinogen Lyophilised Scaffolds for Soft Tissue Regeneration. *Materials (Basel, Switzerland), 10*(6), 568. doi:10.3390/ma10060568

Shimomura, K., Moriguchi, Y., Murawski, C. D., Yoshikawa, H., & Nakamura, N. (2014). Osteochondral tissue engineering with biphasic scaffold: current strategies and techniques. *Tissue Eng Part B Rev, 20*(5), 468-476. doi:10.1089/ten.TEB.2013.0543

Siepmann, J., Faisant, N., Akiki, J., Richard, J., & Benoit, J. (2004). Effect of the size of biodegradable microparticles on drug release: experiment and theory. *Journal of Controlled Release, 96*(1), 123-134.

Singh, Y. P., Moses, J. C., Bhunia, B. K., Nandi, S. K., & Mandal, B. B. (2018). Hierarchically structured seamless silk scaffolds for osteochondral interface tissue engineering. *Journal of materials chemistry. B, 6*(36), 5671-5688. doi:10.1039/c8tb01344f

Siswanta, D., Wahyuni, R., & Mudasir, M. (2020). Synthesis of Glutaraldehyde-Crosslinked Carboxymethyl Cellulose-Polyvinyl Alcohol Film as an Adsorbent for Methylene Blue. *Key Engineering Materials, 840*, 35-42. doi:10.4028/www.scientific.net/KEM.840.35

Stewart, H. L., & Kawcak, C. E. (2018). The Importance of Subchondral Bone in the Pathophysiology of Osteoarthritis. *Frontiers in veterinary science, 5*, 178-178. doi:10.3389/fvets.2018.00178

Su, T., Zhang, M., Zeng, Q., Pan, W., Huang, Y., Qian, Y., . . . Shen, J. (2021). Mussel-inspired agarose hydrogel scaffolds for skin tissue engineering. *Bioactive Materials, 6*(3), 579-588. doi:https://doi.org/10.1016/j.bioactmat.2020.09.004

Subia, B., Kundu, J., & Kundu, S. (2010). Biomaterial scaffold fabrication techniques for potential tissue engineering applications. *Tissue engineering, 141*.

Tack, P., Victor, J., Gemmel, P., & Annemans, L. (2016). 3D-printing techniques in a medical setting: a systematic literature review. *Biomed Eng Online, 15*(1), 115. doi:10.1186/s12938-016-0236-4

Takahashi, K., & Yamanaka, S. (2006). Induction of pluripotent stem cells from mouse embryonic and adult fibroblast cultures by defined factors. *Cell, 126*(4), 663-676. doi:10.1016/j.cell.2006.07.024

Tangchitphisut, P., Srikaew, N., Numhom, S., Tangprasittipap, A., Woratanarat, P., Wongsak, S., . . . Tawonsawatruk, T. (2016). Infrapatellar Fat Pad: An Alternative Source of Adipose-Derived Mesenchymal Stem Cells. *Arthritis, 2016*, 4019873-4019873. doi:10.1155/2016/4019873

Temenoff, J. S., & Mikos, A. G. (2000). Review: tissue engineering for regeneration of articular cartilage. *Biomaterials, 21*(5), 431-440. doi:10.1016/s0142-9612(99)00213-6

Temple, J. P., Hutton, D. L., Hung, B. P., Huri, P. Y., Cook, C. A., Kondragunta, R., . . . Grayson, W. L. (2014). Engineering anatomically shaped vascularized bone grafts with hASCs and 3D-printed PCL scaffolds. *Journal of Biomedical Materials Research Part A, 102*(12), 4317-4325. doi:https://doi.org/10.1002/jbm.a.35107

Thomas-Busani, C., Sarabia-Sainz, J. A., García-Hernández, J., Madera-Santana, T. J., Vázquez-Moreno, L., & Montfort, G. R.-C. (2020). Synthesis of alginate–polycation capsules of different composition: characterization and their adsorption for [As (iii)] and [As (v)] from aqueous solutions. *RSC Advances, 10*(48), 28755-28765.

TOPALOĞLU, U., KETANİ, M. A., & SARUHAN, B. G. (2017). Kemik doku ve kemikleşme çeşitleri. *Dicle Üniversitesi Veteriner Fakültesi Dergisi, 10*(1), 62-71.

Tzelepi, V., Tsamandas, A. C., Zolota, V., & Scopa, C. D. (2009). Bone Anatomy, Physiology and Function. In D. Kardamakis, V. Vassiliou, & E. Chow (Eds.), *Bone Metastases: A translational and clinical approach* (pp. 3-30). Dordrecht: Springer Netherlands.

van der Harst, M. R., Brama, P. A. J., van de Lest, C. H. A., Kiers, G. H., DeGroot, J., & van Weeren, P. R. (2004). An integral biochemical analysis of the main constituents of articular cartilage, subchondral and trabecular bone. *Osteoarthritis and Cartilage, 12*(9), 752-761. doi:https://doi.org/10.1016/j.joca.2004.05.004

Varma, M. J., Breuls, R. G., Schouten, T. E., Jurgens, W. J., Bontkes, H. J., Schuurhuis, G. J., . . . van Milligen, F. J. (2007). Phenotypical and functional characterization of freshly isolated adipose tissue-derived stem cells. *Stem Cells Dev, 16*(1), 91-104. doi:10.1089/scd.2006.0026

Vichi, A., Eliazyan, G., & Kazarian, S. G. (2018). Study of the degradation and conservation of historical leather book covers with macro attenuated total reflection–Fourier transform infrared spectroscopic imaging. *ACS omega, 3*(7), 7150-7157.

Wang, C.-C., Chen, I.-H., Yang, Y.-T., Chen, Y.-R., & Yang, K.-C. (2021). Infrapatellar Fat Pads–Derived Stem Cell Is a Favorable Cell Source for Articular Cartilage Tissue Engineering: An In Vitro and Ex Vivo Study Based on 3D Organized Self-Assembled Biomimetic Scaffold. *Cartilage*, 1947603520988153.

Wang, H., Zou, Q., Boerman, O. C., Nijhuis, A. W., Jansen, J. A., Li, Y., & Leeuwenburgh, S. C. (2013). Combined delivery of BMP-2 and bFGF from nanostructured colloidal gelatin gels and its effect on bone regeneration in vivo. *Journal of Controlled Release, 166*(2), 172-181.

Wang, Z., Wang, Z., Lu, W. W., Zhen, W., Yang, D., & Peng, S. (2017). Novel biomaterial strategies for controlled growth factor delivery for biomedical applications. *NPG Asia Materials, 9*(10), e435-e435. doi:10.1038/am.2017.171

Wickham, M. Q., Erickson, G. R., Gimble, J. M., Vail, T. P., & Guilak, F. (2003). Multipotent stromal cells derived from the infrapatellar fat pad of the knee. *Clinical Orthopaedics and Related Research®, 412*, 196-212.

Woolf, A. D., & Pfleger, B. (2003). Burden of major musculoskeletal conditions. *Bulletin of the World Health Organization, 81*(9), 646-656. Retrieved from https://pubmed.ncbi.nlm.nih.gov/14710506

Wu, L., Cai, X., Zhang, S., Karperien, M., & Lin, Y. (2013). Regeneration of articular cartilage by adipose tissue derived mesenchymal stem cells: perspectives from stem cell biology and molecular medicine. *J Cell Physiol, 228*(5), 938-944. doi:10.1002/jcp.24255

Wu, Z., Su, X., Xu, Y., Kong, B., Sun, W., & Mi, S. (2016). Bioprinting three-dimensional cell-laden tissue constructs with controllable degradation. *Scientific reports, 6*(1), 24474. doi:10.1038/srep24474

Yang, J., Shi, P., Tu, M., Wang, Y., Liu, M., Fan, F., & Du, M. (2014). Bone morphogenetic proteins: Relationship between molecular structure and their osteogenic activity. *Food Science and Human Wellness, 3*(3), 127-135. doi:https://doi.org/10.1016/j.fshw.2014.12.002

Yang, Y., Yang, G., Song, Y., Xu, Y., Zhao, S., & Zhang, W. (2020). 3D Bioprinted Integrated Osteochondral Scaffold-Mediated Repair of Articular Cartilage Defects in the Rabbit Knee. *Journal of Medical and Biological Engineering, 40*(1), 71-81. doi:10.1007/s40846-019-00481-y

Ye, K., Felimban, R., Traianedes, K., Moulton, S. E., Wallace, G. G., Chung, J., . . . Myers, D. E. (2014). Chondrogenesis of Infrapatellar Fat Pad Derived Adipose Stem Cells in 3D Printed Chitosan Scaffold. *PLOS ONE, 9*(6), e99410. doi:10.1371/journal.pone.0099410

Yilgor Huri, P., Cook, C. A., Hutton, D. L., Goh, B. C., Gimble, J. M., DiGirolamo, D. J., & Grayson, W. L. (2013). Biophysical cues enhance myogenesis of human adipose derived stem/stromal cells. *Biochem Biophys Res Commun, 438*(1), 180-185. doi:10.1016/j.bbrc.2013.07.049

Yilgor, P., Sousa, R. A., Reis, R. L., Hasirci, N., & Hasirci, V. (2010). Effect of scaffold architecture and BMP-2/BMP-7 delivery on in vitro bone regeneration. *J Mater Sci Mater Med, 21*(11), 2999-3008. doi:10.1007/s10856-010-4150-1

Yilgor, P., Tuzlakoglu, K., Reis, R. L., Hasirci, N., & Hasirci, V. (2009). Incorporation of a sequential BMP-2/BMP-7 delivery system into chitosan-based scaffolds for bone tissue engineering. *Biomaterials, 30*(21), 3551-3559. doi:https://doi.org/10.1016/j.biomaterials.2009.03.024

Yoshimura, K., Shigeura, T., Matsumoto, D., Sato, T., Takaki, Y., Aiba-Kojima, E., . . . Gonda, K. (2006). Characterization of freshly isolated and cultured cells derived from the fatty and fluid portions of liposuction aspirates. *J Cell Physiol, 208*(1), 64-76. doi:10.1002/jcp.20636

Zhang, M., Li, Y., Rao, P., Huang, K., Luo, D., Cai, X., & Xiao, J. (2018). Blockade of receptors of advanced glycation end products ameliorates diabetic osteogenesis of

adipose-derived stem cells through DNA methylation and Wnt signalling pathway. *Cell proliferation, 51*(5), e12471.

Zhao, X., Lang, Q., Yildirimer, L., Lin, Z. Y., Cui, W., Annabi, N., . . . Khademhosseini, A. (2016). Photocrosslinkable Gelatin Hydrogel for Epidermal Tissue Engineering. *Adv Healthc Mater, 5*(1), 108-118. doi:10.1002/adhm.201500005

Zheng, P., Hu, X., Lou, Y., & Tang, K. (2019). A Rabbit Model of Osteochondral Regeneration Using Three-Dimensional Printed Polycaprolactone-Hydroxyapatite Scaffolds Coated with Umbilical Cord Blood Mesenchymal Stem Cells and Chondrocytes. *Medical science monitor : international medical journal of experimental and clinical research, 25*, 7361-7369. doi:10.12659/MSM.915441

Zhong, Y.-c., Wang, S.-c., Han, Y.-h., & Wen, Y. (2020). Recent advance in source, property, differentiation, and applications of infrapatellar fat pad adipose-derived stem cells. *Stem cells international, 2020*.

Zuk, P. A., Zhu, M., Ashjian, P., De Ugarte, D. A., Huang, J. I., Mizuno, H., . . . Hedrick, M. H. (2002). Human adipose tissue is a source of multipotent stem cells. *Molecular biology of the cell, 13*(12), 4279-4295.

APPENDICES

APPENDIX 1

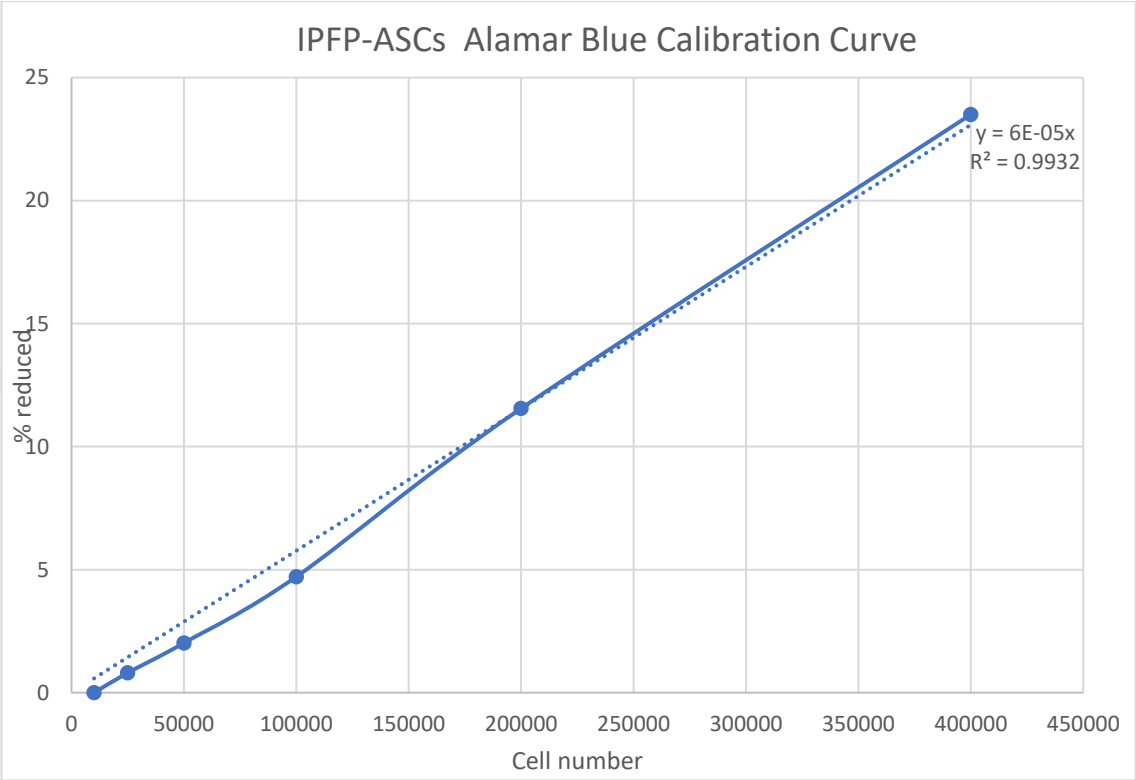

Calibration curve of infrapatellar fat pad derived adipose stem cells (IPFP-ASCs) for Alamar Blue Assay

APPENDIX 2

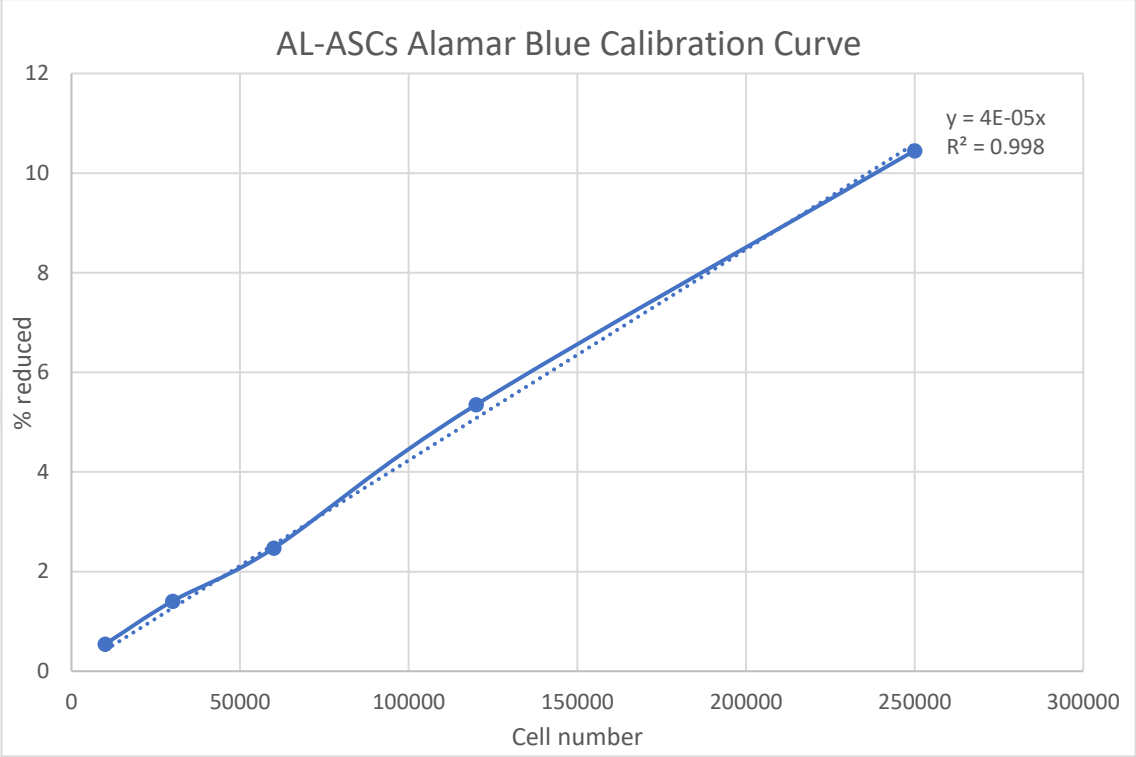

Calibration curve of abdominal lipoaspirate derived adipose stem cells (AL-ASCs) for Alamar Blue Assay

APPENDIX 3

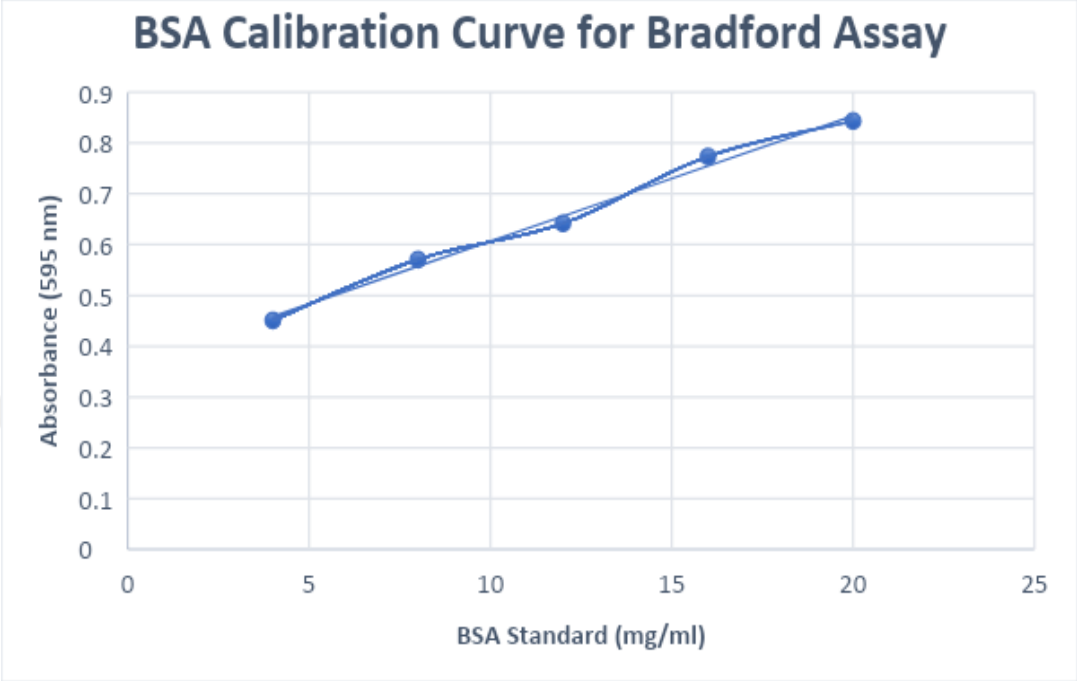

Calibration Curve of BSA concentration for Bradford Assay